Sampling Based on Local Bandwidth

by

Dennis Wei

S.B. Electrical Science and Engineering,
Massachusetts Institute of Technology (2006)
S.B. Physics,
Massachusetts Institute of Technology (2006)

Submitted to the Department of Electrical Engineering and Computer Science
in partial fulfillment of the requirements for the degree of

Master of Engineering in Electrical Engineering and Computer Science

at the

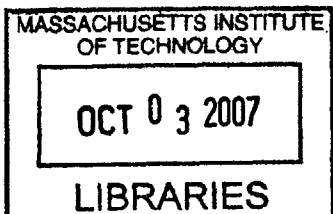MASSACHUSETTS INSTITUTE OF TECHNOLOGY

February 2007

Author ....
Department of Electrical Engineering and Computer Science
December 7, 2006

Certified by ....
....
Alan V. Oppenheim
Ford Professor of Engineering
Thesis Supervisor

Accepted by .....
....
Arthur C. Smith
Professor of Electrical Engineering
Chairman, Department Committee on Graduate Theses

Sampling Based on Local Bandwidth

by

Dennis Wei

Submitted to the Department of Electrical Engineering and Computer Science
on December 7, 2006, in partial fulfillment of the
requirements for the degree of
Master of Engineering in Electrical Engineering and Computer Science

Abstract

The sampling of continuous-time signals based on local bandwidth is considered in this thesis. In an intuitive sense, local bandwidth refers to the rate at which a signal varies locally. One would expect that signals should be sampled at a higher rate in regions of higher local bandwidth, and at a lower rate in regions of lower local bandwidth. In many cases, sampling signals based on local bandwidth can yield more efficient representations as compared with conventional uniform sampling, which does not exploit local signal characteristics.

In the first part of the thesis, a particular definition for a linear time-varying lowpass filter is adopted as a potential model for local bandwidth. A sampling and reconstruction method permitting consistent resampling is developed for signals generated by such filters. The method does not generally result in perfect reconstruction except for a special class of self-similar signals. However, the reconstruction error is shown to decrease with the variation in the cut-off frequency of the filter.

In the second part of the thesis, a definition for local bandwidth based on the time-warping of globally bandlimited signals is reviewed. Using this definition, a method is developed for sampling and reconstructing signals according to local bandwidth. The method employs a time-warping to minimize the energy of a signal above a given maximum frequency. A number of techniques for determining the optimal time-warping are examined.

Thesis Supervisor: Alan V. Oppenheim
Title: Ford Professor of Engineering

Acknowledgments

Contents

List of Figures

List of Tables

Chapter 1

Introduction

1.1 Motivation

Continuous-time signals are traditionally sampled uniformly to obtain a discrete-time representation. The theoretical basis for uniform sampling is provided by the classical uniform sampling theorem (see [1] for a general discussion), which states that a continuous-time signal with a maximum bandwidth of $2W$ cycles per second is completely determined by its samples taken $1/2W$ seconds apart. The signal is reconstructed from its samples using bandlimited interpolation. Specifically, a signal $x(t)$ bandlimited to $[-W, W]$ cycles per second can be expressed as

$$x(t) = \sum_{k=-\infty}^{\infty} x\left(\frac{k}{2W}\right) \frac{\sin(2\pi Wt - k\pi)}{2\pi Wt - k\pi}. \tag{1.1}$$

For non-bandlimited signals, it is a common practice to process the signal with an anti-aliasing lowpass or bandpass filter before sampling, at the cost of some distortion.

For many classes of signals, however, uniform sampling may not yield as efficient a representation as alternative sampling methods. The uniform sampling theorem only assumes knowledge of the bandwidth of the signal. If more detailed information about the signal is available, it is often possible to design sampling strategies that exploit the additional information. For example, if a signal $x(t)$ can be expressed as an expansion involving its

samples $x(t_k)$ and basis functions $\varphi_k(t)$,

$$x(t) = \sum_{k=-\infty}^{\infty} x(t_k)\varphi_k(t), \tag{1.2}$$

then $x(t)$ is completely specified by the samples $x(t_k)$. In particular, the sampling times t_k need not be uniformly spaced, and $x(t)$ need not be bandlimited.

In this thesis, we specifically consider sampling based on the concept of local bandwidth. For the purposes of the present discussion, the term local bandwidth refers to some measure of the rate at which the signal varies locally, e.g. within a nearby interval. Intuitively, we would expect that a signal should be sampled at a higher rate in regions where it varies more quickly, and at a lower rate where it varies more slowly. The intuition leads to a generally non-uniform sampling in which the sampling rate is adapted to the local bandwidth.

As an example, consider sampling the linear frequency-modulation (FM) signal shown in Figure 1-1. FM signals are typically described in terms of an instantaneous frequency, i.e. the instantaneous rate of oscillation, which in our example increases linearly with time. In the upper panel of Figure 1-1, we illustrate a uniform sampling of the signal. Since linear FM signals are not bandlimited except in degenerate cases, it is not possible to attain perfect reconstruction using bandlimited interpolation. We observe that the number of samples per cycle decreases as the instantaneous frequency increases, so intuitively we would expect a bandlimited reconstruction to be less accurate where the signal varies more quickly. In the lower panel, the signal is sampled non-uniformly at a rate proportional to its instantaneous frequency, which we interpret as its local bandwidth. In this case, the number of samples per cycle remains approximately constant. Given that the total number of samples taken is the same in the two approaches, we may reasonably expect the second to yield a more efficient representation.

FM signals arise in a number of contexts, including FM radio and radar waveforms [2]. Many other classes of signals lend themselves to a characterization in terms of local bandwidth. For example, natural images are often decomposed into uniform regions, corresponding to lower local bandwidth, and edges and textures, corresponding to higher local bandwidth [3]. Music can also be thought of as possessing a local bandwidth that depends on the pitches present in a given time interval. For instance, the highest harmonic frequency with significant energy may be taken as the local bandwidth at each point in time.
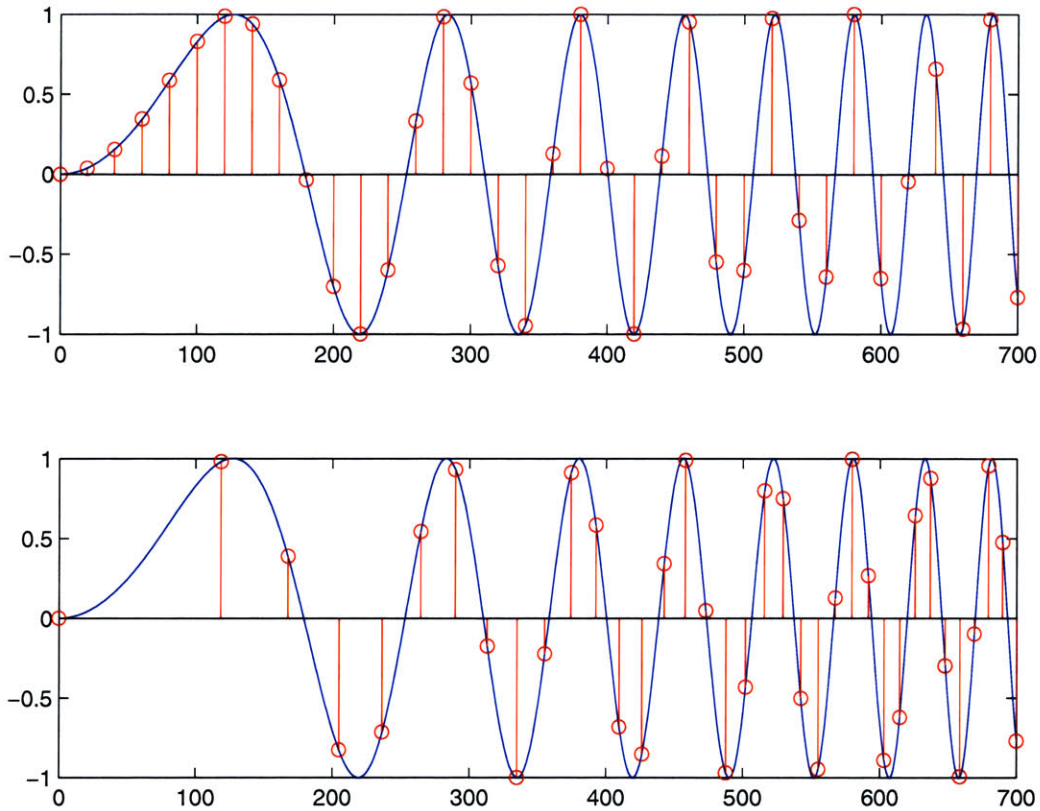
Figure 1-1: Example of a linear FM signal sampled uniformly (upper panel) and non-uniformly according to local bandwidth (lower panel). The number of samples is the same in both cases.

Although the intuition behind sampling according to local bandwidth is seemingly reasonable, more effort is required in developing the underlying theory. In particular, a mathematical definition of local bandwidth is not straightforward because it restores time locality to the concept of bandwidth, a quantity that is by definition completely non-local. A central aim of the thesis is to formulate a definition for local bandwidth, thus providing a framework for the development of sampling and reconstruction strategies. These strategies may be applied to signals that are well-characterized in terms of local bandwidth as possible alternatives to uniform sampling.

1.2   Desirable properties of a definition for local bandwidth

In this section, we summarize some properties that a definition for local bandwidth should possess. These properties will provide a basis for evaluating potential definitions.

A signal is said to be globally bandlimited if it has a finite global bandwidth, in which

17

case the uniform sampling theorem provides an exact reconstruction from uniform samples of the signal. Generalizing, we refer to a signal as locally bandlimited if its local bandwidth is finite and if it can be perfectly reconstructed from its samples. The locations of the sampling times should depend upon the local bandwidth, i.e. they should be more closely spaced in regions of high local bandwidth, and vice versa. In the context of sampling, it is highly desirable to have a perfect reconstruction property for locally bandlimited signals.

If a definition does not allow perfect reconstruction for an appropriately defined class of locally bandlimited signals, it should still have the property that the reconstruction error decreases as the variation in local bandwidth becomes more gradual. In the limit of constant local bandwidth, the signal should also be globally bandlimited and hence exactly reconstructable using the uniform sampling theorem. Accordingly, if the local bandwidth is approximately constant, we expect the reconstruction error to be small.

The choice of sampling grid and reconstruction should permit consistent resampling. In other words, if $\hat{x}(t)$ is the reconstruction from samples $x(t_k)$, $k \in \mathbf{Z}$ of the original signal $x(t)$, then $\hat{x}(t_k) = x(t_k)$ at the sampling instants t_k even if $\hat{x}(t) \neq x(t)$ at other values of t.

A definition for local bandwidth should also correspond to the local rate of variation of the signal, and should provide a measure of the local variation as a function of time.

1.3 Potential models for local bandwidth

In this section, two models are introduced as possible definitions for local bandwidth, the first based on linear time-varying lowpass filters, and the second based on the time-warping of bandlimited signals.

1.3.1 Signals generated by linear time-varying lowpass filters

A globally bandlimited signal may be associated with the output of an ideal linear time-invariant lowpass filter. It is therefore natural to consider a locally bandlimited signal as the output of a linear time-varying lowpass filter. For brevity, we will omit the qualifiers "linear" and "ideal", as all lowpass filters considered in this thesis are linear, and all time-invariant lowpass filters are ideal unless otherwise noted.

Intuitively, a time-varying lowpass filter is a generalization of a time-invariant lowpass filter in which the cut-off frequency $w(t)$ is permitted to vary with time, as represented

18

schematically in Figure 1-2. However, Figure 1-2 is not well-defined mathematically, as it
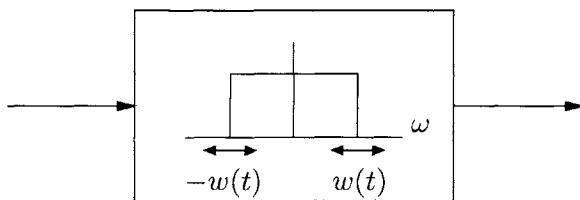
Figure 1-2: Schematic representation of a time-varying lowpass filter.

suggests that the frequency response of the filter is also a function of time. It is unclear how the input-output relations of a time-invariant lowpass filter should be generalized to the time-varying case. In Chapter 3, we will obtain a consistent definition for a time-varying lowpass filter based on a set of desirable properties.

In [4], Horiuchi considered the sampling of signals with time-varying spectra of finite frequency support, viz. bandlimited time-varying spectra. Horiuchi derived an expansion for such signals analogous to the uniform sampling theorem and observed that the expansion does not correspond to a representation of the signal in terms of its samples, except in some special cases. As we will show, the output of a time-varying lowpass filter as defined in Chapter 3 has a bandlimited time-varying spectrum. Following [4], in Chapter 4 we consider the sampling and reconstruction of signals generated by time-varying lowpass filters.

1.3.2 Time-warped bandlimited signals

Clark et al. [5] considered a class of signals that can be mapped into bandlimited signals through an invertible transformation of the time axis, interpreted more informally as a time-warping. These signals are referred to as time-warped bandlimited signals, since they can also be regarded as the result of applying the inverse time-warping to bandlimited signals. Figure 1-3 shows an example of a bandlimited signal and the corresponding time-warped signal. The local bandwidth of the time-warped signal is defined in terms of the local dilation or compression relative to the bandlimited signal, and is higher at earlier times and lower at later times.

It was shown in [5] that the class of time-warped bandlimited signals can be exactly represented by the set of non-uniform samples that are the image under the time-warping of uniform samples of the associated bandlimited signal. In Chapter 5, this result is reviewed for one-dimensional (1-D) signals, although [5] also extended it to two-dimensional (2-D)
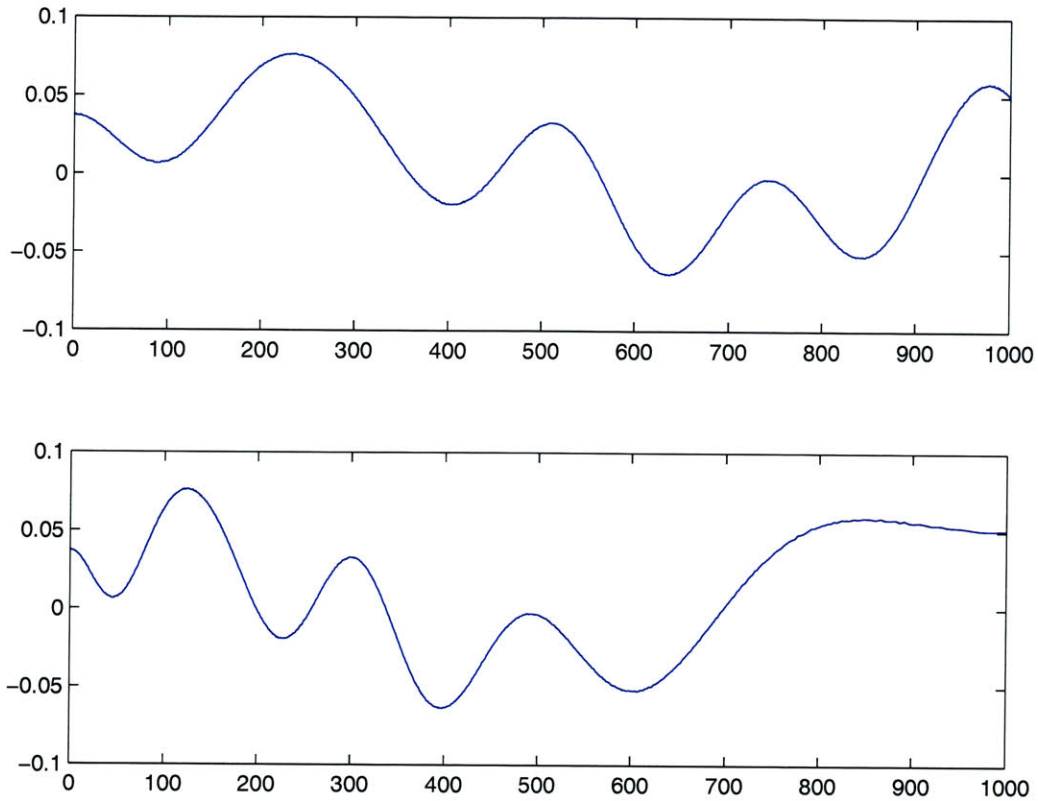
Figure 1-3: Example of a bandlimited signal (upper panel) and the corresponding time-warped signal (lower panel).

signals.

Zeevi and Shlomot [6] showed that the class of time-warped bandlimited signals is a reproducing kernel Hilbert space, and developed a projection filter for signals (1-D or 2-D) to be sampled on a specified non-uniform grid. They also extended the results of [5] to a class of stochastic processes and related the time-warping to certain parameters of the stochastic process.

Both [5] and [6] suggested the use of time-frequency distributions, such as the short-time Fourier transform or the Wigner-Ville distribution (see e.g. [7]), in estimating a time-warping that maps an arbitrary signal into an approximately bandlimited signal. Accordingly, Brueller et al. developed an iterative algorithm in [8], based on the thresholding of time-frequency distributions, that yields a time-warping and an approximately bandlimited signal. The time-warping was incorporated in a non-uniform sampling and reconstruction procedure, and an application to synthetic aperture radar was suggested. In Chapter 6, we discuss alternative approaches to the determination of such a time-warping.

1.4 Outline of thesis

In Chapter 2, the theory of linear time-varying systems is reviewed so as to establish notation and a framework for analyzing time-varying lowpass filters in Chapters 3 and 4.

In Chapter 3, we develop a particular definition of a time-varying lowpass filter that satisfies a number of desirable properties. We then analyze the spectral input-output relation for time-varying lowpass filters, treating separately the cases of aperiodic and periodic cut-off frequency.

Chapter 4 considers the sampling of signals with bandlimited time-varying spectra, i.e. signals generated by time-varying lowpass filters as defined in Chapter 3. We develop a non-uniform sampling and reconstruction method based on the time-varying cut-off frequency. It is shown that this reconstruction is not exact in general, but that the reconstruction error decreases with the variation in the cut-off frequency, as supported by numerical simulations. The method does however yield a perfect reconstruction for a class of self-similar signals with bandlimited time-varying spectra.

In Chapter 5, we review a definition of local bandwidth based on the time-warping of globally bandlimited signals. The definition specifies a class of locally bandlimited signals that can be perfectly reconstructed from samples taken according to local bandwidth. We also discuss the pre-filtering and pre-warping of signals to be sampled on a specified non-uniform grid.

Chapter 6 develops an approach to sampling and reconstruction based on the definition of local bandwidth in Chapter 5. In particular, a time-warping is sought that minimizes the energy of a signal above a given maximum frequency. We examine a number of analytical and numerical techniques to determine the optimal time-warping. Simulations of the numerical algorithms are summarized.

Chapter 2

Linear Time-Varying Systems

In this chapter, the theory of linear time-varying (LTV) systems is reviewed in order to establish notation and a framework for analyzing time-varying lowpass filters in Chapters 3 and 4. Following Claasen and Mecklenbräuker [9], we summarize some of the more common forms for the input-output relation of an LTV system.

2.1 Impulse response

LTV systems may be characterized by their responses to impulses, as is the case for linear time-invariant (LTI) systems. The input $x(t)$ is decomposed into an integral over weighted and shifted impulses:

$$x(t) = \int_{-\infty}^{\infty} x(\tau)\delta(t - \tau)d\tau.$$

Let $h_1(t,\tau)$ denote the response, evaluated at time t, to the impulse $\delta(t - \tau)$. Applying superposition, the output $y(t)$ is given by

$$y(t) = \int_{-\infty}^{\infty} x(\tau)h_1(t,\tau)d\tau. \tag{2.1}$$

Equation (2.1) is typically referred to as the superposition integral. For a general LTV system, the impulse response $h_1(t,\tau)$ can depend on both the excitation time τ and the observation time t. In contrast, for an LTI system, the impulse response depends only on the time difference $t - \tau$, i.e. $h_1(t,\tau)$ reduces to a function of the form $h(t - \tau)$ and (2.1) reduces to the convolution integral.

Figure 2-1 shows the (t, τ) plane, the domain of the 2-D function $h_1(t, \tau)$. The response

$h_1(t, t_0)$ to the impulse $\delta(t - t_0)$ is represented by a horizontal dashed line along $\tau = t_0$. From (2.1), the output evaluated at $t = t_1$ is the integral of the product of $x(\tau)$ with the vertical slice $h_1(t_1, \tau)$ indicated by a dotted line in Figure 2-1.
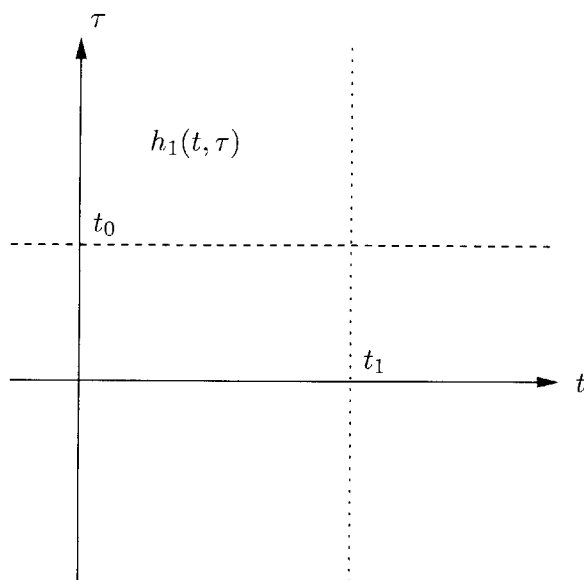
Figure 2-1: Slices of the impulse response $h_1(t, \tau)$. The dashed horizontal line represents the response $h_1(t, t_0)$ to the impulse $\delta(t - t_0)$. The dotted vertical line represents the slice $h_1(t_1, \tau)$ involved in computing the output value $y(t_1)$.

2.2 Time-varying frequency response

Complex exponentials are an important class of signals in LTI system theory because they are eigenfunctions of all LTI systems. The response of an LTI system to a complex exponential $e^{j\omega t}$ is the same exponential scaled by its eigenvalue $H(\omega)$, i.e. the frequency response evaluated at frequency ω. The concept of frequency response can be generalized to LTV systems, as we now summarize.

Complex exponentials are not eigenfunctions of all LTV systems. Nevertheless, the decomposition of signals into complex exponentials can still be useful. For example, we may wish to analyze an LTV system in the context of LTI systems to which it is connected, and/or the input signals may be better characterized in the frequency domain.

Using the inverse Fourier transform, the input $x(t)$ is decomposed into a superposition of complex exponentials:

$$x(t) = \frac{1}{2\pi} \int_{-\infty}^{\infty} X(\omega) e^{j\omega t} d\omega,$$

24

where $X(\omega)$ denotes the Fourier transform of $x(t)$. To describe the response of an LTV system to a complex exponential, Zadeh [10] introduced the time-varying frequency response $H_2(t, \omega)$, defined by

$$\text{response to } e^{j\omega t} \equiv H_2(t, \omega)e^{j\omega t}. \tag{2.2}$$

From (2.2), the output $y(t)$ is

$$y(t) = \frac{1}{2\pi} \int_{-\infty}^{\infty} X(\omega)H_2(t, \omega)e^{j\omega t}d\omega. \tag{2.3}$$

Equation (2.3) relates the output signal $y(t)$ to the input spectrum $X(\omega)$. It can be recast as a relation between $y(t)$ and the input signal $x(t)$. We define the following Fourier pair:

$$h_2(t, \tau) = \frac{1}{2\pi} \int_{-\infty}^{\infty} H_2(t, \omega)e^{j\omega\tau}d\omega, \tag{2.4a}$$

$$H_2(t, \omega) = \int_{-\infty}^{\infty} h_2(t, \tau)e^{-j\omega\tau}d\tau. \tag{2.4b}$$

Substituting (2.4b) into (2.3),

$$\begin{aligned}
y(t) &= \frac{1}{2\pi} \int_{-\infty}^{\infty} X(\omega) \int_{-\infty}^{\infty} h_2(t, \tau)e^{-j\omega\tau}d\tau\ e^{j\omega t}d\omega, \\
&= \int_{-\infty}^{\infty} \left[\frac{1}{2\pi} \int_{-\infty}^{\infty} X(\omega)e^{j\omega(t-\tau)}d\omega \right] h_2(t, \tau)d\tau, \\
&= \int_{-\infty}^{\infty} x(t - \tau)h_2(t, \tau)d\tau,
\end{aligned}$$

which has the form of a convolution. The convolution is commutative, i.e. replacing τ with $t - \tau$,

$$y(t) = \int_{-\infty}^{\infty} x(\tau)h_2(t, t - \tau)d\tau. \tag{2.5}$$

The function $h_2(t, \tau)$ can also be interpreted as an impulse response, for which t is the observation time and $t - \tau$ is the excitation time. Comparing (2.5) and (2.1), the impulse responses $h_1(t, \tau)$ and $h_2(t, \tau)$ correspond to the same LTV system if

$$h_1(t, \tau) = h_2(t, t - \tau). \tag{2.6}$$

To obtain an alternative to (2.3), we define $H_1(t, \omega)$ as the Fourier transform of $h_1(t, \tau)$

with respect to τ, but with a positive sign in the complex exponential $e^{j\omega\tau}$:

$$H_1(t,\omega) = \int_{-\infty}^{\infty} h_1(t,\tau)e^{j\omega\tau}d\tau. \tag{2.7}$$

Then it follows from (2.6) that $H_1(t,\omega) = H_2(t,\omega)e^{j\omega t}$, which yields

$$y(t) = \frac{1}{2\pi}\int_{-\infty}^{\infty} X(\omega)H_1(t,\omega)d\omega \tag{2.8}$$

upon substitution into (2.3).

It is sometimes convenient to consider the output $y(t)$ as having a time-varying spectrum $\tilde{Y}(t,\omega)$ defined by the following relations:

$$Y(t,\omega) = X(\omega)H_2(t,\omega), \tag{2.9a}$$

$$y(t) = \frac{1}{2\pi}\int_{-\infty}^{\infty} Y(t,\omega)e^{j\omega t}d\omega. \tag{2.9b}$$

Taking the inverse Fourier transform of $\tilde{Y}(t,\omega)$, we obtain a 2-D signal $\tilde{y}(t,\tau)$, i.e.

$$\tilde{y}(t,\tau) = \frac{1}{2\pi}\int_{-\infty}^{\infty} \tilde{Y}(t,\omega)e^{j\omega\tau}d\omega, \tag{2.10a}$$

$$\tilde{Y}(t,\omega) = \int_{-\infty}^{\infty} \tilde{y}(t,\tau)e^{-j\omega\tau}d\tau. \tag{2.10b}$$

The variables τ and ω form a Fourier pair. The 1-D signal $y(t)$ is the diagonal slice of $\tilde{y}(t,\tau)$ obtained by setting $\tau = t$, i.e. $y(t) = \tilde{y}(t,t)$. In Chapter 4, we will make explicit use of the time-varying spectrum $\tilde{Y}(t,\omega)$ and the 2-D signal $\tilde{y}(t,\tau)$.

In Figure 2-2, we again show the (t,τ) plane, the domain of the impulse response $h_2(t,\tau)$. The dotted vertical line indicates the slice $h_2(t_1,\tau)$ that is involved in computing the output value $y(t_1)$. The impulse response $h_2(t,t-t_0)$, obtained by substituting $x(\tau) = \delta(\tau - t_0)$ into (2.5), is marked in Figure 2-2 by a dashed diagonal line.

2.3 Bifrequency function

We have discussed representations of LTV systems relating the output signal $y(t)$ to the input signal $x(t)$, and the output signal to the input spectrum $X(\omega)$. It is also desirable to
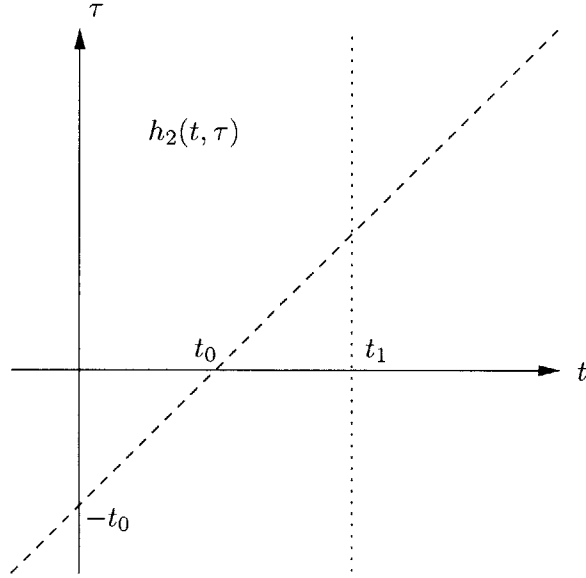
Figure 2-2: Slices of the impulse response $h_2(t, \tau)$. The dotted vertical line represents the slice $h_2(t_1, \tau)$ involved in computing the output value $y(t_1)$. The diagonal dashed line represents the response $h_2(t, t - t_0)$ to the impulse $\delta(t - t_0)$.

obtain representations that directly relate the output spectrum $Y(\omega)$ to the input spectrum. Taking the Fourier transform with respect to t of both sides of (2.8),

$$Y(\Omega) = \int_{-\infty}^{\infty} y(t)e^{-j\Omega t}dt = \frac{1}{2\pi} \int_{-\infty}^{\infty} X(\omega)\tilde{H}_1(\Omega, \omega)d\omega. \tag{2.11}$$

The function $\tilde{H}_1(\Omega, \omega)$ is referred to as the bifrequency function and is related to $h_1(t, \tau)$ and $H_1(t, \omega)$ by

$$\tilde{H}_1(\Omega, \omega) = \int_{-\infty}^{\infty} \int_{-\infty}^{\infty} h_1(t, \tau)e^{-j\Omega t}e^{j\omega\tau}dt \, d\tau, \tag{2.12}$$

$$= \int_{-\infty}^{\infty} H_1(t, \omega)e^{-j\Omega t}dt. \tag{2.13}$$

We note that (2.11) can also be derived using the projection-slice theorem from 2-D signal processing [3].

An alternative bifrequency function $\tilde{H}_2(\Omega, \omega)$ results from taking the Fourier transform of $H_2(t, \omega)$ with respect to t:

$$\tilde{H}_2(\Omega, \omega) = \int_{-\infty}^{\infty} H_2(t, \omega)e^{-j\Omega t}dt. \tag{2.14}$$

27

Since $H_1(t, \omega) = H_2(t, \omega)e^{j\omega t}$, we have $\tilde{H}_1(\Omega, \omega) = \tilde{H}_2(\Omega - \omega, \omega)$. Substituting into (2.11),

$$Y(\Omega) = \frac{1}{2\pi} \int_{-\infty}^{\infty} X(\omega)\tilde{H}_2(\Omega - \omega, \omega)d\omega. \qquad (2.15)$$

In Section 3.3.1, we will find it more convenient to use (2.15) rather than (2.11) in analyzing the spectral input-output relation for a time-varying lowpass filter.

For the special case of periodically time-varying systems, there exists an alternative expression relating $Y(\omega)$ to $X(\omega)$. If the system varies periodically with period T, the time-varying frequency response $H_2(t, \omega)$ is also periodic in t and can be expanded in the following Fourier series:

$$H_2(t, \omega) = \sum_{k=-\infty}^{\infty} H_k(\omega)e^{jk(2\pi/T)t}. \qquad (2.16)$$

Substituting (2.16) into (2.3), performing a change of variables, and identifying the resulting integrand as $Y(\omega)$, we obtain

$$Y(\omega) = \sum_{k=-\infty}^{\infty} H_k\left(\omega - \frac{2\pi k}{T}\right) X\left(\omega - \frac{2\pi k}{T}\right), \qquad (2.17)$$

i.e. the output spectrum is the sum of weighted and shifted copies of the input spectrum. For LTI systems, only the $k = 0$ term is present. In Section 3.3.4, we will use (2.17) to analyze periodically time-varying lowpass filters.

It is also possible to relate the output spectrum $Y(\omega)$ to the input signal $x(t)$. Taking the Fourier transform with respect to t of both sides of (2.1),

$$Y(\Omega) = \int_{-\infty}^{\infty} x(\tau)\bar{H}_1(\Omega, \tau)d\tau, \qquad (2.18)$$

where

$$\bar{H}_1(\Omega, \tau) = \int_{-\infty}^{\infty} h_1(t, \tau)e^{-j\Omega t}dt. \qquad (2.19)$$

However, the relation in (2.18) is not commonly used, and we will not require it in later chapters.

Chapter 3

Linear Time-Varying Lowpass Filters

In this chapter, we present a specific definition for a time-varying lowpass filter based on a set of desirable properties. We derive a relation between the input and output spectra of a time-varying lowpass filter, treating separately the cases of aperiodic and periodic cut-off frequency.

3.1 Desirable properties

There are many well-defined ways in which a lowpass filter can be made to vary with time. In this section, we summarize some properties that a time-varying lowpass filter should possess, to be used as criteria before adopting a specific definition.

1. We assume that a time-varying lowpass filter is described in terms of a single time-varying parameter, namely the cut-off frequency $w(t)$. Furthermore, $w(t)$ has a finite minimum and maximum value, i.e. $0 < w_{min} \leq w(t) \leq w_{max} < \infty \; \forall \; t$ for some w_{min} and w_{max}.

2. A time-varying lowpass filter should be time-varying in the following sense: The response of the filter to the impulse $\delta(t - t_0)$ should depend not only on $w(t_0)$, the cut-off frequency at the excitation time, but also on $w(t)$ at other times $t \neq t_0$.

3. A time-varying lowpass filter should exactly reproduce the complex exponential input $e^{j\omega_0 t}$ when $w(t) > \omega_0$, and should produce an output of zero when $w(t) < \omega_0$. This

property is analogous to the behaviour of a time-invariant lowpass filter with cut-off frequency w and input $e^{j\omega_0 t}$, for which the response is $e^{j\omega_0 t}$ for $w > \omega_0$ and zero for $w < \omega_0$.

4. The output of a time-varying lowpass filter is not necessarily bandlimited, except in the special case of a constant cut-off frequency $w(t) = w$. Accordingly, if $w(t)$ is approximately constant, i.e. if $w(t) = w + \Delta w(t)$ where $\Delta w(t)$ is a small perturbation relative to w, we expect most of the output spectrum to be concentrated within a finite bandwidth. In the limit as $\Delta w(t)$ approaches zero, the output should become bandlimited.

5. A time-varying lowpass filter should be idempotent, i.e. if $y(t)$ is the output of a time-varying lowpass filter, and $z(t)$ is the output of an identical time-varying lowpass filter with $y(t)$ as input, then $z(t) = y(t)$. If a time-varying lowpass filter is to be interpreted as a filter that shapes the local bandwidth of its output, then the output should be unchanged by a second, identical shaping.

3.2   Definition

In this section, we develop a specific definition for a time-varying lowpass filter based on the generalization of a time-invariant lowpass filter and the properties summarized in Section 3.1.

For a time-invariant lowpass filter with cut-off frequency w, the output $y(t)$ is the convolution of the input $x(t)$ with the impulse response $h_1(t, \tau)$ of the filter,

$$h_1(t, \tau) = h(t - \tau) = \frac{\sin(w(t - \tau))}{\pi(t - \tau)}, \tag{3.1}$$

using the notation of Chapter 2. Hence,

$$y(t) = \int_{-\infty}^{\infty} x(\tau) \frac{\sin(w(t - \tau))}{\pi(t - \tau)} d\tau. \tag{3.2}$$

A natural generalization of (3.1) is to allow the cut-off frequency to vary with the excitation time τ, i.e. $w = w(\tau)$. However, as we will show, this generalization does not satisfy Property 2 of Section 3.1.

Letting $w = w(\tau)$, (3.1) becomes

$$h_1(t, \tau) = \frac{\sin(w(\tau)(t - \tau))}{\pi(t - \tau)}.$$ (3.3)

Substituting (3.3) into (2.1),

$$y(t) = \int_{-\infty}^{\infty} x(\tau) \frac{\sin(w(\tau)(t - \tau))}{\pi(t - \tau)} d\tau.$$ (3.4)

Figure 3-1 provides a pictorial interpretation of (3.4). On the left-hand side, the input $x(t)$ is decomposed into weighted and shifted impulses. Each impulse drives a time-invariant lowpass filter with a cut-off frequency that depends on the location of the impulse. The output $y(t)$ is formed by superimposing the filter outputs. For clarity, Figure 3-1 shows branches corresponding to specific values of τ in (3.4), with the understanding that the continuous nature of τ implies an uncountable number of branches.
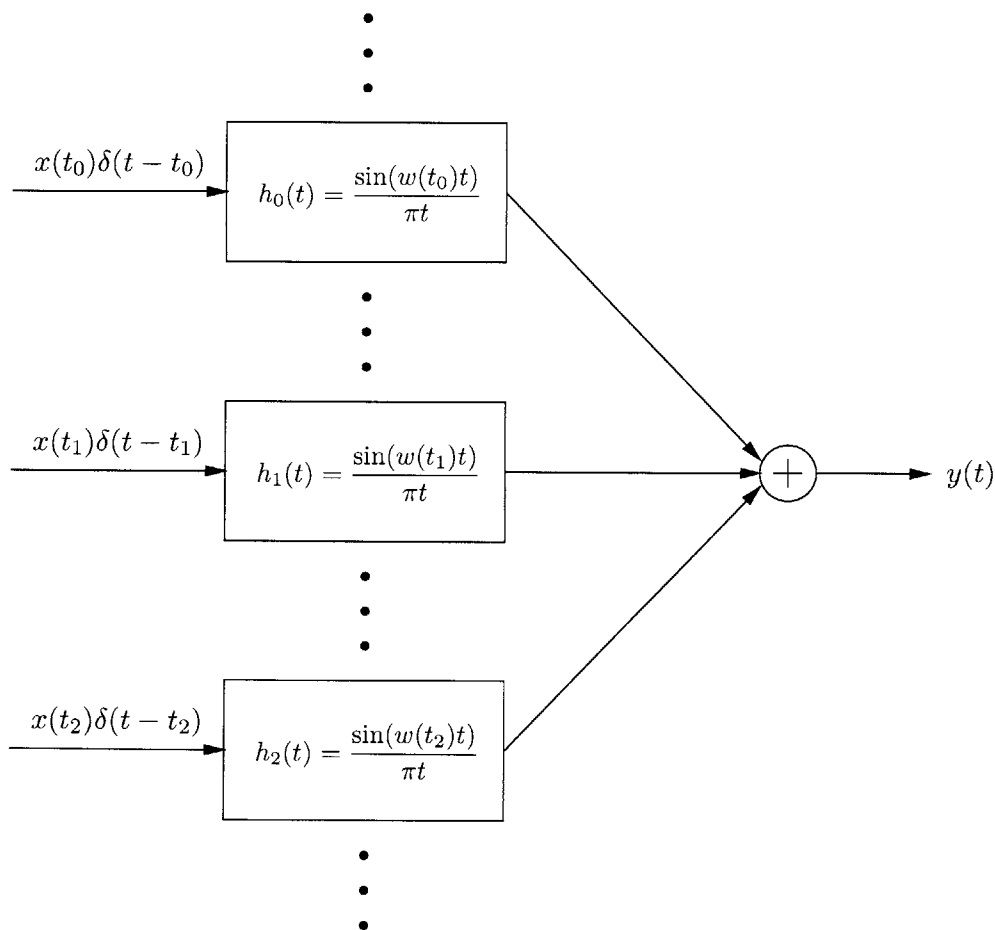
Figure 3-1: Block diagram representation of equation (3.4).

31

From (3.3) and Figure 3-1, we observe that the response to the impulse $\delta(t - t_0)$ depends only on $w(t_0)$ and not on other values of $w(t)$, and thus Property 2 of Section 3.1 is not satisfied. Consequently, we are led to consider an alternative generalization of a time-invariant lowpass filter, specifically in terms of its frequency response.

A time-invariant lowpass filter with cut-off frequency w has a frequency response $H(\omega)$ given by

$$H(\omega) = \begin{cases} 1, & |\omega| < w, \\ 0, & |\omega| > w. \end{cases} \tag{3.5}$$

In terms of $H(\omega)$ and the input spectrum $X(\omega)$, the output $y(t)$ is expressed as

$$\begin{aligned} y(t) &= \frac{1}{2\pi} \int_{-\infty}^{\infty} X(\omega) H(\omega) e^{j\omega t} d\omega, \\ &= \frac{1}{2\pi} \int_{-w}^{w} X(\omega) e^{j\omega t} d\omega. \end{aligned} \tag{3.6}$$

We generalize (3.5) to a time-varying frequency response $H_2(t, \omega)$ by allowing w to vary with the observation time t, i.e. $w = w(t)$ and

$$H_2(t, \omega) = \begin{cases} 1, & |\omega| < w(t), \\ 0, & |\omega| > w(t). \end{cases} \tag{3.7}$$

An example of such a time-varying frequency response is sketched in Figure 3-2.
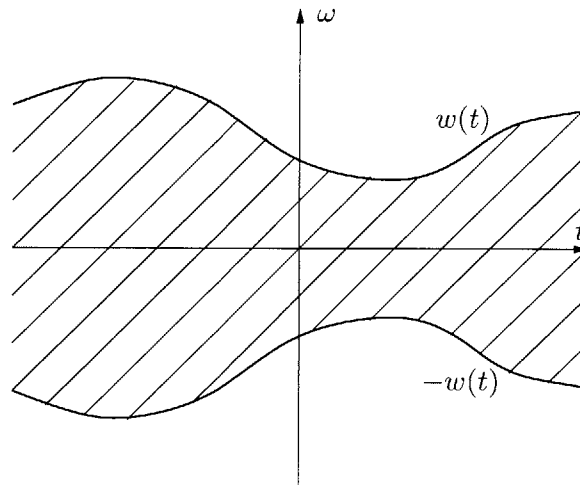
Figure 3-2: Sketch of the time-varying frequency response $H_2(t, \omega)$ for a time-varying lowpass filter. $H_2(t, \omega)$ is unity in the shaded region and zero elsewhere.

Substituting (3.7) into (2.3),

$$y(t) = \frac{1}{2\pi} \int_{-w(t)}^{w(t)} X(\omega)e^{j\omega t}d\omega. \tag{3.8}$$

Equation (3.8) can be rewritten as

$$y(t) = \int_{-\infty}^{\infty} x(\tau)\frac{\sin(w(t)(t-\tau))}{\pi(t-\tau)}d\tau, \tag{3.9}$$

where the corresponding impulse response $h_2(t,\tau)$ defined by (2.4a) and (2.5) is given by

$$h_2(t,\tau) = \frac{\sin(w(t)\tau)}{\pi\tau}. \tag{3.10}$$

The time-varying spectrum $\tilde{Y}(t,\omega)$ of $y(t)$, defined in (2.9a), takes the specific form

$$\tilde{Y}(t,\omega) = \begin{cases} X(\omega), & |\omega| < w(t), \\ 0, & |\omega| > w(t). \end{cases} \tag{3.11}$$

Since for each value of t, $\tilde{Y}(t,\omega)$ is non-zero only on the finite interval $-w(t) < \omega < w(t)$, we refer to $y(t)$ as having a bandlimited time-varying spectrum. Substituting (3.11) in (2.10a), the 2-D signal $\tilde{y}(t,\tau)$ is expressed as

$$\tilde{y}(t,\tau) = \frac{1}{2\pi} \int_{-w(t)}^{w(t)} X(\omega)e^{j\omega\tau}d\omega, \tag{3.12}$$

with $y(t) = \tilde{y}(t,t)$.

We can interpret (3.12) as describing a filter bank with an infinite number of branches, as illustrated in Figure 3-3. The input $x(t)$ is simultaneously processed by a continuum of time-invariant lowpass filters, indexed by the continuous variable t and having cut-off frequencies $w(t)$. As in Figure 3-1, we show only a few specific branches for clarity. From (3.12), we identify $\tilde{y}(t,\tau)$ as the output of the tth filter evaluated at time τ. The diagonal slice $\tilde{y}(t,t)$ corresponds to the output $y(t)$.

We verify that the generalization of a time-invariant lowpass filter specified by (3.8) and (3.9) satisfies Properties 2 and 3 of Section (3.1). From (3.9), the response to the impulse
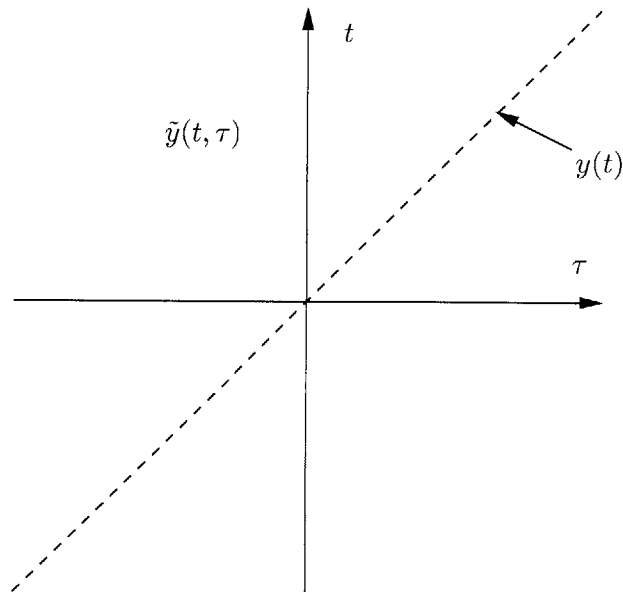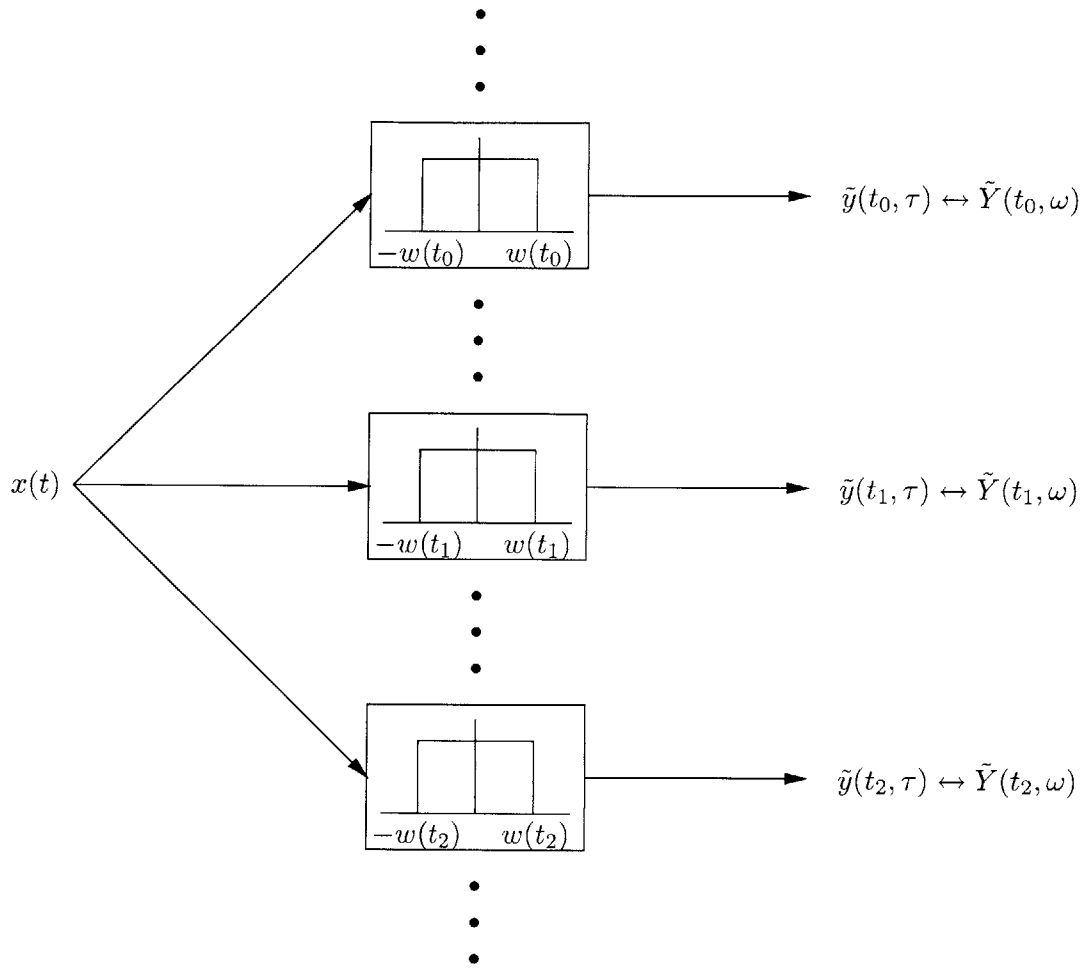
Figure 3-3: Filter bank interpretation of $\tilde{y}(t, \tau)$ for a time-varying lowpass filter.

$x(t) = \delta(t - t_0)$ is given by

$$y(t) = \frac{\sin(w(t)(t - t_0))}{\pi(t - t_0)},$$

which does depend on values of $w(t)$ for $t \neq t_0$. To evaluate the response to the complex exponential $x(t) = e^{j\omega_0 t}$, we substitute $X(\omega) = 2\pi\delta(\omega - \omega_0)$ in (3.8):

$$y(t) = \frac{1}{2\pi} \int_{-w(t)}^{w(t)} 2\pi\delta(\omega - \omega_0)e^{j\omega t} d\omega,$$

$$= \begin{cases} e^{j\omega_0 t}, & w(t) > \omega_0, \\ \\ 0, & w(t) < \omega_0, \end{cases}$$

which verifies Property 3.

Henceforth, we will define a time-varying lowpass filter to be the filter specified by equations (3.7) through (3.12). As we will show in the next section, this definition also satisfies Property 4, but not Property 5 of Section 3.1.

3.3 Spectral input-output relations

We derive relations between the input and output spectra of a time-varying lowpass filter based on the definition adopted in Section 3.2. In Section 3.3.1, we analyze the case in which the cut-off frequency varies aperiodically with time, from which some additional properties of our definition are inferred. The analysis of Section 3.3.1 is applied to the specific case of a linear cut-off frequency in Section 3.3.2 and simulation results are presented in Section 3.3.3. In Section 3.3.4, we treat the case of periodic cut-off frequency, and discuss its relationship to the short-time Fourier transform in Section 3.3.5.

3.3.1 Aperiodic cut-off frequency

For the general case of an aperiodic cut-off frequency, we first determine the bifrequency function $\tilde{H}_2(\Omega, \omega)$ defined by (2.14). The spectral input-output relation follows using (2.15).

From (3.7) and Property 1 of Section 3.1,

$$H_2(t, \omega) = \begin{cases} 1, & \forall\, t,\ |\omega| < w_{min}, \\ \\ 0, & \forall\, t,\ |\omega| > w_{max}. \end{cases} \tag{3.13}$$

35

Taking the Fourier transform,

$$\tilde{H}_2(\Omega, \omega) = \begin{cases} 2\pi\delta(\Omega), & |\omega| < w_{min}, \\ \\ 0, & |\omega| > w_{max}. \end{cases} \qquad (3.14)$$

It remains to specify $\tilde{H}_2(\Omega, \omega)$ in the region $w_{min} < |\omega| < w_{max}$ where $H_2(t, \omega)$ alternates between 1 and 0 depending on the exact shape of $w(t)$.

Toward this end, we decompose $H_2(t, \omega)$ into a sum of step functions as follows: Let $t_1(\omega), t_2(\omega), \ldots, t_{L(\omega)}(\omega)$ denote the values of t at which $w(t) = |\omega|$, labelled in increasing order, and excluding tangent points. Then for each value of ω, $w_{min} < |\omega| < w_{max}$, $H_2(t, \omega)$ alternates between 1 and 0 at the times $t_\ell(\omega)$ as illustrated in Figure 3-4. We can therefore
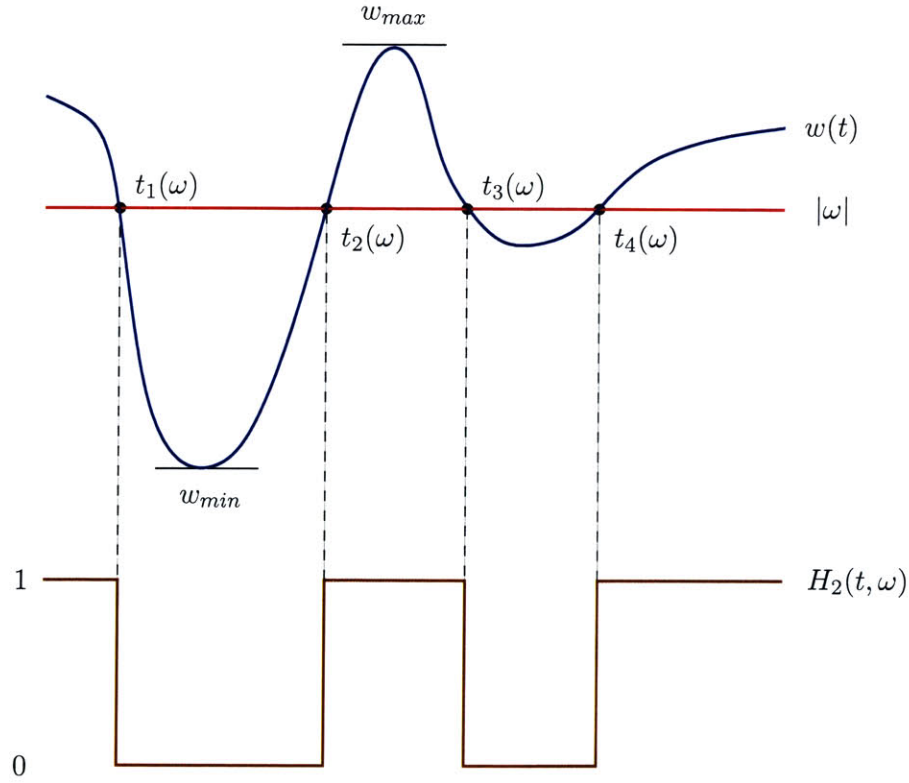
Figure 3-4: Sketch of $w(t)$ and $|\omega|$ for the case $w_{min} < |\omega| < w_{max}$. $H_2(t, \omega)$ alternates between 1 and 0 at the times $t_\ell(\omega)$.

express $H_2(t, \omega)$ as the following sum of step functions with alternating signs:

$$H_2(t, \omega) = \sum_{\ell=1}^{L(\omega)} (-1)^{\ell+1} u(t - t_\ell(\omega)), \quad w_{min} < |\omega| < w_{max}, \qquad (3.15)$$

where we have assumed that $\lim_{t\to-\infty} H_2(t,\omega) = 0$. A similar expression can be written for the case $\lim_{t\to-\infty} H_2(t,\omega) = 1$.

Taking the Fourier transform of (3.15) with respect to t,

$$\tilde{H}_2(\Omega,\omega) = 2\pi H_0(\omega)\delta(\Omega) \pm \frac{1}{j\Omega}\sum_{\ell=1}^{L(\omega)}(-1)^\ell e^{-j\Omega t_\ell(\omega)}, \quad w_{min} < |\omega| < w_{min}, \qquad (3.16)$$

where the plus sign corresponds to $\lim_{t\to-\infty} H_2(t,\omega) = 1$, the minus sign to $\lim_{t\to-\infty} H_2(t,\omega) = 0$, and $H_0(\omega)$ is given by

$$H_0(\omega) = \begin{cases} 1, & \lim_{t\to-\infty} H_2(t,\omega) = 1 \text{ and } L(\omega) \text{ even,} \\ \dfrac{1}{2}, & L(\omega) \text{ odd,} \qquad\qquad\qquad w_{min} < |\omega| < w_{max}. \\ 0, & \lim_{t\to-\infty} H_2(t,\omega) = 0 \text{ and } L(\omega) \text{ even,} \end{cases} \qquad (3.17)$$

For $|\omega| < w_{min}$ and $|\omega| > w_{max}$, we define $H_0(\omega)$ as

$$H_0(\omega) = \begin{cases} 1, & |\omega| < w_{min}, \\ 0, & |\omega| > w_{max}. \end{cases} \qquad (3.18)$$

Combining (3.14) and (3.16), and using the definition of $H_0(\omega)$ in (3.17) and (3.18),

$$\tilde{H}_2(\Omega,\omega) = \begin{cases} 2\pi H_0(\omega)\delta(\Omega), & |\omega| < w_{min} \text{ and } |\omega| > w_{max}, \\ 2\pi H_0(\omega)\delta(\Omega) \pm \dfrac{1}{j\Omega}\displaystyle\sum_{\ell=1}^{L(\omega)}(-1)^\ell e^{-j\Omega t_\ell(\omega)}, & w_{min} < |\omega| < w_{max}. \end{cases} \qquad (3.19)$$

Figure 3-5 shows a sketch of the bifrequency function $\tilde{H}_2(\Omega,\omega)$. The heavy vertical line represents a column of impulses along the line segment ($\Omega = 0$, $|\omega| < w_{max}$). The two shaded horizontal bands represent the second term in (3.19) for the case $w_{min} < |\omega| < w_{max}$. The diagonal dotted line indicates the slice $\tilde{H}_2(\Omega_0 - \omega, \omega)$ involved in determining $Y(\Omega)$ at the single frequency $\Omega = \Omega_0$ according to (2.15).

Substituting (3.19) into (2.15), we obtain the desired spectral input-output relation for

37
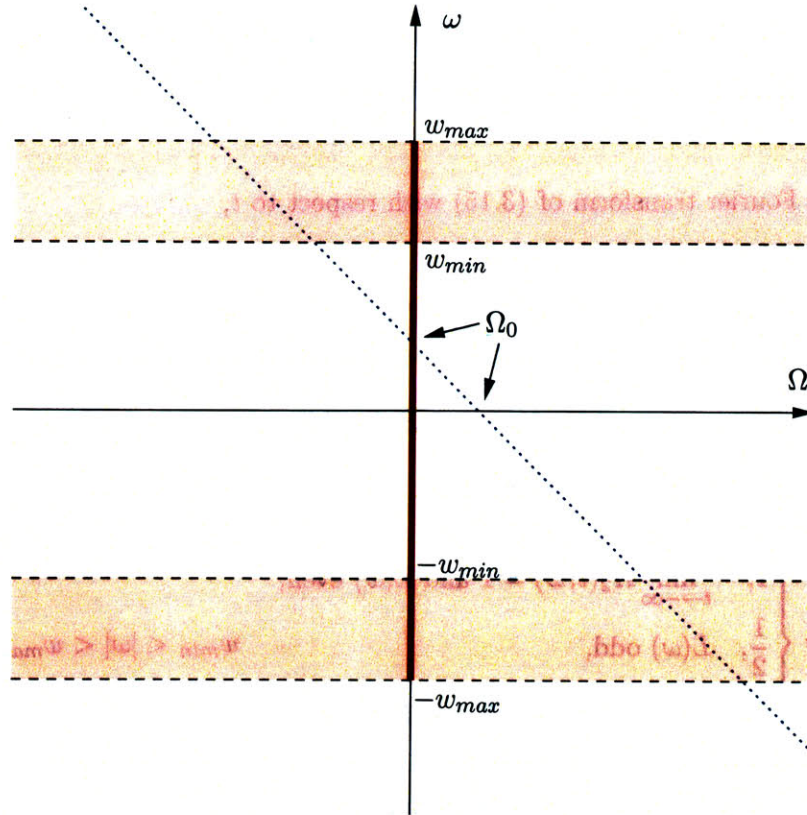
Figure 3-5: Sketch of the bifrequency function $\tilde{H}_2(\Omega, \omega)$ for an aperiodically time-varying lowpass filter.

a time-varying lowpass filter:

$$Y(\Omega) = H_0(\Omega)X(\Omega) \pm \frac{1}{2\pi j} \int_{|\omega|=w_{min}}^{|\omega|=w_{max}} \left[\frac{X(\omega)}{\Omega - \omega} \sum_{\ell=1}^{L(\omega)} (-1)^\ell e^{-j(\Omega-\omega)t_\ell(\omega)} \right] d\omega, \qquad (3.20)$$

where the plus sign corresponds to $\lim_{t \to -\infty} H_2(t, \omega) = 1$ and the minus sign to $\lim_{t \to -\infty} H_2(t, \omega) = 0$ as before.

We consider separately the two terms on the right-hand side of (3.20). The first term,

$$Y_1(\Omega) = H_0(\Omega)X(\Omega), \qquad (3.21)$$

can be interpreted as the effect of an LTI filter with frequency response $H_0(\Omega)$ on the input. Since $H_0(\Omega) = 0$ for $|\Omega| > w_{max}$, $Y_1(\Omega)$ is bandlimited to w_{max}, the maximum cut-off

frequency of the filter. The second term,

$$Y_2(\Omega) = \pm \frac{1}{2\pi j} \int_{|\omega|=w_{min}}^{|\omega|=w_{max}} \frac{X(\omega)}{\Omega - \omega} \sum_{\ell=1}^{L(\omega)} (-1)^\ell e^{-j(\Omega-\omega)t_\ell(\omega)} d\omega, \qquad (3.22)$$

represents the redistribution of the input frequency content in the bands $w_{min} < |\omega| < w_{max}$ over all frequencies Ω in the output spectrum. As a result, if $w(t)$ is not constant, $Y_2(\Omega)$ and $Y(\Omega)$ are generally not bandlimited.

To show that our definition of a time-varying lowpass filter satisfies Property 4 of Section 3.1, we first derive an upper bound on the non-bandlimited component $Y_2(\Omega)$ and show that the bound decreases to zero as the cut-off frequency approaches a constant. $|Y_2(\Omega)|$ is bounded as follows:

$$|Y_2(\Omega)| = \left| \frac{1}{2\pi j} \int_{|\omega|=w_{min}}^{|\omega|=w_{max}} \frac{X(\omega)}{\Omega - \omega} \sum_{\ell=1}^{L(\omega)} (-1)^\ell e^{-j(\Omega-\omega)t_\ell(\omega)} d\omega \right|,$$

$$\leq \frac{1}{2\pi} \int_{|\omega|=w_{min}}^{|\omega|=w_{max}} \frac{|X(\omega)|}{|\Omega - \omega|} \left| \sum_{\ell=1}^{L(\omega)} (-1)^\ell e^{-j(\Omega-\omega)t_\ell(\omega)} \right| d\omega.$$

The magnitude of the summation may be bounded as

$$\left| \sum_{\ell=1}^{L(\omega)} (-1)^\ell e^{-j(\Omega-\omega)t_\ell(\omega)} \right| \leq L(\omega) \leq L_{max},$$

where

$$L_{max} = \max_{w_{min}<|\omega|<w_{max}} L(\omega). \qquad (3.23)$$

Hence,

$$|Y_2(\Omega)| \leq \frac{L_{max}}{2\pi} \int_{|\omega|=w_{min}}^{|\omega|=w_{max}} \frac{|X(\omega)|}{|\Omega - \omega|} d\omega. \qquad (3.24)$$

The bound in (3.24) is proportional to L_{max}, which is the maximum number of level crossings of $w(t)$. As the variation in $w(t)$ decreases, L_{max} generally decreases as well. For example, if $w(t)$ is a polynomial of order p, then $L_{max} \leq p$ since the equation $w(t) = |\omega|$ can have at most p real solutions. Furthermore, the domain of integration $w_{min} < |\omega| < w_{max}$ is determined by the range $w_{max} - w_{min}$ of $w(t)$. As $w(t)$ approaches a constant, both $w_{max} - w_{min}$ and $|Y_2(\Omega)|$ approach zero. We have thus verified Property 4.

Two additional properties of the non-bandlimited component $Y_2(\Omega)$ may be inferred

39

from (3.24). First, by virtue of the $1/|\Omega - \omega|$ factor in the integrand of (3.24), $|Y_2(\Omega)|$ tends to decay as Ω increases or decreases from the range $w_{min} < |\Omega| < w_{max}$. Second, if $|X(\omega)|$ is small for $w_{min} < |\omega| < w_{max}$, i.e. if there is little frequency content in the range over which $w(t)$ varies, then $|Y_2(\Omega)|$ is also small. In particular, if $X(\omega) = 0$ for $w_{min} < |\omega| < w_{max}$, then $Y_2(\omega) = 0$, and $Y(\omega) = X(\omega)$ for $|\omega| < w_{min}$ and is zero otherwise. This result is intuitively reasonable: the filter admits frequencies below w_{min}, blocks frequencies above w_{max}, and no input frequency components exist between w_{min} and w_{max}.

Our definition of a time-varying lowpass filter does not however satisfy Property 5 of Section 3.1. In analogy with (3.8), the output $z(t)$ of a second, identical time-varying lowpass filter with $y(t)$ as input can be written as

$$z(t) = \frac{1}{2\pi} \int_{-w(t)}^{w(t)} Y(\omega)e^{j\omega t}d\omega.$$

We have $z(t) = y(t)$ if $Y(\omega) = X(\omega)$ for $|\omega| < w_{max}$. But according to (3.20) and (3.17), $Y(\omega)$ may differ from $X(\omega)$ in the range $w_{min} < |\omega| < w_{max}$ since $H_0(\omega)$ may be non-unity. Even in the range $|\omega| < w_{min}$, in general $Y(\omega) \neq X(\omega)$ because of the contribution of $Y_2(\Omega)$. Hence, a time-varying lowpass filter with non-constant cut-off frequency is not idempotent. The case of constant cut-off frequency is an exception, since it corresponds to a time-invariant lowpass filter which is idempotent.

3.3.2 Linear cut-off frequency

As an example of an aperiodic choice for $w(t)$, we choose $w(t)$ to be linear over the interval $[0, T]$ and constant elsewhere, i.e.

$$w(t) = \begin{cases} w_{min}, & t \leq 0, \\ w_{min} + \alpha t, & 0 \leq t \leq T, \\ w_{max} = w_{min} + \alpha T, & t \geq T. \end{cases} \tag{3.25}$$

We assume for simplicity that the slope α is positive; a similar analysis could be conducted for $\alpha < 0$.

For this choice of $w(t)$, $L(\omega) = 1$ in equation (3.15), and $t_1(\omega)$ is given by

$$t_1(\omega) = \frac{|\omega| - w_{min}}{\alpha}, \quad w_{min} < |\omega| < w_{max}.$$

Thus,

$$H_2(t, \omega) = u\left(t - \frac{|\omega| - w_{min}}{\alpha}\right), \quad w_{min} < |\omega| < w_{max}, \tag{3.26}$$

$$\tilde{H}_2(\Omega, \omega) = \pi\delta(\Omega) + \frac{1}{j\Omega} \exp\left\{-j\Omega\frac{|\omega| - w_{min}}{\alpha}\right\}, \quad w_{min} < |\omega| < w_{max}. \tag{3.27}$$

The function $H_0(\omega)$ defined by (3.17) and (3.18) is given by

$$H_0(\omega) = \begin{cases} 1, & |\omega| < w_{min}, \\ \dfrac{1}{2}, & w_{min} < |\omega| < w_{max}, \\ 0, & |\omega| > w_{max}. \end{cases} \tag{3.28}$$

From (3.20), the Fourier transform $Y(\Omega)$ of the output is expressed as

$$Y(\Omega) = H_0(\Omega)X(\Omega) + \frac{1}{2\pi j} \int_{|\omega|=w_{min}}^{|\omega|=w_{max}} \frac{X(\omega)}{\Omega - \omega} \exp\left\{-j(\Omega - \omega)\frac{|\omega| - w_{min}}{\alpha}\right\} d\omega,$$

$$= H_0(\Omega)X(\Omega)$$

$$+ \frac{1}{2\pi j} \exp\left\{-j\frac{(\Omega - w_{min})^2}{4\alpha}\right\} \int_{w_{min}}^{w_{max}} \frac{X(\omega)}{\Omega - \omega} \exp\left\{\frac{j}{\alpha}\left(\omega - \frac{\Omega + w_{min}}{2}\right)^2\right\} d\omega$$

$$+ \frac{1}{2\pi j} \exp\left\{j\frac{(\Omega + w_{min})^2}{4\alpha}\right\} \int_{-w_{max}}^{-w_{min}} \frac{X(\omega)}{\Omega - \omega} \exp\left\{-\frac{j}{\alpha}\left(\omega - \frac{\Omega - w_{min}}{2}\right)^2\right\} d\omega.$$

$$\tag{3.29}$$

The second equality is obtained by dividing the domain of integration into positive and negative ranges of ω and by completing the squares in the exponents.

3.3.3 Discrete-time simulation with a linear cut-off frequency

A discrete-time simulation was implemented in MATLAB for time-varying lowpass filters with linearly increasing cut-off frequencies. The simulation demonstrates that the corresponding output spectra are spread over an increasingly wider range of frequencies as the slope of the cut-off frequency increases.

41

The input was chosen to be an impulse, i.e. $x[n] = \delta[n]$ and correspondingly $X(e^{j\omega}) = 1$, in order to focus on the spectral characteristics of the filters. The output is given by the discrete-time analogues to (3.10) and (3.9), i.e. replacing t by n, τ by m, and integration by summation,

$$h_2[n, m] = \frac{\sin(w[n]m)}{\pi m}, \tag{3.30}$$

$$\begin{aligned}
y[n] &= \sum_{m=-\infty}^{\infty} x[m]h_2[n, n-m], \\
&= \sum_{m=-\infty}^{\infty} \delta[m]\frac{\sin(w[n](n-m))}{\pi(n-m)}, \\
&= \frac{\sin(w[n]n)}{\pi n}. \tag{3.31}
\end{aligned}$$

The time index n was restricted to the range $[-L, L]$ with $L = 2000$ and the output sequences were truncated outside of this range.

The cut-off frequency takes the specific form

$$w[n] = w_0 + \alpha n, \quad -L \le n \le L, \tag{3.32}$$

where $w_0 = 0.3\pi$ and the slope $\alpha = \{0.0, 2.5, 5.0, 7.5, 10.0\} \times 10^{-5}\pi$. For instance, if $\alpha = 10.0 \times 10^{-5}\pi$, then the minimum cut-off frequency is 0.1π and the maximum is 0.5π.

For each value of α, the output $y[n]$ and the 8192-point, zero-padded DFT $Y[k]$ of $y[n]$ were computed. Figure 3-6 plots the magnitude of $Y[k]$, interpolated for the purposes of display, for the various choices of α.

As α increases, we observe that the output spectra decay more slowly and at higher frequencies. In particular, the curve corresponding to $\alpha = 0$ represents a constant cut-off frequency, while the curve corresponding to $\alpha = 10 \times 10^{-5}\pi$ represents a five-fold increase over the interval $[-L, L]$. Thus, the results are consistent with Property 4 of Section 3.1 and with the analysis of Section 3.3.1.

3.3.4 Periodic cut-off frequency

In this section, we consider the specific case of a cut-off frequency that varies periodically with time. We derive a spectral input-output relation for this class of time-varying lowpass
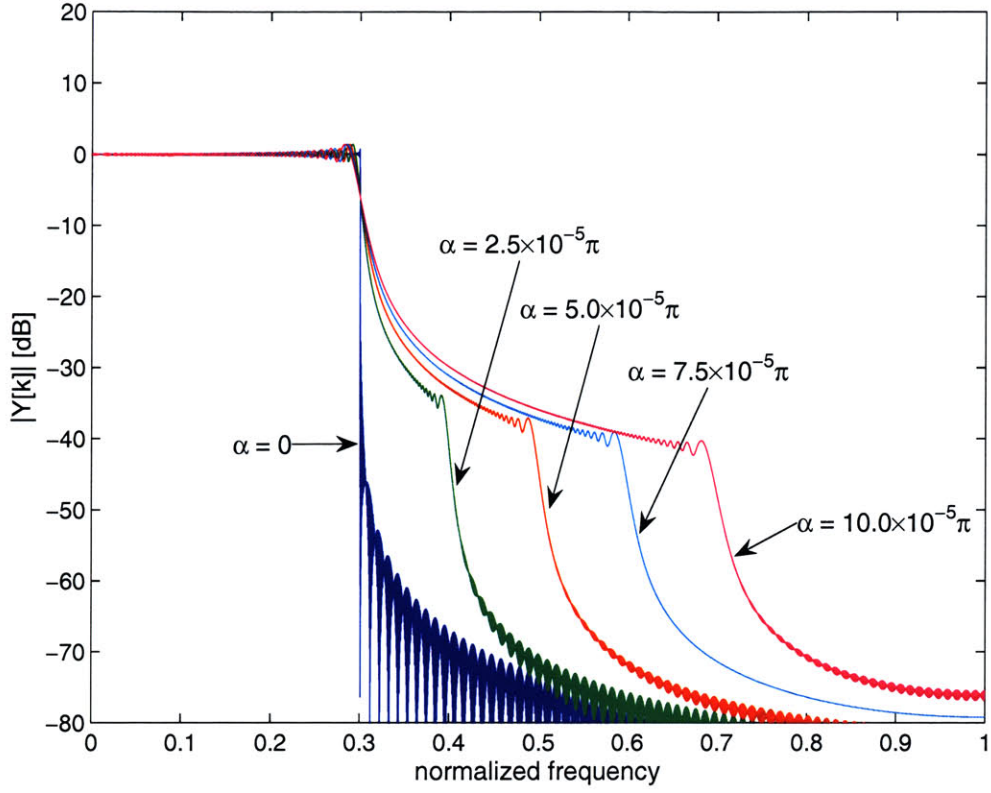
Figure 3-6: Magnitude of the output DFT $Y[k]$ in decibels (dB) for discrete-time time-varying lowpass filters with linearly increasing cut-off frequencies.

filters.

We use T to denote the period of the cut-off frequency $w(t)$. For every value of ω, $H_2(t,\omega)$ is also periodic in t with period T. As a consequence, (2.17) applies, with the Fourier series coefficients $H_k(\omega)$ partially given by

$$H_k(\omega) = \begin{cases} \delta[k], & |\omega| < w_{min}, \\ 0, & |\omega| > w_{max}, \end{cases} \tag{3.33}$$

where we have used Property 1 of Section 3.1. It remains to determine $H_k(\omega)$ for $w_{min} < |\omega| < w_{max}$.

For $w_{min} < |\omega| < w_{max}$, $H_2(t,\omega)$ can be decomposed into a sum of periodic square waves. As in Section 3.3.1, we consider the times $t_\ell(\omega)$, $\ell = 1, 2, \ldots, L(\omega)$, at which $w(t) = |\omega|$, but only within a single period $[t_0(\omega), t_0(\omega)+T]$ since $w(t)$ is periodic. Furthermore, $L(\omega)$ must

be even, and $t_0(\omega)$ can be chosen such that $H_2(t_0(\omega), \omega) = 0$ without loss of generality. It follows that $H_2(t, \omega) = 1$ between $t_{2\ell-1}(\omega)$ and $t_{2\ell}(\omega)$ for $\ell = 1, 2, \ldots, L(\omega)/2$, as illustrated in Figure 3-7. Thus, $H_2(t, \omega)$ can be expressed as

$$H_2(t, \omega) = \sum_{\ell=1}^{L(\omega)/2} s\left[t_{2\ell-1}(\omega), t_{2\ell}(\omega)\right], \quad w_{min} < |\omega| < w_{max}, \qquad (3.34)$$

where

$$s\left[t_{2\ell-1}(\omega), t_{2\ell}(\omega)\right] = \begin{cases} 1, & t_{2\ell-1}(\omega) < t < t_{2\ell}(\omega), \\ 0, & t_0(\omega) < t < t_{2\ell-1}(\omega) \text{ and } t_{2\ell}(\omega) < t < t_0(\omega) + T, \end{cases} \qquad (3.35)$$

and $s[t_{2\ell-1}(\omega), t_{2\ell}(\omega)]$ is periodic with period T.
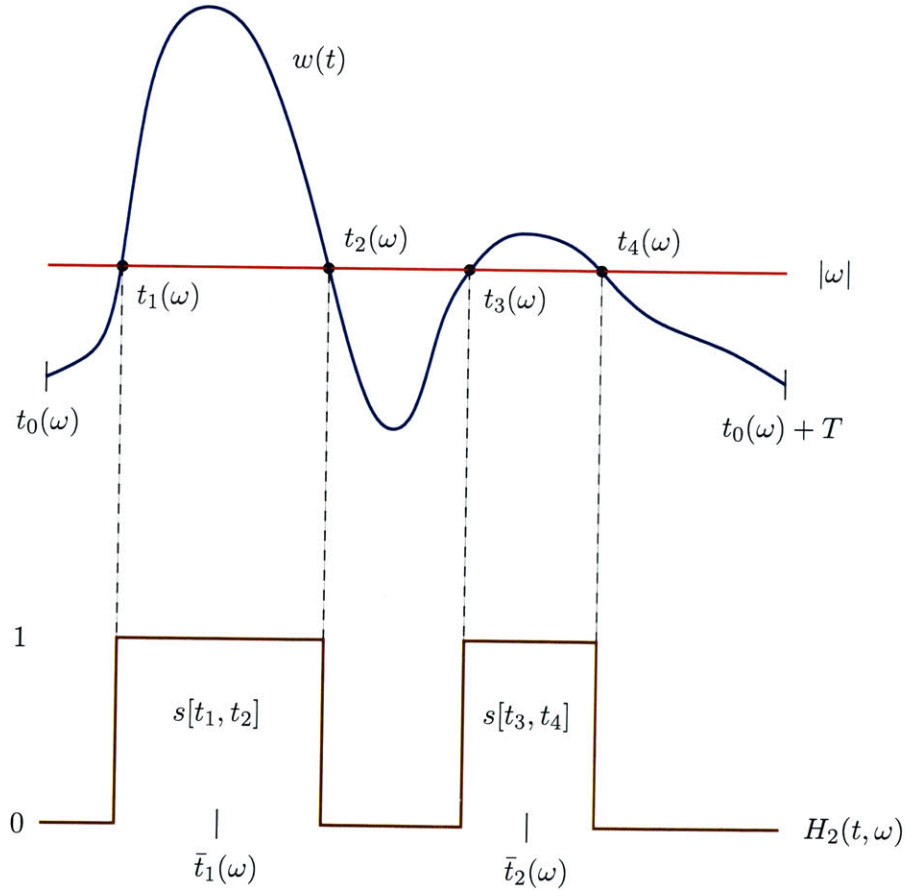
Figure 3-7: Decomposition of $H_2(t, \omega)$ into periodic square waves $s[t_{2\ell-1}(\omega), t_{2\ell}(\omega)]$ for the case of periodic cut-off frequency.

Define

$$\bar{t}_\ell(\omega) = \frac{t_{2\ell-1}(\omega) + t_{2\ell}(\omega)}{2}, \qquad (3.36)$$

$$D_\ell(\omega) = \frac{t_{2\ell}(\omega) - t_{2\ell-1}(\omega)}{T}, \qquad (3.37)$$

to be the point of symmetry and the duty cycle respectively of the square wave $s[t_{2\ell-1}(\omega), t_{2\ell}(\omega)]$ (see Figure 3-7). Then $H_k(\omega)$ can be expressed in terms of $\bar{t}_\ell(\omega)$ and $D_\ell(\omega)$ as

$$H_0(\omega) = \sum_{\ell=1}^{L(\omega)/2} D_\ell(\omega) \equiv D(\omega), \quad w_{min} < |\omega| < w_{max}, \qquad (3.38\text{a})$$

$$H_k(\omega) = \sum_{\ell=1}^{L(\omega)/2} \frac{\sin\left(k\pi D_\ell(\omega)\right)}{k\pi} e^{-jk\omega_0 \bar{t}_\ell(\omega)}, \quad w_{min} < |\omega| < w_{max}, \ k \neq 0, \qquad (3.38\text{b})$$

where $\omega_0 \equiv 2\pi/T$ is the fundamental frequency of $w(t)$ and $D(\omega)$ is the overall duty cycle of $H_2(t, \omega)$. $H_k(\omega)$ decays as $1/|k|$ as expected for the sum of periodic square waves.

Combining (3.33) and (3.38a),

$$H_0(\omega) = \begin{cases} 1, & |\omega| < w_{min}, \\ D(\omega), & w_{min} < |\omega| < w_{max}, \\ 0, & |\omega| > w_{max}. \end{cases} \qquad (3.39)$$

For k not equal to zero, $H_k(\omega) = 0$ for $|\omega| < w_{min}$ and $|\omega| > w_{max}$. As a result, the summation in (2.17) includes only the following ranges of non-zero k:

$$\left\lceil \frac{\omega - w_{max}}{\omega_0} \right\rceil \leq k \leq \left\lfloor \frac{\omega - w_{min}}{\omega_0} \right\rfloor,$$

$$\left\lceil \frac{\omega + w_{min}}{\omega_0} \right\rceil \leq k \leq \left\lfloor \frac{\omega + w_{max}}{\omega_0} \right\rfloor,$$

$$k \neq 0, \qquad (3.40)$$

which we will abbreviate using $\mathcal{A}$. Substituting (3.38b) for $H_k(\omega)$ in (2.17) and incorporating (3.39) and (3.40), we obtain the desired spectral input-output relation:

$$Y(\omega) = H_0(\omega)X(\omega) + \sum_{\mathcal{A}} \left[X(\omega - k\omega_0) \sum_{\ell=1}^{L(\omega - k\omega_0)/2} \frac{\sin\left(k\pi D_\ell(\omega - k\omega_0)\right)}{k\pi} e^{-jk\omega_0 \bar{t}_\ell(\omega - k\omega_0)} \right].$$

(3.41)

As in Section 3.3.1, the component $Y_1(\omega)$ defined by (3.21) is bandlimited to w_{max} by virtue of (3.39). The second term in (3.41),

$$Y_2(\omega) = \sum_{\mathcal{A}} \left[X(\omega - k\omega_0) \sum_{\ell=1}^{L(\omega - k\omega_0)/2} \frac{\sin\left(k\pi D_\ell(\omega - k\omega_0)\right)}{k\pi} e^{-jk\omega_0 \bar{t}_\ell(\omega - k\omega_0)} \right],$$

(3.42)

consists of contributions from shifted copies of $X(\omega)$. As in the aperiodic case, $Y_2(\omega)$ represents the redistribution of the input frequency content in the bands $w_{min} < |\omega| < w_{max}$ over all output frequencies.

We verify that Property 4 of Section 3.1 holds in the case of periodic cut-off frequency. As in Section 3.3.1, we determine an upper bound on the non-bandlimited component $Y_2(\Omega)$ and show that the bound decreases to zero as the cut-off frequency approaches a constant.

From (3.42),

$$|Y_2(\omega)| = \left| \sum_{\mathcal{A}} X(\omega - k\omega_0) \sum_{\ell=1}^{L(\omega - k\omega_0)/2} \frac{\sin\left(k\pi D_\ell(\omega - k\omega_0)\right)}{k\pi} e^{-jk\omega_0 \bar{t}_\ell(\omega - k\omega_0)} \right|,$$

$$\leq \sum_{\mathcal{A}} |X(\omega - k\omega_0)| \left| \sum_{\ell=1}^{L(\omega - k\omega_0)/2} \frac{\sin\left(k\pi D_\ell(\omega - k\omega_0)\right)}{k\pi} e^{-jk\omega_0 \bar{t}_\ell(\omega - k\omega_0)} \right|,$$

$$\leq \sum_{\mathcal{A}} |X(\omega - k\omega_0)| \sum_{\ell=1}^{L(\omega - k\omega_0)/2} \frac{|\sin\left(k\pi D_\ell(\omega - k\omega_0)\right)|}{|k|\pi} \left| e^{-jk\omega_0 \bar{t}_\ell(\omega - k\omega_0)} \right|.$$

Since $|\sin(\cdot)| \leq 1$,

$$|Y_2(\omega)| \leq \sum_{\mathcal{A}} |X(\omega - k\omega_0)| \frac{L(\omega - k\omega_0)}{2\pi|k|},$$

$$|Y_2(\omega)| \leq \frac{L_{max}}{2\pi} \sum_{\mathcal{A}} \frac{|X(\omega - k\omega_0)|}{|k|},$$

(3.43)

where L_{max} now denotes the maximum number of level crossings within a single period. Consequently, as $w(t)$ varies more slowly in time, L_{max} and $|Y_2(\omega)|$ both decrease.

According to (3.40), the maximum number of terms in the summation over $\mathcal{A}$ is

$2 \left\lceil \frac{w_{max} - w_{min}}{\omega_0} \right\rceil$, which is approximately proportional to the range $w_{max} - w_{min}$ of $w(t)$. As $w(t)$ approaches a constant, there will be fewer terms in the summation and the bound on $|Y_2(\omega)|$ will be tighter.

Additionally, we observe from (3.40) that $1/|k| \sim \omega_0/|\omega - w|$, where $|\omega - w|$ represents the distance between the output frequency ω and frequencies within the range of $w(t)$. Therefore, $|Y_2(\omega)|$ decays as ω increases or decreases away from the range of $w(t)$. Furthermore, if $|X(\omega)|$ is small for $w_{min} < |\omega| < w_{max}$, $|Y_2(\omega)|$ is likewise small, and if $X(\omega) = 0$ for $w_{min} < |\omega| < w_{max}$, $Y_2(\omega) = 0$ as in the aperiodic case.

3.3.5 Relationship to the short-time Fourier transform

In this section, we show that the short-time Fourier transform (STFT) of the output of any time-varying lowpass filter (as defined in Section 3.2) is related to the Fourier transform of the output of a certain periodically time-varying lowpass filter. The latter can be analyzed as in Section 3.3.4.

The STFT is one of many time-frequency distributions that characterize the frequency content of a signal as it evolves in time. In the case of a time-varying lowpass filter, the STFT may be useful in estimating the time-varying spectrum of the output. The STFT $\hat{Y}(t, \omega)$ of a signal $y(t)$ can be defined (see [7]) as the windowed Fourier transform of $y(t)$:

$$\hat{Y}(t, \omega) = \int_{t-T/2}^{t+T/2} y(\tau) v(\tau - t) e^{-j\omega\tau} d\tau, \tag{3.44}$$

where the window $v(t)$ is supported only on $[-T/2, T/2]$. Equivalently, in the frequency domain we have

$$\hat{Y}(t, \omega) = \frac{1}{2\pi} \int_{-\infty}^{\infty} Y(\theta) V(\omega - \theta) e^{-j(\omega-\theta)t} d\theta, \tag{3.45}$$

i.e. $\hat{Y}(t, \omega)$ is the convolution of $Y(\omega)$ with the Fourier transform $V(\omega)e^{-j\omega t}$ of the time-shifted window.

From (3.44), we observe that the STFT $\hat{Y}(t, \omega)$, when evaluated at a single instant $t = t_0$, does not depend on values of $y(t)$ outside the interval $I = [t_0 - T/2, t_0 + T/2]$. Therefore, $y(t)$ can be chosen arbitrarily outside of I without affecting the value of $\hat{Y}(t_0, \omega)$. The same observation extends to the frequency domain relation (3.45).

Now consider $y(t)$ to be the output of a time-varying lowpass filter with cut-off frequency

$w(t)$. Since $\hat{Y}(t_0, \omega)$ depends only on $y(t)$ for $t \in I$, and from (3.8) or (3.9), $y(t)$, $t \in I$ depends only on $w(t)$, $t \in I$, we conclude that $\hat{Y}(t_0, \omega)$ is independent of $w(t)$ for $t \notin I$.

The foregoing discussion suggests the following approach: We consider a new cut-off frequency $\tilde{w}(t)$ that is the periodic replication of the segment of $w(t)$ in I. Specifically, we define

$$\widehat{w}(t) = \begin{cases} w(t), & t_0 - \frac{T}{2} \leq t \leq t_0 + \frac{T}{2}, \\ 0, & \text{otherwise}, \end{cases} \tag{3.46}$$

$$\tilde{w}(t) = \sum_{r=-\infty}^{\infty} \widehat{w}(t - rT). \tag{3.47}$$

The Fourier transform $Y(\omega)$ corresponding to $\tilde{w}(t)$ can be determined according to the analysis of Section 3.3.4. The value of $\hat{Y}(t_0, \omega)$ corresponding to the original time-varying lowpass filter with cut-off frequency $w(t)$ is then related to $Y(\omega)$ through (3.45).

Chapter 4

Sampling of Signals With Bandlimited Time-Varying Spectra

In Chapter 3, we adopted a particular definition of a time-varying lowpass filter and showed that the output of such a filter possesses a bandlimited time-varying spectrum. In this chapter, we develop a non-uniform sampling and reconstruction for signals with bandlimited time-varying spectra. Our approach does not achieve perfect reconstruction in general; however, the reconstruction error is shown to decrease with the variation in the cut-off frequency. Furthermore, perfect reconstruction does result for a class of self-similar signals with bandlimited time-varying spectra. We also consider uniform sampling at a rate corresponding to the maximum cut-off frequency and show that exact reconstruction is not possible using the time-varying lowpass filter of Chapter 3.

4.1 Series expansion for signals with bandlimited time-varying spectra

In this section, we review a series expansion for signals $y(t)$ with bandlimited time-varying spectra, as originally derived by Horiuchi in [4]. The expansion forms the basis for the sampling and reconstruction discussed in Section 4.2.

We can equivalently consider $y(t)$ to be the output of a time-varying lowpass filter (as defined in Section 3.2) with input $x(t)$. For every value of t, the time-varying spectrum $\tilde{Y}(t, \omega)$ in (3.11) is zero for $|\omega| > w(t)$, and hence $\tilde{y}(t, \tau)$ in (3.12) is a 1-D function of τ

bandlimited to a maximum frequency of $w(t)$. Using the uniform sampling theorem, $\tilde{y}(t, \tau)$ can be represented as

$$\tilde{y}(t, \tau) = \sum_{k=-\infty}^{\infty} \tilde{y}\left(t, \frac{k\pi}{w(t)}\right) \frac{\sin\left[w(t)(\tau - k\pi/w(t))\right]}{w(t)(\tau - k\pi/w(t))}, \tag{4.1}$$

where the samples $\tilde{y}(t, k\pi/w(t))$ are taken in the τ dimension at the Nyquist rate corresponding to $w(t)$. The samples still vary continuously with t since there is no sampling in the t dimension. Setting $y(t) = \tilde{y}(t, t)$, we obtain the following series expansion:

$$y(t) = \sum_{k=-\infty}^{\infty} \tilde{y}\left(t, \frac{k\pi}{w(t)}\right) \frac{\sin\left[w(t)t - k\pi\right]}{w(t)t - k\pi}. \tag{4.2}$$

Equation (4.1) assumes that the samples of $\tilde{y}(t, \tau)$ corresponding to $k = 0$ occur at $\tau = 0$ for all values of t. More generally, (4.1) still holds if the $k = 0$ samples occur at $\tau = \tau_0(t)$ for some $\tau_0(t)$ that may vary with t. Equation (4.2) then becomes

$$y(t) = \sum_{k=-\infty}^{\infty} \tilde{y}\left(t, \frac{k\pi}{w(t)} + \tau_0(t)\right) \frac{\sin\left[w(t)t - k\pi - w(t)\tau_0(t)\right]}{w(t)t - k\pi - w(t)\tau_0(t)}. \tag{4.3}$$

Equation (4.3) requires that a second function $\tau_0(t)$ be specified in addition to the cut-off frequency $w(t)$. However, we are interested in an expansion that depends on the specific signal only through its samples and through $w(t)$. Thus, we will henceforth take $\tau_0(t) = 0$.

4.2 Non-uniform sampling and consistent reconstruction

In this section, we develop a sampling and reconstruction method based on the expansion in (4.2) for signals with bandlimited time-varying spectra. Our choice of reconstruction permits consistent resampling and can thus be interpreted as a projection. We show that our method does not in general result in perfect reconstruction. Nevertheless, the reconstruction error decreases with the variation in the cut-off frequency, as demonstrated in numerical simulations.

4.2.1 Sampling grid

We assume that the 2-D signal $\tilde{y}(t, \tau)$ is only available along the slice $\tau = t$ where it corresponds to $y(t)$. Consequently, the coefficients $\tilde{y}(t, k\pi/w(t))$ in (4.2) do not correspond

to samples of $y(t)$ except at certain values of t. We seek instead an expansion in which the coefficients $\tilde{y}(t, k\pi/w(t))$ are replaced with samples of $y(t)$, i.e. an expansion of the form

$$\hat{y}(t) = \sum_{k=-\infty}^{\infty} y(t_k) \frac{\sin\left[w(t)t - k\pi\right]}{w(t)t - k\pi}, \tag{4.4}$$

where t_k is the kth sampling instant. In this section, we determine the sampling instants that are naturally suggested by (4.2).

In Figure 4-1, the loci of the sample locations $(t, k\pi/w(t))$ are sketched in the (t, τ) plane. The $k = 0$ locus is the line $\tau = 0$, i.e. the t-axis. The dashed diagonal line represents the slice corresponding to $y(t) = \tilde{y}(t, t)$. Hence, $y(t)$ is equal to $\tilde{y}(t, k\pi/w(t))$ only at the intersections marked by filled circles.
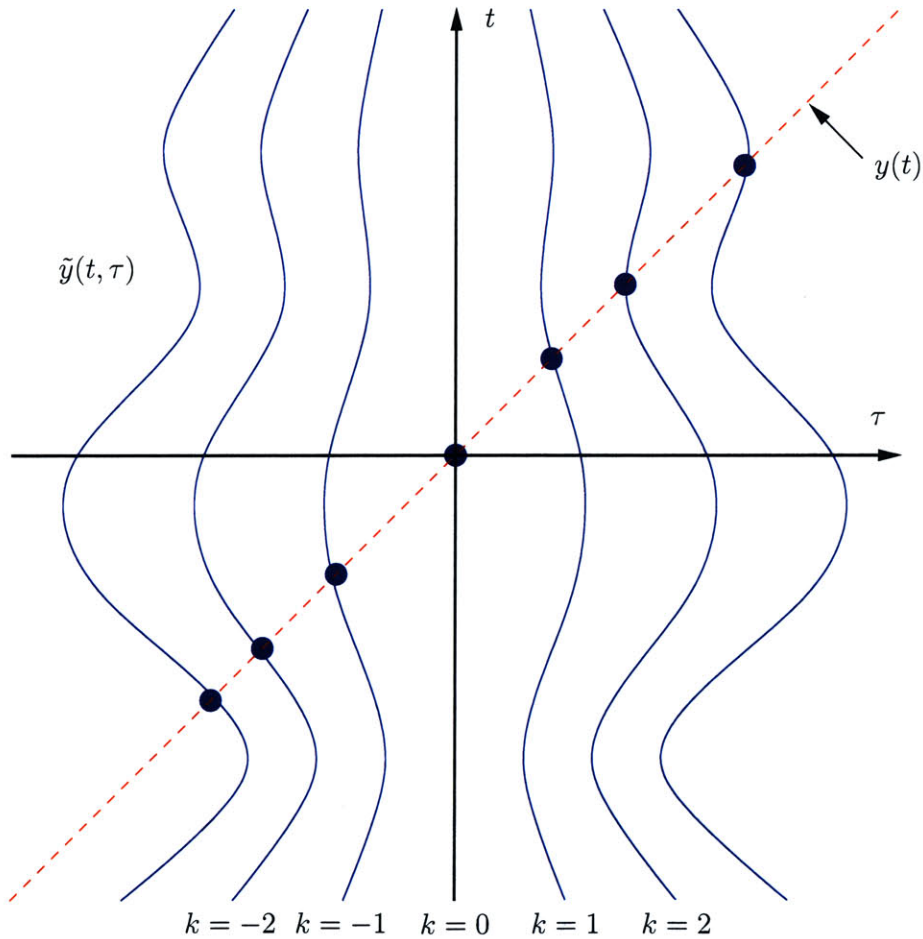
Figure 4-1: Loci of sample locations $(t, k\pi/w(t))$ and slice corresponding to $y(t) = \tilde{y}(t, t)$ in the (t, τ) plane.

Based on Figure 4-1, we consider sampling $y(t)$ at the intersections, i.e. the values of

t at which $y(t) = \tilde{y}(t, k\pi/w(t))$. Then the sampling instants t_k are the solutions to the following equation:

$$w(t_k)t_k - k\pi = 0, \quad k \in \mathbf{Z}. \tag{4.5}$$

We show that (4.5) has at least one solution for every k, i.e. that each t_k exists. We assume that $w(t)$ is continuous as well as being positive and bounded. Then the function $w(t)t$ is surjective onto the real line, i.e. it must take on all real values as t ranges from $-\infty$ to $+\infty$. Consequently, for all k, there is at least one value of t_k that satisfies (4.5). In addition, we have that

$$w(t)t \mid_{t=0} = 0,$$

which implies that (4.5) always has the solution $t_0 = 0$.

In order for (4.5) to have only one solution for every k, i.e. for t_k to be unique, $w(t)t$ must not equal $k\pi$ for more than one value of t. To ensure this, we can impose the additional constraint that $w(t)t$ increases monotonically, so that no two values of t yield the same value of $w(t)t$. As a result, $w(t)t$ is also injective and hence invertible. The derivative of $w(t)t$ must then be positive, leading to the following constraint:

$$\frac{d}{dt}[w(t)t] = w(t) + t\dot{w}(t) \geq 0,$$

$$\frac{\dot{w}(t)}{w(t)} \begin{cases} \leq -\dfrac{1}{t}, & t < 0, \\[2mm] \geq -\dfrac{1}{t}, & t > 0, \end{cases} \tag{4.6}$$

where $w(t) > 0$ and $\dot{w}(t) = \frac{dw(t)}{dt}$. The constraint in (4.6) becomes more restrictive for larger $|t|$.

If, for certain values of k, there exist multiple solutions $t_{k1}, t_{k2}, \ldots$ to (4.5), the kth coefficient in (4.4) is not determined uniquely. For example, the kth coefficient may be chosen as an arbitrary linear combination of all samples $y(t_{ki})$ such that t_{ki} satisfies (4.5). However, for simplicity of analysis, we will assume henceforth that a single sample $y(t_k)$ is chosen to be the kth coefficient, even when multiple solutions exist.

The solutions to (4.5) generally form a non-uniform sampling grid. As Figure 4-2 suggests, the sampling rate should increase with the cut-off frequency $w(t)$ as we would intuitively expect. The function $w(t)t$ is sketched with a solid curve and the levels $k\pi$ are

indicated by horizontal dashed lines. At the intersection between $w(t)t$ and $k\pi$, the sampling instant t_k is marked on the t axis. In regions where $w(t)$ is low, $w(t)t$ rises slowly, and the sampling instants are spaced farther apart. When $w(t)$ is high, $w(t)t$ increases quickly, and the sampling instants are more closely spaced.
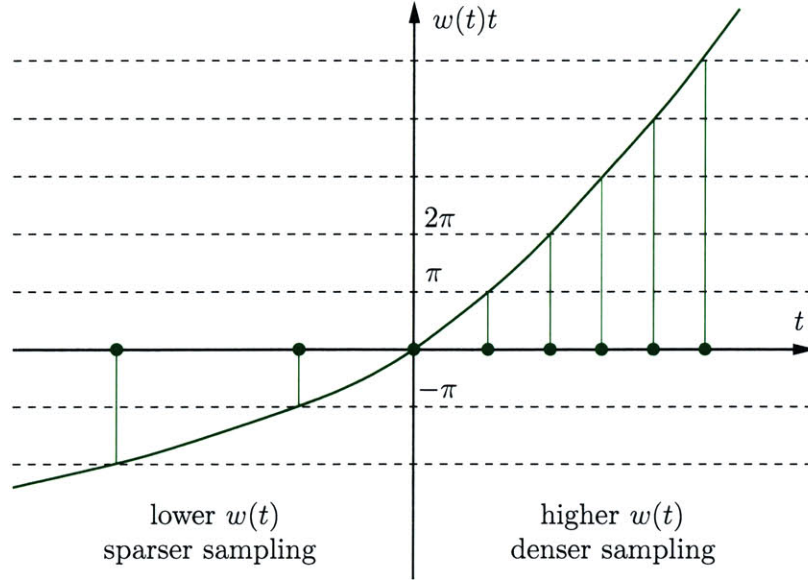
Figure 4-2: Sketch of $w(t)t$ showing the dependence of the sampling rate on $w(t)$.

4.2.2 Synthesis functions

Equation (4.4) can be interpreted as a sampling and reconstruction of $y(t)$. Specifically, the sampling of $y(t)$ can be represented as the product of $y(t)$ with a train of impulses:

$$s(t) = \sum_{k=-\infty}^{\infty} y(t_k)\delta(t - t_k), \tag{4.7}$$

where the sampling instants t_k are given by (4.5). We wish to express the reconstruction in (4.4) as the output of an LTV reconstruction filter with input $s(t)$. The impulse response $\bar{h}_1(t, \tau)$ of the required filter is given by

$$\bar{h}_1(t, \tau) = \frac{\sin\left[w(t)t - w(\tau)\tau\right]}{w(t)t - w(\tau)\tau}. \tag{4.8}$$

Using (2.1), we verify our choice of $\bar{h}_1(t, \tau)$ by determining the corresponding output:

$$
\begin{aligned}
\int_{-\infty}^{\infty} s(\tau)\bar{h}_1(t, \tau)d\tau &= \sum_{k=-\infty}^{\infty} y(t_k) \int_{-\infty}^{\infty} \delta(\tau - t_k) \frac{\sin[w(t)t - w(\tau)\tau]}{w(t)t - w(\tau)\tau}, \\
&= \sum_{k=-\infty}^{\infty} y(t_k) \frac{\sin[w(t)t - w(t_k)t_k]}{w(t)t - w(t_k)t_k}, \\
&= \sum_{k=-\infty}^{\infty} y(t_k) \frac{\sin[w(t)t - k\pi]}{w(t)t - k\pi}, \\
&= \hat{y}(t),
\end{aligned}
$$

where we have used (4.5).

The reconstruction filter with impulse response $\bar{h}_1(t, \tau)$ is not a time-varying lowpass filter in the sense of Section 3.2. For comparison, the impulse response $h_1(t, \tau)$ of a (scaled) time-varying lowpass filter with the same cut-off frequency $w(t)$ is

$$
h_1(t, \tau) = \frac{\sin[w(t)(t - \tau)]}{w(t)(t - \tau)} \neq \bar{h}_1(t, \tau). \tag{4.9}
$$

For convenience, we rewrite (4.4) as

$$
\hat{y}(t) = \sum_{k=-\infty}^{\infty} y(t_k)\varphi_k(t), \tag{4.10}
$$

where $\varphi_k(t)$ denotes the kth synthesis function:

$$
\varphi_k(t) = \frac{\sin[w(t)t - k\pi]}{w(t)t - k\pi}. \tag{4.11}
$$

It follows from (4.5) that the functions $\varphi_k(t)$ possess an interpolating property with respect to the sampling times t_k:

$$
\varphi_k(t_m) = \delta[k - m]. \tag{4.12}
$$

As will be shown in the next section, the interpolating property allows for consistent resampling of $\hat{y}(t)$.

From the interpolating property, we prove that the functions $\varphi_k(t)$ are linearly independent, i.e. if

$$
\sum_{k=-\infty}^{\infty} a_k\varphi_k(t) = 0 \quad \forall \, t, \tag{4.13}
$$

54

then $a_k = 0$ for all k. Evaluating the left-hand side of (4.13) at an arbitrary sampling instant t_m and using (4.12),

$$\sum_{k=-\infty}^{\infty} a_k \varphi_k(t_m) = \sum_{k=-\infty}^{\infty} a_k \delta[k-m],$$

$$= a_m = 0$$

for all m as desired.

4.2.3 Consistent resampling and projection

It is shown that the reconstruction $\hat{y}(t)$ in (4.4) can be consistently resampled on the grid $\{t_k, k \in \mathbf{Z}\}$ defined by (4.5), i.e. $\hat{y}(t_k) = y(t_k)$ for all k. Thus, our reconstruction fulfills one of the desired properties summarized in Section 1.2. We then show that $\hat{y}(t)$ is a projection of $y(t)$ onto the reconstruction space spanned by the functions $\{\varphi_k(t), k \in \mathbf{Z}\}$.

Using (4.4), the samples $\hat{y}(t_m)$, $m \in \mathbf{Z}$, at the times t_m satisfying (4.5) are expressed as

$$\hat{y}(t_m) = \sum_{k=-\infty}^{\infty} y(t_k)\varphi_k(t_m),$$

$$= \sum_{k=-\infty}^{\infty} y(t_k)\delta[k-m],$$

$$= y(t_m), \tag{4.14}$$

where we have used the interpolating property in (4.12). Therefore, the samples $\hat{y}(t_m)$ are consistent with the original samples $y(t_m)$.

We define P to be an operator that consists of sampling on the grid $\{t_k, k \in \mathbf{Z}\}$ followed by reconstruction using the synthesis functions $\{\varphi_k(t), k \in \mathbf{Z}\}$, i.e.

$$P(y(t)) = \sum_{k=-\infty}^{\infty} y(t_k)\varphi_k(t) = \hat{y}(t). \tag{4.15}$$

The operator P is depicted in Figure 4-3, where $\bar{h}_1(t, \tau)$ as defined in (4.8) is the impulse response of the reconstruction filter.

By definition, in order for P to be a projection operator, P must be idempotent. Con-
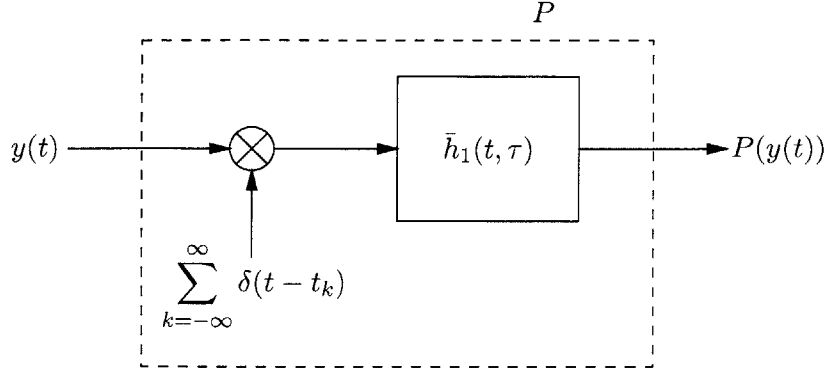
Figure 4-3: The operator P.

sequently, $P(\hat{y}(t)) = \hat{y}(t)$ must hold, which is verified below:

$$P(\hat{y}(t)) = \sum_{k=-\infty}^{\infty} \hat{y}(t_k)\varphi_k(t).$$

Using the consistent resampling property in (4.14),

$$P(\hat{y}(t)) = \sum_{k=-\infty}^{\infty} y(t_k)\varphi_k(t),$$

which is equal to $\hat{y}(t)$ from (4.10). Thus, P may be interpreted as a projection onto the reconstruction space spanned by $\{\varphi_k(t), k \in \mathbf{Z}\}$. Since the signal $y(t)$ may not lie in the reconstruction space, the first projection $\hat{y}(t) = P(y(t))$ generally incurs some error, which we will examine in Sections 4.2.5 and 4.2.6.

4.2.4 Conditions for perfect reconstruction

In this section, we derive necessary conditions for perfect reconstruction, i.e. conditions under which $\hat{y}(t) = y(t)$ for all t. A class of signals satisfying a sufficient condition for perfect reconstruction is discussed in Section 4.5.

We first express the reconstruction in the form $\hat{y}(t) = r(w(t)t)$ for a signal $r(t)$,

$$r(t) = \sum_{k=-\infty}^{\infty} y(t_k)\frac{\sin(t - k\pi)}{t - k\pi}, \tag{4.16}$$

that is bandlimited to a maximum frequency of 1. The signal $r(t)$ is the bandlimited interpolation obtained by assuming that the samples $y(t_k)$ were taken uniformly. To attain

56

perfect reconstruction, i.e. $y(t) = r(w(t)t)$, $y(t)$ must be a time-warped bandlimited signal in the sense to be discussed in Chapter 5, with $r(t)$ as the corresponding bandlimited signal.

A more explicit form for the condition for perfect reconstruction can be obtained by first replacing ω with $w(t)\omega$ as the variable of integration in (3.8):

$$y(t) = w(t) \int_{-1}^{1} X(w(t)\omega)e^{j\omega(w(t)t)}d\omega.$$

Expressing $\hat{y}(t)$ as

$$\hat{y}(t) = \int_{-1}^{1} R(\omega)e^{j\omega(w(t)t)}d\omega,$$

the condition for perfect reconstruction is equivalent to

$$\int_{-1}^{1} \left[w(t)X(w(t)\omega) - R(\omega)\right] e^{j\omega(w(t)t)}d\omega = 0 \quad \forall\, t \in \mathbf{R}, \tag{4.17}$$

in which the Fourier transform $R(\omega)$ also depends on $X(\omega)$ through the sample values $y(t_k)$. Equation (4.17) imposes a restriction on the signals $x(t)$, i.e. the inputs to the time-varying lowpass filter, that result in signals $y(t)$ that can be perfectly reconstructed.

We conclude that not all signals with bandlimited time-varying spectra can be sampled and perfectly reconstructed using the method we have developed. Given our method, it is unsatisfying to interpret signals with bandlimited time-varying spectra as being locally bandlimited since the perfect reconstruction property of Section 1.2 does not hold in general. Our method does however satisfy the property that the reconstruction error $e(t) \equiv \hat{y}(t) - y(t)$ decreases to zero as the cut-off frequency $w(t)$ approaches a constant, as is shown in the next section.

4.2.5 Bound on reconstruction error

We first derive a bound on the reconstruction error and show that the bound decreases to zero as $w(t)$ becomes constant. First, using (3.8) and (3.12), we express both sets of coefficients in terms of $X(\omega)$:

$$y(t_k) = \frac{1}{2\pi} \int_{-w(t_k)}^{w(t_k)} X(\omega)e^{j\omega t_k}d\omega,$$

$$\tilde{y}\left(t, \frac{k\pi}{w(t)}\right) = \frac{1}{2\pi} \int_{-w(t)}^{w(t)} X(\omega)e^{j\omega k\pi/w(t)}d\omega.$$

Let $e_k(t)$ be the error in the kth coefficient, i.e.

$$e_k(t) \equiv y(t_k) - \tilde{y}\left(t, \frac{k\pi}{w(t)}\right)$$

$$= \frac{1}{2\pi} \int_{-w(t)}^{w(t)} X(\omega)\left(e^{j\omega t_k} - e^{j\omega k\pi/w(t)}\right) d\omega + \frac{1}{2\pi} \int_{|\omega|=w(t)}^{|\omega|=w(t_k)} X(\omega)e^{j\omega t_k} d\omega. \quad (4.18)$$

The magnitude of $e_k(t)$ can be bounded using the triangle inequality:

$$|e_k(t)| \leq \frac{1}{2\pi} \left| \int_{-w(t)}^{w(t)} X(\omega)\left(e^{j\omega t_k} - e^{j\omega k\pi/w(t)}\right) d\omega \right| + \frac{1}{2\pi} \left| \int_{|\omega|=w(t)}^{|\omega|=w(t_k)} X(\omega)e^{j\omega t_k} d\omega \right|. \quad (4.19)$$

The first term on the right-hand side of (4.19) can be bounded using the Cauchy-Schwarz inequality:

$$\frac{1}{2\pi} \left| \int_{-w(t)}^{w(t)} X(\omega)\left(e^{j\omega t_k} - e^{j\omega k\pi/w(t)}\right) d\omega \right|$$

$$\leq \frac{1}{2\pi} \left(\int_{-w(t)}^{w(t)} |X(\omega)|^2 d\omega\right)^{1/2} \left(\int_{-w(t)}^{w(t)} |e^{j\omega t_k} - e^{j\omega k\pi/w(t)}|^2 d\omega\right)^{1/2},$$

$$= \frac{1}{2\pi} \left(2\int_0^{w(t)} |X(\omega)|^2 d\omega\right)^{1/2} \left[4w(t)\left(1 - \frac{\sin[w(t)t_k - k\pi]}{w(t)t_k - k\pi}\right)\right]^{1/2},$$

$$= \frac{1}{\pi}\sqrt{2w(t)} \left(\int_0^{w(t)} |X(\omega)|^2 d\omega\right)^{1/2} \left(1 - \frac{\sin[w(t)t_k - k\pi]}{w(t)t_k - k\pi}\right)^{1/2}, \quad (4.20)$$

where $|X(\omega)|$ is an even function of ω because $x(t)$ is real. The second term on the right-hand side of (4.19) can be bounded as follows:

$$\frac{1}{2\pi} \left| \int_{|\omega|=w(t)}^{|\omega|=w(t_k)} X(\omega)e^{j\omega t_k} d\omega \right| \leq \frac{1}{2\pi} \int_{|\omega|=w(t)}^{|\omega|=w(t_k)} |X(\omega)| d\omega,$$

$$= \frac{1}{\pi} \int_{\omega=w(t)}^{\omega=w(t_k)} |X(\omega)| d\omega. \quad (4.21)$$

Combining (4.19), (4.20), and (4.21),

$$|e_k(t)| \leq \frac{1}{\pi} \left\{ \sqrt{2w(t)} \left(1 - \frac{\sin[w(t)t_k - k\pi]}{w(t)t_k - k\pi}\right)^{1/2} \left(\int_0^{w(t)} |X(\omega)|^2 d\omega\right)^{1/2} + \int_{w(t)}^{w(t_k)} |X(\omega)| d\omega \right\}.$$

$$(4.22)$$

Expressing $w(t)$ as $w(t) = w + \Delta w(t)$, we wish to show that the bound on $|e_k(t)|$ in (4.22) goes to zero as $\Delta w(t)$ goes to zero, i.e. as $w(t)$ approaches a constant. Considering first the second term on the right-hand side of (4.22), the limits of integration converge as $\Delta w(t) \to 0$, and hence the integral tends to zero.

We show that the first term on the right-hand side of (4.22) also decreases to zero as $\Delta w(t) \to 0$. The first term is proportional to the quantity λ, defined as

$$\lambda \equiv \left(1 - \frac{\sin[w(t)t_k - k\pi]}{w(t)t_k - k\pi} \right)^{1/2}. \tag{4.23}$$

Rewriting the quantity $w(t)t_k - k\pi$ that appears in (4.23),

$$
\begin{aligned}
w(t)t_k - k\pi &= t_k[w(t) - w(t_k)], \\
&= t_k[\Delta w(t) - \Delta w(t_k)], \tag{4.24}
\end{aligned}
$$

where we have used (4.5) to substitute for $k\pi$ in the first line. Thus, as $\Delta w(t)$ approaches zero, $w(t)t_k - k\pi$ and λ also approach zero. However, if $|t_k|$ is large, $|\Delta w(t) - \Delta w(t_k)|$ must be very small in order for their product to be small. Thus, for large $|t_k|$, i.e. for samples distant from the origin, λ is more sensitive to deviations from a constant cut-off frequency.

We remark that it seems unnatural for $|e_k(t)|$ to become more sensitive to the variation of $w(t)$ as $|k|$ increases. The fact that $|e_k(t)|$ is better controlled for sampling times close to the origin may be a consequence of setting $\tau_0(t) = 0$ in Section 4.1. We recall that $t_0 = 0$ is always a solution to (4.5), and hence is always included in the sampling grid. It may be possible to address the bias toward the origin by introducing a non-zero $\tau_0(t)$.

The total reconstruction error $e(t)$ may be bounded in terms of $e_k(t)$:

$$
\begin{aligned}
|e(t)| &= \left| \sum_{k=-\infty}^{\infty} e_k(t) \frac{\sin[w(t)t - k\pi]}{w(t)t - k\pi} \right|, \\
&\leq \sum_{k=-\infty}^{\infty} |e_k(t)| \frac{|\sin[w(t)t - k\pi]|}{|w(t)t - k\pi|}, \\
&\leq \sum_{k=-\infty}^{\infty} \frac{|e_k(t)|}{|w(t)t - k\pi|}, \tag{4.25}
\end{aligned}
$$

where we have used the triangle inequality and the fact that $|\sin(\cdot)| \leq 1$. Each coefficient error $e_k(t)$ is weighted by $1/|w(t)t - k\pi|$. If $w(t)$ is approximately constant, $w(t)t - k\pi \approx$

$w(t)(t - t_k)$, which corresponds to a $1/|t - t_k|$ decay. Assuming that $|e_k(t)|$ itself does not increase faster than $O(|t - t_k|)$, the error due to the kth sample decays as $|t - t_k|$ increases.

4.2.6 Discrete-time simulation

In this section, we present MATLAB simulations of the sampling and reconstruction of signals with bandlimited time-varying spectra, in which the sampling is based on (4.5) and the reconstruction on (4.4). We verify that the reconstruction error increases as the variation in $w(t)$ increases.

The cut-off frequency $w(t)$ is chosen to be a linear function parameterized by an intercept $w_0 = 0.1\pi$ and a slope α ranging from 0 to $5 \times 10^{-5}\pi$. For the purposes of simulation, $w(t)$ is sampled at $t = n$, $n \in \mathbf{Z}$, yielding the sequence

$$w[n] = w_0 + \alpha n, \quad -L \leq n \leq L. \tag{4.26}$$

The time index n is restricted to the range $-L \leq n \leq L$ with $L = 1000$, so that all signals in the simulation are of length $2L + 1$. Consequently, when $\alpha = 5 \times 10^{-5}\pi$, $w[n]$ ranges from 0.05π at $n = -L$ to 0.15π at $n = L$.

For each choice of $w[n]$ corresponding to a different choice of α, 1000 test sequences, denoted by $y[n]$, were generated according to the following equation:

$$y[n] = \sum_{m=-L}^{L} h[n, m]x[m], \quad -L \leq n \leq L, \tag{4.27}$$

where $x[n]$ is a realization of a white noise sequence consisting of samples uniformly distributed on $[-1, 1]$, and $h[n, m]$ is a matrix implementing a time-varying lowpass filter with cut-off frequency $w[n]$. We consider $y[n]$ to be a sequence of samples from a signal $y(t)$ with a bandlimited time-varying spectrum.

The matrix $h[n, m]$ is formed according to the following procedure: For each value of n, $-L \leq n \leq L$, a $2L + 1$-point lowpass filter with cut-off frequency $w[n]$ is designed using the Parks-McClellan algorithm. Let $b[m; w[n]]$, $0 \leq m \leq 2L$ denote the impulse response of this lowpass filter, indexed so that it is symmetric about $m = L$. Then, for each value of n,

the vector $h[n,m]$ is obtained by circularly shifting $b[m; w[n]]$ by $n - L$:

$$h[n,m] = b\left[(m - n + L) \bmod (2L + 1); w[n]\right], \quad -L \leq n, m \leq L. \tag{4.28}$$

In terms of the output $y[n]$, the circular shift in (4.28) is equivalent to linearly shifting $b[m; w[n]]$ and periodically replicating $x[n]$ outside of $-L \leq n \leq L$ with period $2L + 1$.

For each test sequence $y[n]$, the sampling and reconstruction of the underlying signal $y(t)$ were simulated. Substituting $w(t) = w_0 + \alpha t$ into (4.5) yields a quadratic equation specifying the sampling instants t_k for $y(t)$. The restriction $-L \leq t_k \leq L$ limits the sample numbers to the range $k_{min} \leq k \leq k_{max}$, where

$$
\begin{aligned}
k_{min} &= \left\lceil \frac{w(-L)(-L)}{\pi} \right\rceil, \\
k_{max} &= \left\lfloor \frac{w(L)L}{\pi} \right\rfloor.
\end{aligned} \tag{4.29}
$$

The restriction $-L \leq t_k \leq L$ and the particular values chosen for w_0 and α allow one of the roots of (4.5) to be eliminated, leaving

$$
t_k = \begin{cases} \dfrac{\sqrt{w_0^2 + 4\pi\alpha k} - w_0}{2\alpha}, & \alpha \neq 0, \\[3mm] \dfrac{k\pi}{w_0}, & \alpha = 0, \end{cases} \tag{4.30}
$$

as the single sampling instant for each value of k. When t_k is not an integer, the sample $y(t_k)$ is computed by interpolating between the uniform samples $y[n]$ using cubic spline functions. The parameter $w_0 = 0.1\pi$ was chosen in part so that $y(t)$ varies slowly compared to the unit sample spacing for $y[n]$.

The discrete-time reconstruction $\hat{y}[n]$ of $y[n]$ is obtained by setting $t = n$ in (4.4) and restricting k to $k_{min} \leq k \leq k_{max}$:

$$\hat{y}[n] = \sum_{k=k_{min}}^{k_{max}} y(t_k) \frac{\sin\left[w[n]n - k\pi\right]}{w[n]n - k\pi}, \quad -L \leq n \leq L. \tag{4.31}$$

For each test sequence, we evaluate the energy in the error sequence $e[n] \equiv \hat{y}[n] - y[n]$

normalized by the energy in $y[n]$, i.e.

$$\varepsilon = \frac{\displaystyle\sum_{n=-L/2}^{L/2} e^2[n]}{\displaystyle\sum_{n=-L/2}^{L/2} y^2[n]}. \tag{4.32}$$

The computation in (4.32) is performed only over the range $-L/2 \leq n \leq L/2$ in order to mitigate end effects caused by the finite number of terms in (4.31).

For each value of α, the normalized error energy ε is averaged over all the corresponding test sequences. In Figure 4-4, the average normalized error energy is plotted as a function of α. As suggested by the analysis in Section 4.2.5, the error increases with α, which corresponds to the rate of variation of $w(t)$. In fact, the dependence appears to be nearly linear.
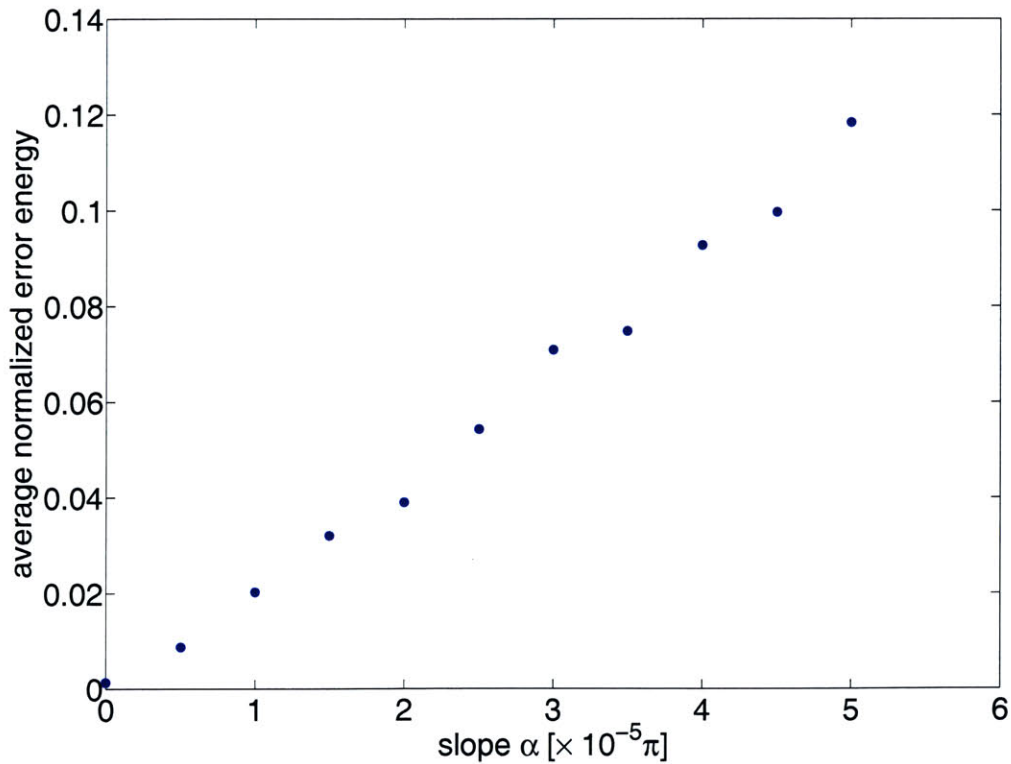
Figure 4-4: Average normalized error energy as a function of slope α for the case of linearly increasing cut-off frequency.

4.3 Non-uniform sampling and reconstruction using a time-varying lowpass filter

In this section, we consider a different method of reconstructing from the non-uniform samples $y(t_k)$ of $y(t)$. Specifically, the sampling instants t_k are still given by (4.5), but the reconstruction filter is a second time-varying lowpass filter having the same cut-off frequency $w(t)$ as the time-varying lowpass filter that generated $y(t)$. This choice of reconstruction filter is analogous to the reconstruction of globally bandlimited signals. A signal globally bandlimited to w may be viewed as the output of a time-invariant lowpass filter with cut-off frequency w. The signal may be reconstructed from uniform, Nyquist rate samples using a second time-invariant lowpass filter with the same cut-off frequency w.

For convenience, we apply a normalizing weighting to the impulse train $s(t)$ specified in (4.7):

$$s(t) = \sum_{k=-\infty}^{\infty} \frac{\pi}{w(t_k)} y(t_k) \delta(t - t_k). \tag{4.33}$$

The Fourier transform $S(\omega)$ of $s(t)$ is given by

$$S(\omega) = \sum_{k=-\infty}^{\infty} \frac{\pi}{w(t_k)} y(t_k) e^{-j\omega t_k}, \tag{4.34}$$

which can be related to $X(\omega)$ by using (3.8) to substitute for $y(t_k)$:

$$S(\omega) = \sum_{k=-\infty}^{\infty} \frac{1}{2w(t_k)} \int_{-w(t_k)}^{w(t_k)} X(\theta) e^{j(\theta-\omega)t_k} d\theta. \tag{4.35}$$

The reconstruction $\hat{y}(t)$ is obtained by processing $s(t)$ with a time-varying lowpass filter having cut-off frequency $w(t)$. Replacing $X(\omega)$ with $S(\omega)$ in (3.8), we have

$$\hat{y}(t) = \frac{1}{2\pi} \int_{-w(t)}^{w(t)} S(\omega) e^{j\omega t} d\omega. \tag{4.36}$$

The error $e(t) \equiv \hat{y}(t) - y(t)$ is found by subtracting (3.8) from (4.36). It can be bounded by the integral of the absolute difference $|S(\omega) - X(\omega)|$ over the frequency band $|\omega| < w(t)$,

i.e.

$$|e(t)| = \frac{1}{2\pi} \left| \int_{-w(t)}^{w(t)} (S(\omega) - X(\omega)) e^{j\omega t} d\omega \right|,$$

$$\leq \frac{1}{2\pi} \int_{-w(t)}^{w(t)} |S(\omega) - X(\omega)| d\omega. \tag{4.37}$$

We show that $S(\omega) = X(\omega)$ for $|\omega| < w(t)$ when $w(t)$ is constant, i.e. $w(t) = w_0$, and hence that $e(t) = 0$. With this assumption, $w(t_k) = w_0$ in (4.35), allowing the summation over k to be exchanged with the integral, and $t_k = k\pi/w_0$. Therefore,

$$S(\omega) = \int_{-w_0}^{w_0} X(\theta) \left\{ \frac{1}{2w_0} \sum_{k=-\infty}^{\infty} e^{j(\theta-\omega)k\pi/w_0} \right\} d\theta.$$

Recognizing the quantity in braces as the Fourier series expansion of a periodic impulse train in frequency with period $2w_0$,

$$S(\omega) = \int_{-w_0}^{w_0} X(\theta) \left\{ \sum_{k=-\infty}^{\infty} \delta(\theta - \omega - 2kw_0) \right\} d\theta.$$

For $|\theta| < w_0$ and $|\omega| < w_0$, the integral is non-zero only for $k = 0$. Hence $S(\omega) = X(\omega)$ for $|\omega| < w_0$ and $e(t) = 0$ as desired.

4.4 Uniform sampling and reconstruction using a time-varying lowpass filter

In Section 4.2, we showed that a signal $y(t)$ with a bandlimited time-varying spectrum cannot in general be exactly reconstructed using (4.4) from its non-uniform samples taken according to (4.5). In this section, we consider sampling $y(t)$ uniformly at a rate corresponding to the maximum cut-off frequency w_{max}. Even in this case, $y(t)$ cannot be perfectly reconstructed from its samples using the time-varying lowpass filter defined in Section 3.2. A bound on the reconstruction error is derived.

The sampling instants t_k that we now consider are given by

$$t_k = \frac{k\pi}{w_{max}}, \tag{4.38}$$

corresponding to the Nyquist rate associated with w_{max}. The sampling of $y(t)$ on the grid $\{t_k, k \in \mathbf{Z}\}$ is represented as a product with an impulse train scaled by π/w_{max}, i.e.

$$s(t) = \frac{\pi}{w_{max}} \sum_{k=-\infty}^{\infty} y\left(\frac{k\pi}{w_{max}}\right) \delta\left(t - \frac{k\pi}{w_{max}}\right). \tag{4.39}$$

Since the samples of $y(t)$ are taken uniformly, the Fourier transform $S(\omega)$ consists of copies of $Y(\omega)$ replicated at intervals of $2w_{max}$:

$$S(\omega) = \sum_{k=-\infty}^{\infty} Y(\omega - 2kw_{max}). \tag{4.40}$$

To obtain a reconstruction $\hat{y}(t)$, we consider processing $s(t)$ with a time-varying lowpass filter having cut-off frequency $w(t)$. Using (3.8) and (4.40), $\hat{y}(t)$ can be expressed as

$$\begin{aligned} \hat{y}(t) &= \frac{1}{2\pi} \int_{-w(t)}^{w(t)} S(\omega)e^{j\omega t}d\omega, \\ &= \frac{1}{2\pi} \sum_{k=-\infty}^{\infty} \int_{2kw_{max}-w(t)}^{2kw_{max}+w(t)} Y(\omega)e^{j(\omega-2kw_{max})t}d\omega. \end{aligned} \tag{4.41}$$

Alternatively, using (3.9) and (4.39),

$$\begin{aligned} \hat{y}(t) &= \int_{-\infty}^{\infty} s(u)\frac{\sin[w(t)(t-u)]}{\pi(t-u)}du, \\ &= \sum_{k=-\infty}^{\infty} y\left(\frac{k\pi}{w_{max}}\right)\frac{\sin[w(t)(t-k\pi/w_{max})]}{w_{max}(t-k\pi/w_{max})}. \end{aligned} \tag{4.42}$$

Based on (4.41), we derive a bound on the reconstruction error $e(t) \equiv \hat{y}(t) - y(t)$. From Section 3.3.1, $Y(\omega)$ can be written as

$$Y(\omega) = H_0(\omega)X(\omega) + Y_2(\omega), \tag{4.43}$$

where $H_0(\omega)$ is given by (3.17) and (3.18) and $Y_2(\omega)$ by (3.22). Substituting (4.43) in (4.41),

$$\hat{y}(t) = \frac{1}{2\pi}\left\{\int_{-w(t)}^{w(t)} H_0(\omega)X(\omega)e^{j\omega t}d\omega + \sum_{k=-\infty}^{\infty}\int_{2kw_{max}-w(t)}^{2kw_{max}+w(t)} Y_2(\omega)e^{j(\omega-2kw_{max})t}d\omega\right\}, \tag{4.44}$$

using the fact that $H_0(\omega) = 0$ for $|\omega| > w_{max}$ according to (3.18).

Subtracting (3.8) from (4.44),

$$e(t) = \frac{1}{2\pi} \left\{ \int_{|\omega|=w_{min}}^{|\omega|=w(t)} [H_0(\omega)-1]X(\omega)e^{j\omega t}d\omega + \sum_{k=-\infty}^{\infty} \int_{2kw_{max}-w(t)}^{2kw_{max}+w(t)} Y_2(\omega)e^{j(\omega-2kw_{max})t}d\omega \right\},$$

$$(4.45)$$

where the range of integration in the first integral is now $w_{min} < |\omega| < w(t)$ since $H_0(\omega) = 1$ for $|\omega| < w_{min}$. For arbitrary choices of $X(\omega)$ and non-constant $w(t)$, the right-hand side of (4.45) is generally non-zero, and the reconstruction is not exact. Using the triangle inequality to bound $e(t)$,

$$|e(t)| \leq \frac{1}{2\pi} \left\{ \left| \int_{|\omega|=w_{min}}^{|\omega|=w(t)} [H_0(\omega)-1]X(\omega)e^{j\omega t}d\omega \right| + \sum_{k=-\infty}^{\infty} \left| \int_{2kw_{max}-w(t)}^{2kw_{max}+w(t)} Y_2(\omega)e^{j(\omega-2kw_{max})t}d\omega \right| \right\},$$

$$\leq \frac{1}{2\pi} \left\{ \int_{|\omega|=w_{min}}^{|\omega|=w(t)} [1-H_0(\omega)]|X(\omega)|d\omega + \sum_{k=-\infty}^{\infty} \int_{2kw_{max}-w(t)}^{2kw_{max}+w(t)} |Y_2(\omega)|d\omega \right\}. \qquad (4.46)$$

As in Section 4.2.5, we wish to show that the bound on $|e(t)|$ decreases to zero as $w(t)$ approaches a constant. The first term on the right-hand side of (4.46) goes to zero as the range of $w(t)$, and therefore the range of integration, approach zero. The summation over k represents the integral of $|Y_2(\omega)|$ over an infinite set of frequency bands having width $2w(t)$ and centre frequencies $\omega = 2kw_{max}, k \in \mathbf{Z}$. As discussed in Section 3.3.1, $|Y_2(\omega)|$ is bounded according to (3.24) and approaches zero as $w(t)$ approaches a constant. The integral of $|Y_2(\omega)|$ behaves similarly.

4.5 Self-similar signals with bandlimited time-varying spectra

In Section 4.2.5, it was observed that a signal $y(t)$ with a bandlimited time-varying spectrum is in general not perfectly reconstructable according to the procedure summarized in (4.5) and (4.4). However, as demonstrated in this section, perfect reconstruction does result for a class of self-similar signals with bandlimited time-varying spectra. We also discuss the stochastic analogue to these results.

66

4.5.1 Definition and perfect reconstruction property

Comparing the expansions in (4.4) and (4.2), a sufficient condition for perfect reconstruction is met if $\tilde{y}(t, k\pi/w(t))$ is independent of t, so that $\tilde{y}(t, k\pi/w(t)) = y(t_k)$ for all t and $\hat{y}(t) = y(t)$. More generally, if the quantity $w(t)^{\gamma-1}\tilde{y}(t, k\pi/w(t))$ is independent of t, where γ is a real constant, an exact expansion can be obtained for $y(t)$ in terms of its samples $y(t_k)$ and the cut-off frequency $w(t)$. The conditions under which this holds will define a class of self-similar signals with bandlimited time-varying spectra.

Using (3.12), we write $\tilde{y}(t, k\pi/w(t))$ as

$$\tilde{y}\left(t, \frac{k\pi}{w(t)}\right) = \frac{1}{2\pi}\int_{-w(t)}^{w(t)} X(\omega)e^{j\omega k\pi/w(t)}d\omega.$$

Replacing ω with $w(t)\omega$ as the variable of integration,

$$\tilde{y}\left(t, \frac{k\pi}{w(t)}\right) = \frac{w(t)}{2\pi}\int_{-1}^{1} X(w(t)\omega)e^{j\omega k\pi}d\omega. \tag{4.47}$$

We consider cases in which $X(w(t)\omega)$ can be separated into a product of two functions:

$$X(w(t)\omega) = X_a(w(t))X_b(\omega), \tag{4.48}$$

which allows (4.47) to be rearranged as follows:

$$\frac{\tilde{y}(t, k\pi/w(t))}{w(t)X_a(w(t))} = \frac{1}{2\pi}\int_{-1}^{1} X_b(\omega)e^{j\omega k\pi}d\omega. \tag{4.49}$$

Then the left-hand side of (4.49) is independent of t.

Specifically, we restrict our attention to Fourier transforms $X(\omega)$ that obey a power-law:

$$X(\omega) = \frac{C}{|\omega|^\gamma}, \tag{4.50}$$

where C and γ are real constants. Then $X(w(t)\omega)$ satisfies (4.48) with $X_a(w(t)) = w(t)^{-\gamma}$ and $X_b(\omega) = X(\omega)$. Substituting into (4.49),

$$(w(t))^{\gamma-1}\tilde{y}\left(t, \frac{k\pi}{w(t)}\right) = \frac{1}{2\pi}\int_{|\omega|=\epsilon}^{|\omega|=1} \frac{C}{|\omega|^\gamma}e^{j\omega k\pi}d\omega, \tag{4.51}$$

where ϵ is an arbitrarily small positive constant so that the range of integration does

67

not include $\omega = 0$. Thus, if $X(\omega)$ is a power-law spectrum as in (4.50), the quantity $w(t)^{\gamma-1}\tilde{y}(t, k\pi/w(t))$ is independent of t. Signals with power-law spectra are known as self-similar signals or homogeneous signals and are discussed in detail in [11].

From (3.8), the signal $y(t)$ corresponding to (4.50) is given by

$$y(t) = \frac{1}{2\pi} \int_{|\omega|=\epsilon w(t)}^{|\omega|=w(t)} \frac{C}{|\omega|^\gamma} e^{j\omega t} d\omega. \tag{4.52}$$

We refer to signals of the form in (4.52) as self-similar signals with bandlimited time-varying spectra. In Section 4.5.2, we discuss the stochastic analogue to (4.52).

We now show that self-similar signals with bandlimited time-varying spectra can be perfectly reconstructed from samples taken at the times specified by (4.5). Toward this end, we first use (4.5) to substitute $w(t_k)t_k$ for $k\pi$ on the right-hand side of (4.51). Next, replacing ω with $\omega/w(t_k)$ as the variable of integration,

$$(w(t))^{\gamma-1} \tilde{y}\left(t, \frac{k\pi}{w(t)}\right) = (w(t_k))^{\gamma-1} \left\{ \frac{1}{2\pi} \int_{|\omega|=\epsilon w(t_k)}^{|\omega|=w(t_k)} \frac{C}{|\omega|^\gamma} e^{j\omega t_k} d\omega \right\}. \tag{4.53}$$

From (4.52), we recognize the quantity in braces as $y(t_k)$. Rearranging (4.53),

$$\tilde{y}\left(t, \frac{k\pi}{w(t)}\right) = (w(t))^{1-\gamma} (w(t_k))^{\gamma-1} y(t_k). \tag{4.54}$$

Substituting (4.54) into (4.2), we arrive at the desired reconstruction:

$$y(t) = (w(t))^{1-\gamma} \sum_{k=-\infty}^{\infty} (w(t_k))^{\gamma-1} y(t_k) \frac{\sin[w(t)t - k\pi]}{w(t)t - k\pi}. \tag{4.55}$$

Hence $y(t)$ is completely determined by its samples $y(t_k)$ and the cut-off frequency $w(t)$.

4.5.2 Stochastic analogue

The uniform sampling theorem can be extended to wide-sense stationary (WSS) random processes with bandlimited power spectral densities (PSD) (see [1] for a discussion). Specifically, the autocorrelation function of the random process is completely specified by its uniform samples taken at the Nyquist rate associated with the PSD. Accordingly, this leads us to consider the stochastic analogue to a signal with a bandlimited time-varying spectrum. Taking (3.8) and replacing $y(t)$ with the autocorrelation function $R_{yy}(\tau)$ and $X(\omega)$ with

the PSD $S_{xx}(\omega)$, we define

$$R_{yy}(\tau) = \frac{1}{2\pi} \int_{-w(\tau)}^{w(\tau)} S_{xx}(\omega) e^{j\omega\tau} d\omega \qquad (4.56)$$

to be an autocorrelation function with a bandlimited lag-varying PSD. In order for $R_{yy}(\tau)$ to be a valid autocorrelation, it must be an even function of τ, i.e. $R_{yy}(\tau) = R_{yy}(-\tau)$. Thus, $w(\tau)$ must also be an even function.

Consider cases in which the PSD $S_{xx}(\omega)$ is distributed according to a power-law:

$$S_{xx}(\omega) = \frac{C}{|\omega|^\gamma}. \qquad (4.57)$$

WSS random processes having PSDs of the form in (4.57) are known as $1/f$ processes, a rich class of random processes discussed extensively in [11]. Substituting (4.57) into (4.56),

$$R_{yy}(\tau) = \frac{1}{2\pi} \int_{|\omega|=\epsilon w(\tau)}^{|\omega|=w(\tau)} \frac{C}{|\omega|^\gamma} e^{j\omega\tau} d\omega, \qquad (4.58)$$

where $\omega = 0$ has been excluded from the range of integration as in (4.52). The stochastic analogue to (4.55) follows:

$$R_{yy}(\tau) = (w(\tau))^{1-\gamma} \sum_{k=-\infty}^{\infty} (w(\tau_k))^{\gamma-1} R_{yy}(\tau_k) \frac{\sin[w(\tau)\tau - k\pi]}{w(\tau)\tau - k\pi}, \qquad (4.59)$$

where the sampling times τ_k satisfy (4.5). Hence, an autocorrelation function $R_{yy}(\tau)$ of the form in (4.58) is completely determined by its samples $R_{yy}(\tau_k)$ and the cut-off frequency $w(\tau)$.

An autocorrelation function of the form in (4.56) does not correspond however to a random process obtained by filtering a WSS random process with a time-varying lowpass filter. In fact, such a random process is not even WSS, as we show by determining its autocorrelation function. From (3.9), the output $y(t)$ of a time-varying lowpass filter with cut-off frequency $w(t)$ when driven by a WSS random process $x(t)$ is given by

$$y(t) = \int_{-\infty}^{\infty} x(t-u) \frac{\sin[w(t)u]}{\pi u} du. \qquad (4.60)$$

Let $y_1(t)$ and $y_2(t)$ denote the outputs of two time-invariant lowpass filters with cut-off

69

frequencies $w(t_1)$ and $w(t_2)$ respectively when driven by $x(t)$:

$$y_1(t) = \int_{-\infty}^{\infty} x(t - u) \frac{\sin[w(t_1)u]}{\pi u} du, \qquad (4.61)$$

$$y_2(t) = \int_{-\infty}^{\infty} x(t - u) \frac{\sin[w(t_2)u]}{\pi u} du. \qquad (4.62)$$

In particular, $y_1(t_1) = y(t_1)$ and $y_2(t_2) = y(t_2)$. The processes $y_1(t)$ and $y_2(t)$ are jointly WSS and their cross-correlation $R_{y_1 y_2}(\tau)$ is given by

$$R_{y_1 y_2}(\tau) \equiv E\left[y_1(t + \tau)y_2(t)\right] = \frac{\sin[w(t_1)\tau]}{\pi \tau} * \frac{\sin[w(t_2)(-\tau)]}{\pi(-\tau)} * R_{xx}(\tau),$$

where $E[\cdot]$ denotes the ensemble expectation. Since the sinc function is even,

$$R_{y_1 y_2}(\tau) = \frac{\sin[w(t_1)\tau]}{\pi \tau} * \frac{\sin[w(t_2)\tau]}{\pi \tau} * R_{xx}(\tau).$$

The convolution between the two sinc functions, one with maximum frequency $w(t_1)$, the other with maximum frequency $w(t_2)$, yields a sinc function with maximum frequency $\min\{w(t_1), w(t_2)\}$, a result obtained straightforwardly in the Fourier domain. Thus,

$$R_{y_1 y_2}(\tau) = \frac{\sin[\min\{w(t_1), w(t_2)\}\tau]}{\pi \tau} * R_{xx}(\tau). \qquad (4.63)$$

Consider evaluating the autocorrelation $R_{yy}(t, s)$ at the specific times $t = t_1$, $s = t_2$.

$$R_{yy}(t_1, t_2) = E\left[y(t_1)y(t_2)\right] = E\left[y_1(t_1)y_2(t_2)\right] = R_{y_1 y_2}(t_1 - t_2),$$

$$R_{yy}(t_1, t_2) = \int_{-\infty}^{\infty} \frac{\sin[\min\{w(t_1), w(t_2)\}\tau]}{\pi \tau} R_{xx}(t_1 - t_2 - \tau) d\tau. \qquad (4.64)$$

Since $\min\{w(t_1), w(t_2)\}$ is not a function of $t_1 - t_2$ except for special choices of $w(\tau)$, t_1, and t_2, $R_{yy}(t, s)$ is generally not a function of $t - s$ only, and hence $y(t)$ cannot be WSS.

Chapter 5

Time-Warped Bandlimited Signals

In Chapter 4, we concluded that the output of a time-varying lowpass filter as defined in Section 3.2 should not be regarded as a locally bandlimited signal, since the perfect reconstruction property of Section 1.2 does not hold in general for the sampling and reconstruction method developed in Section 4.2. As an alternative approach, in this chapter we consider a definition for local bandwidth based on the time-warping of globally bandlimited signals. This definition was proposed by Clark, Palmer, and Lawrence in [5], and by Zeevi and Shlomot in [6]. We also discuss the pre-filtering and pre-warping of signals to be sampled on a specified non-uniform grid.

5.1 Definition of local bandwidth based on time-warping

In this section, we closely follow the ideas in [5] and [6]. We define a continuous-time signal $f(t)$ to be locally bandlimited if there exists a continuous, invertible function $\alpha(t)$ such that the signal

$$g(t) = f(\alpha(t)) \tag{5.1}$$

is bandlimited to a maximum frequency ω_0, i.e.

$$G(\omega) = 0, \quad |\omega| > \omega_0. \tag{5.2}$$

The signal $g(t)$ is obtained from $f(t)$ by the transformation $t \to \alpha(t)$ of the time variable. More informally, we will refer to this transformation as a time-warping, and to $\alpha(t)$ as the warping function.

71

The signal $f(t)$ can be expressed in terms of $g(t)$ as

$$f(t) = g(\gamma(t)), \tag{5.3}$$

where the warping function $\gamma(t)$ is the unique inverse of $\alpha(t)$, i.e.

$$\gamma(\alpha(t)) = \alpha(\gamma(t)) = t. \tag{5.4}$$

In order for ω_0 to be uniquely specified, the following additional constraint on the warping function $\alpha(t)$ is imposed:

$$\lim_{t \to \pm\infty} \frac{\alpha(t)}{t} = 1, \tag{5.5}$$

which also implies

$$\lim_{t \to \pm\infty} \frac{\gamma(t)}{t} = 1. \tag{5.6}$$

Together with the constraints that $\alpha(t)$ be continuous and invertible, (5.5) and (5.6) restrict $\alpha(t)$ and $\gamma(t)$ to be monotonically increasing with t.

To illustrate the necessity of (5.5), suppose that $g_1(t) = f(\alpha_1(t))$ is bandlimited to ω_1 for some $\alpha_1(t)$ satisfying (5.5), so that $f(t)$ is locally bandlimited. Let $\alpha_2(t) = \alpha_1(at)$, where $|a| \neq 1$ is a real constant, and $g_2(t) = f(\alpha_2(t)) = g_1(at)$, i.e. $g_2(t)$ is a globally time-scaled version of $g_1(t)$. Using the time-scaling property of Fourier transforms,

$$G_2(\omega) = \frac{1}{|a|} G_1\left(\frac{\omega}{a}\right). \tag{5.7}$$

Hence, $g_2(t)$ is bandlimited to $|a|\omega_1 \neq \omega_1$, and we may equally well use $\alpha_2(t)$, $g_2(t)$, and $|a|\omega_1$ to define $f(t)$ as a locally bandlimited signal. Note that

$$\lim_{t \to \pm\infty} \frac{\alpha_2(t)}{t} = \lim_{t \to \pm\infty} \frac{\alpha_1(at)}{t} = \lim_{t \to \pm\infty} a\frac{\alpha_1(at)}{at} = a,$$

so that $g_2(t)$ does not satisfy (5.5). The constraint in (5.5) may be interpreted as fixing the value of ω_0 by excluding any global dilation or compression from the warping function. For simplicity, global time reversal, corresponding to $a = -1$, is also excluded.

Since $g(t)$ is globally bandlimited, we exploit the uniform sampling theorem to show that

$f(t)$ is perfectly reconstructable from knowledge of its samples and the warping function. Specifically, $g(t)$ can be expanded as

$$g(t) = \sum_{k=-\infty}^{\infty} g(kT) \frac{\sin(\omega_0 t - k\pi)}{\omega_0 t - k\pi}, \tag{5.8}$$

where $T = \pi/\omega_0$ is the Nyquist sampling period. Rewriting (5.8) as an expansion for $f(t)$,

$$f(t) = g(\gamma(t)) = \sum_{k=-\infty}^{\infty} f(t_k) \frac{\sin(\omega_0 \gamma(t) - k\pi)}{\omega_0 \gamma(t) - k\pi}, \tag{5.9}$$

where the sampling instants t_k are given by

$$t_k = \alpha(kT), \tag{5.10}$$

so that $g(kT) = f(t_k)$. Equation (5.9) may be interpreted as an exact reconstruction of the locally bandlimited signal $f(t)$ from its samples. The synthesis functions in the reconstruction are time-warped sinc functions obtained by replacing t with $\gamma(t)$.

From the warping function $\gamma(t)$, we can construct a quantity that has the units of frequency and that provides an intuitive measure of the rate at which the signal $f(t)$ varies. As motivation, consider first the special case in which $\gamma(t) = at$ with a a positive constant (and ignoring (5.6) for the moment), corresponding to a time compression if $a > 1$ and a dilation if $a < 1$. Using the property in (5.7), if $g(t)$ is bandlimited to ω_0, then $f(t) = g(\gamma(t))$ is bandlimited to $a\omega_0$, i.e. to a higher maximum frequency for compression and a lower one for dilation. We also observe that the time-scaling a is given by $\gamma'(t)$, the derivative of $\gamma(t)$.

In the more general case in which $\gamma(t)$ is not a linear function of t, $\gamma'(t)$ indicates the amount by which $g(t)$ is locally compressed or dilated to yield $f(t)$. Specifically, $f(t)$ on the infinitesimal interval $[t_0, t_0 + dt]$ is the image of $g(t)$ on the interval $[\gamma(t_0), \gamma(t_0) + \gamma'(t_0)dt]$, which corresponds to compression if $\gamma'(t_0) > 1$ and to dilation if $\gamma'(t_0) < 1$. The monotonically increasing property ensures $\gamma'(t_0) > 0$. Thus, $f(t)$ on the interval $[t_0, t_0 + dt]$ can be said to vary more quickly by the factor $\gamma'(t)$ than $g(t)$ on the corresponding interval. Since the maximum frequency ω_0 is a measure of the variation in $g(t)$, we may interpret the quantity

$$\omega_0 \gamma'(t) \tag{5.11}$$

as a local measure of the variation in $f(t)$. We emphasize, however, that for the purposes of sampling and reconstructing $f(t)$, the warping function $\gamma(t)$ and its inverse $\alpha(t)$ are the fundamental quantities.

In some contexts, we may only require $\gamma(t)$ and not its inverse $\alpha(t)$. Such an example is presented in Section 5.2. In these cases, $\gamma(t)$ does not need to be invertible, although it must still be surjective onto the real line. Accordingly, we consider the following, less restrictive definition of a locally bandlimited signal: A signal $f(t)$ is said to be locally bandlimited if there exists a continuous, surjective warping function $\gamma(t)$ satisfying (5.6) such that $f(t) = g(\gamma(t))$ and $g(t)$ is bandlimited to ω_0 as in (5.2). Given this definition, (5.9) remains valid as an expansion for $f(t)$ in terms of its samples. However, the sampling instants t_k are now specified implicitly by

$$\gamma(t_k) = kT. \tag{5.12}$$

Since $\gamma(t)$ is surjective, (5.12) always has at least one solution. However, the solution may no longer be unique, in which case $g(kT) = f(t_k)$ for all values of t_k satisfying (5.12), and any one of the samples $f(t_k)$ may be chosen as the kth coefficient in (5.9). In addition, we note that in principle, $g(t)$ can still be recovered from $f(t)$ if $\gamma(t)$ is surjective but not invertible, because the value of g at any time $\gamma(t)$, $\gamma(t) \in \mathbf{R}$, is taken by $f(t)$ at time t.

The locally bandlimited signal $f(t) = g(\gamma(t))$ is generally not globally bandlimited. To show this, we relate the Fourier transform $F(\omega)$ to $G(\omega)$ as follows:

$$
\begin{aligned}
F(\omega) &= \int_{-\infty}^{\infty} f(t)e^{-j\omega t}dt, \\
&= \int_{-\infty}^{\infty} g(\gamma(t))e^{-j\omega t}dt, \\
&= \int_{-\infty}^{\infty} \left\{ \int_{-\omega_0}^{\omega_0} G(\lambda)e^{j\lambda\gamma(t)}d\lambda \right\} e^{-j\omega t}dt,
\end{aligned}
$$

where the limits of integration over λ incorporate the fact that $G(\lambda)$ is zero outside the interval $[-\omega_0, \omega_0]$. Interchanging the order of integration,

$$
\begin{aligned}
F(\omega) &= \int_{-\omega_0}^{\omega_0} \left\{ \int_{-\infty}^{\infty} e^{j\lambda\gamma(t)}e^{-j\omega t}dt \right\} G(\lambda)d\lambda, \\
F(\omega) &= \int_{-\omega_0}^{\omega_0} P(\omega, \lambda)G(\lambda)d\lambda, \tag{5.13}
\end{aligned}
$$

where $P(\omega, \lambda)$ is the Fourier transform of the angle-modulated signal

$$p_\lambda(t) = e^{j\lambda\gamma(t)}. \tag{5.14}$$

Since $p_\lambda(t)$ is in general not a bandlimited signal, $f(t)$ is also not bandlimited.

5.2   Pre-filtering and pre-warping for a specified non-uniform sampling grid

In this section, we consider the pre-processing of signals that are to be sampled on a specified non-uniform grid. We present a strategy in which the signal is filtered and time-warped such that the samples taken on the non-uniform grid are equal to uniform, Nyquist-rate samples of a bandlimited version of the signal, which may then be reconstructed.

A possible alternative approach makes use of the non-uniform sampling theorem, which essentially states that a bandlimited signal may be perfectly reconstructed from its non-uniform samples provided that the average sampling rate exceeds the Nyquist rate, and that the sampling times do not differ too greatly from a uniform sequence (see e.g. [12, 13, 14]). In an approach employing the non-uniform sampling theorem, the signal is lowpass filtered to a sufficiently low bandwidth so that it can be exactly represented on the non-uniform grid. The bandlimited version of the signal is then reconstructed by performing Lagrange interpolation between its non-uniform samples.

As an alternative approach, we now consider the system shown in Figure 5-1, consisting of pre-filtering, pre-warping, sampling, and reconstruction. In Figure 5-1, $x(t)$ denotes the original signal, $g(t)$ the output of a time-invariant lowpass filter with cut-off frequency ω_0, and $f(t) = g(\gamma(t))$ the result of time-warping $g(t)$. The overall effect of the pre-filtering and pre-warping is to map an arbitrary signal $x(t)$ into a locally bandlimited signal $f(t)$ in the sense of Section 5.1. The signal $f(t)$ is sampled at the specified times t_k, $k \in \mathbf{Z}$. We note that the time-warping approach of Figure 5-1 does not require the sampling grid to be close to a uniform sampling grid in any sense. In the reconstruction, the samples $f(t_k)$ can be viewed as the coefficients of a uniform impulse train that drives a time-invariant lowpass filter with cut-off frequency ω_0, yielding $g(t)$ as the output.

Based on the sampling grid $\{t_k, k \in \mathbf{Z}\}$, we wish to specify the cut-off frequency ω_0 and
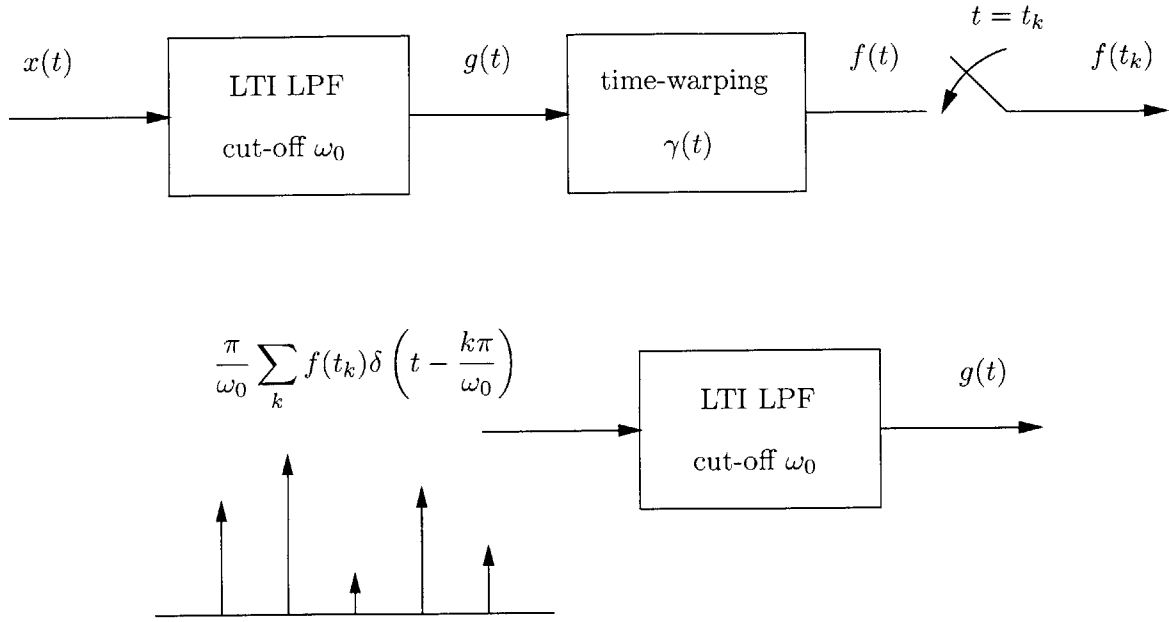
Figure 5-1: Pre-filtering and pre-warping for signals to be sampled on a non-uniform grid. "LTI LPF" denotes a time-invariant lowpass filter.

a continuous, surjective warping function $\gamma(t)$ subject to (5.6) and such that the samples $f(t_k)$ are equal to uniform, Nyquist-rate samples of $g(t)$. In particular, (5.6) implies that the average sample spacing cannot change when the non-uniform sampling grid $\{t_k, k \in \mathbf{Z}\}$ is mapped through $\gamma(t)$ into a uniform, Nyquist-rate sampling grid, i.e.

$$\frac{\pi}{\omega_0} = \lim_{k \to \infty} \frac{t_k}{k},$$

where the right-hand side represents the average sample spacing in $\{t_k, k \in \mathbf{Z}\}$. Thus,

$$\omega_0 = \pi \lim_{k \to \infty} \frac{k}{t_k}. \tag{5.15}$$

We also require that

$$f(t_k) = g(\gamma(t_k)) = g\left(\frac{k\pi}{\omega_0}\right), \tag{5.16}$$

and hence

$$\gamma(t_k) = \frac{k\pi}{\omega_0}. \tag{5.17}$$

Comparing (5.17) with (5.12), we infer that $f(t)$ may be exactly represented by its samples on the grid $\{t_k, k \in \mathbf{Z}\}$. From these samples, $g(t)$ may also be perfectly reconstructed, as is

76

done in this context.

Equation (5.17) only constrains the values of $\gamma(t)$ at $t = t_k, k \in \mathbf{Z}$. As an example, we may choose $\gamma(t)$ to be a linear interpolation between the points $(t_k, k\pi/\omega_0)$, as illustrated in Figure 5-2 and given by

$$\gamma(t) = \frac{\pi}{\omega_0} \frac{k\,(t_{k+1} - t) + (k+1)\,(t - t_k)}{t_{k+1} - t_k}, \quad t_k \le t \le t_{k+1}, \ k \in \mathbf{Z}. \tag{5.18}$$

Although this piecewise linear choice is invertible, in general, it is not necessary for $\gamma(t)$ to be invertible because its inverse $\alpha(t)$ is not required.
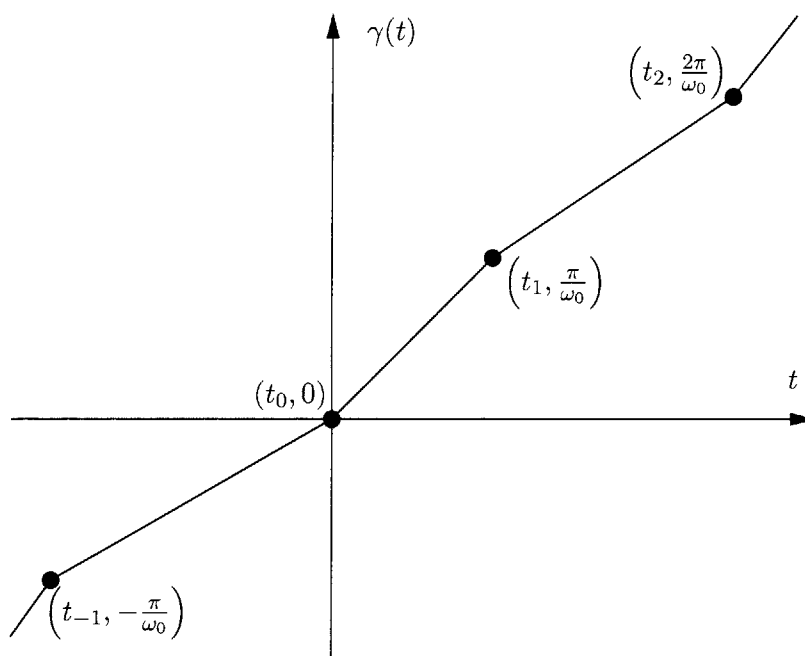
Figure 5-2: Example of a piecewise linear warping function $\gamma(t)$.

To reconstruct the bandlimited signal $g(t)$, we may consider the samples $f(t_n)$ to be the coefficients of a uniform impulse train with spacing π/ω_0. The impulse train is the input to a time-invariant lowpass filter with cut-off frequency ω_0, resulting in the output

$$\sum_{k=-\infty}^{\infty} f(t_k) \frac{\sin[\omega_0(t - k\pi/\omega_0)]}{\omega_0(t - k\pi/\omega_0)} = \sum_{k=-\infty}^{\infty} g\left(\frac{k\pi}{\omega_0}\right) \frac{\sin[\omega_0 t - k\pi]}{\omega_0 t - k\pi},$$
$$= g(t),$$

using (5.16) and (5.8). Thus, the method of pre-filtering and pre-warping allows a bandlimited version of the original signal to be perfectly reconstructed, which is the same result

obtained using the non-uniform sampling theorem. In addition, the signal $f(t)$ may also be recovered by time-warping $g(t)$ with $\gamma(t)$ at the output.

Chapter 6

Sampling and Reconstruction Using an Optimal Time-Warping

In this chapter, we develop a sampling and reconstruction strategy based on the definition of local bandwidth in Chapter 5. In particular, the strategy employs a time-warping that minimizes the energy of a signal above a certain maximum frequency. We examine a number of analytical and numerical approaches to the problem of determining the optimal time-warping. We also present a method for determining a time-warping based on the zero-crossings of the signal to be sampled.

6.1 Sampling and reconstruction method

In this section, we present a method for sampling and reconstructing a signal based on the relationship between time-warping and local bandwidth discussed in Section 5.1. Figure 6-1 depicts the sampling and reconstruction system to be considered, where $f(t)$ denotes the signal to be reconstructed from its samples.

In the first step, we determine the warping function $\alpha_*(t)$ that minimizes the energy above a maximum frequency ω_0 of $g(t) = f(\alpha(t))$ over all possible $\alpha(t)$. Defining the energy as

$$\varepsilon_g = \frac{1}{2\pi} \int_{|\omega|=\omega_0}^{\infty} |G(\omega)|^2 d\omega, \tag{6.1}$$

where $G(\omega)$ is the Fourier transform of $g(t)$, we have

$$\alpha_*(t) = \underset{\alpha(t)}{\operatorname{argmin}} \, \varepsilon_g. \qquad (6.2)$$

The possible warping functions $\alpha(t)$ are constrained to be continuous, invertible functions satisfying (5.5), as discussed in Section 5.1. Consequently, the inverse $\gamma_*(t)$ of $\alpha_*(t)$ also has these properties. In Section 6.2, we consider some approaches to the optimization in (6.2). Once $\alpha_*(t)$ is determined, the signal $g_*(t)$ is obtained by warping $f(t)$ with $\alpha_*(t)$, i.e. $g_*(t) = f(\alpha_*(t))$.
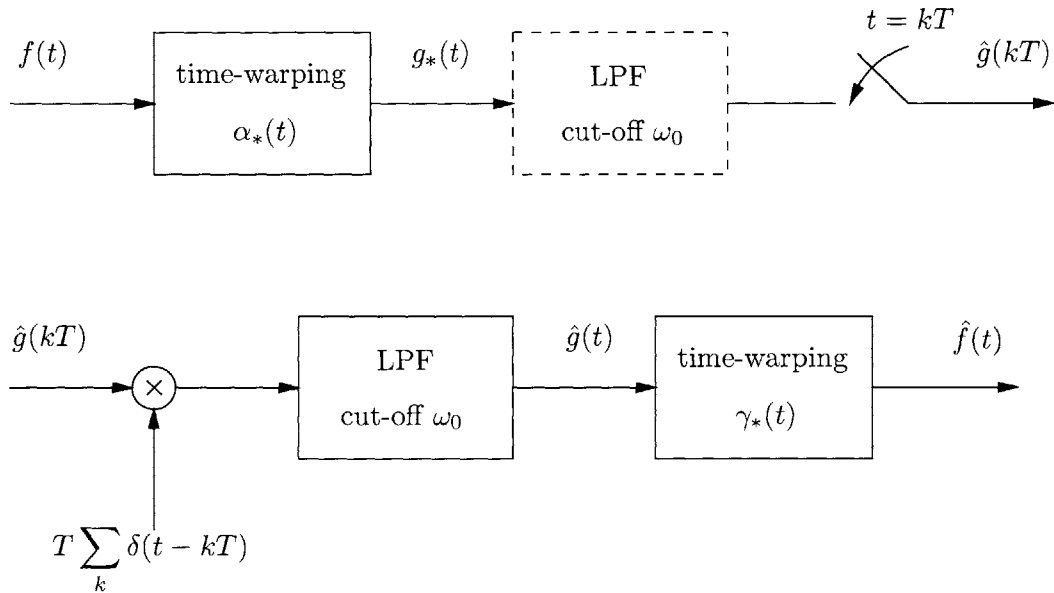
Figure 6-1: System for sampling and reconstructing $f(t)$ using an optimal warping function $\alpha_*(t)$.

We assume that there is a constraint on the average sampling rate, so that the sampling period T in Figure 6-1 can be regarded as fixed. It follows that the maximum frequency ω_0 should be chosen as

$$\omega_0 = \frac{\pi}{T}. \qquad (6.3)$$

If the minimum value of ε_g is zero, then $f(t)$ is locally bandlimited as defined in Section 5.1. Accordingly, the system should yield an exact reconstruction of $f(t)$, i.e. the overall output $\hat{f}(t) = f(t)$, as will be shown.

We consider two choices for the system in Figure 6-1 corresponding to the inclusion or exclusion of the anti-aliasing lowpass filter indicated by a dashed box. In Section 6.1.1,

we analyze the case in which the anti-aliasing filter is included, while in Section 6.1.2 we analyze the case in which it is excluded.

6.1.1   Inclusion of an anti-aliasing filter

With the inclusion of an anti-aliasing filter having cut-off frequency ω_0, the uniform samples $\hat{g}(kT)$ are given by

$$\hat{g}(kT) = \frac{\omega_0}{\pi} \int_{-\infty}^{\infty} f(\alpha_*(t)) \frac{\sin(\omega_0 t - k\pi)}{\omega_0 t - k\pi} dt. \tag{6.4}$$

Equivalently,

$$\hat{g}(kT) = \frac{\omega_0}{\pi} \int_{-\infty}^{\infty} f(t) \frac{\sin(\omega_0 \gamma_*(t) - k\pi)}{\omega_0 \gamma_*(t) - k\pi} \gamma_*'(t) dt, \tag{6.5}$$

as a result of changing the variable of integration from t to $\gamma_*(t)$. The samples $\hat{g}(kT)$ do not correspond to samples of $f(t)$ except when $f(t)$ is locally bandlimited, in which case $g_*(t)$ is globally bandlimited to ω_0 and is unchanged by the lowpass filter. In this special case,

$$\hat{g}(kT) = g_*(kT) = f(\alpha_*(kT)),$$
$$= f(t_k), \tag{6.6}$$

where the sampling instants t_k are those in (5.10).

The bandlimited signal $\hat{g}(t)$ is reconstructed from its samples, represented by a weighted impulse train, using a second time-invariant lowpass filter with cut-off frequency ω_0. The reconstruction $\hat{f}(t)$ of $f(t)$ is obtained by time-warping $\hat{g}(t)$ with $\gamma_*(t)$:

$$\hat{f}(t) = \sum_{k=-\infty}^{\infty} \hat{g}(kT) \frac{\sin(\omega_0 \gamma_*(t) - k\pi)}{\omega_0 \gamma_*(t) - k\pi}. \tag{6.7}$$

In the case where $f(t)$ is locally bandlimited and (6.6) holds, the right-hand side of (6.7) matches the right-hand side of (5.9). Thus, $\hat{f}(t) = f(t)$ and perfect reconstruction is achieved.

The only source of error in the system is the anti-aliasing filter used to process $g_*(t)$. Specifically, the energy in the error $\hat{g}(t) - g_*(t)$ is equal to ε_g, which may also be expressed

in terms of $f(t)$ as follows:

$$\varepsilon_g = \int_{-\infty}^{\infty} [\hat{g}(t) - g_*(t)]^2 dt,$$

$$= \int_{-\infty}^{\infty} [\hat{f}(\alpha_*(t)) - f(\alpha_*(t))]^2 dt.$$

Again invoking the change of variable $t \rightarrow \gamma_*(t)$,

$$\varepsilon_g = \int_{-\infty}^{\infty} [\hat{f}(t) - f(t)]^2 \gamma_*'(t) dt. \tag{6.8}$$

The optimal warping function $\alpha_*(t)$ minimizes the weighted error energy in (6.8), which is the same optimality criterion used by Zeevi and Shlomot [6] in defining a projection onto the space of locally bandlimited signals. If $f(t)$ is already locally bandlimited, then $\varepsilon_g = 0$, corresponding to the fact that $f(t)$ is equal to its projection.

Define

$$\varepsilon_f = \int_{-\infty}^{\infty} |\hat{f}(t) - f(t)|^2 dt \tag{6.9}$$

to be the unweighted energy in the reconstruction error $\hat{f}(t) - f(t)$. Using (6.8), ε_f may be bounded above and below by

$$\frac{\varepsilon_g}{\gamma_{max}'} \leq \varepsilon_f \leq \frac{\varepsilon_g}{\gamma_{min}'}, \tag{6.10}$$

where γ_{min}' and γ_{max}' are the minimum and maximum values of $\gamma_*'(t)$. We note that $\gamma_*'(t)$ is positive because $\gamma_*(t)$ is monotonically increasing.

6.1.2 Exclusion of an anti-aliasing filter

With the exclusion of an anti-aliasing filter, $g_*(t)$ is sampled directly and (6.6) holds regardless of whether or not $g_*(t)$ is bandlimited. Consequently, the reconstruction $\hat{f}(t)$ is given by

$$\hat{f}(t) = \sum_{k=-\infty}^{\infty} f(t_k) \frac{\sin(\omega_0 \gamma_*(t) - k\pi)}{\omega_0 \gamma_*(t) - k\pi}. \tag{6.11}$$

If $f(t)$ is locally bandlimited, we conclude by comparing (5.9) and (6.11) that $\hat{f}(t) = f(t)$.

If $g_*(t)$ is not bandlimited, the sampling and reconstruction results in some error due to

aliasing of $g_*(t)$. Weiss [1, 15] provides the following bound for the aliasing error:

$$|\hat{g}(t) - g_*(t)| \leq \frac{2}{\pi} \int_{\omega_0}^{\infty} |G_*(\omega)| d\omega. \tag{6.12}$$

Substituting $\gamma_*(t)$ for t and noting that the right-hand side of (6.12) does not depend on t, we obtain

$$|\hat{f}(t) - f(t)| \leq \frac{2}{\pi} \int_{\omega_0}^{\infty} |G_*(\omega)| d\omega \tag{6.13}$$

as a bound on the reconstruction error. If $f(t)$ is locally bandlimited, the right-hand side of (6.13) is zero and we have perfect reconstruction.

6.2 Determination of the optimal time-warping

In this section, we discuss two approaches to determining the optimal warping $\alpha_*(t)$ that minimizes ε_g over all possible warping functions $\alpha(t)$, as formulated in Section 6.1. In Section 6.2.1, the calculus of variations is applied to the minimization. In Section 6.2.2, we seek to minimize ε_g over a class of piecewise linear functions by minimizing with respect to a set of parameters. We present a gradient-descent algorithm in Section 6.2.3 based on the piecewise linear parameterization of Section 6.2.2.

6.2.1 Calculus of variations

In this section, we employ the calculus of variations (see for example [16]) in minimizing ε_g. We consider ε_g to be the integral of a functional $\mathcal{F}[\alpha(t)]$ by expressing ε_g as

$$\varepsilon_g = \int_{-\infty}^{\infty} \left\{ \int_{-\infty}^{\infty} g(\tau) h(t - \tau) d\tau \right\}^2 dt, \tag{6.14}$$

where $h(t)$ is the impulse response of an ideal highpass filter with cut-off frequency ω_0:

$$h(t) = \delta(t) - \frac{\sin(\omega_0 t)}{\pi t}. \tag{6.15}$$

Substituting $g(t) = f(\alpha(t))$ in (6.14),

$$\varepsilon_g = \int_{-\infty}^{\infty} \left\{ \int_{-\infty}^{\infty} f(\alpha(\tau)) h(t - \tau) d\tau \right\}^2 dt. \tag{6.16}$$

We identify the squared quantity in braces as $\mathcal{F}[\alpha(t)]$:

$$\mathcal{F}[\alpha(t)] = \left\{ \int_{-\infty}^{\infty} f(\alpha(\tau))h(t-\tau)d\tau \right\}^2. \tag{6.17}$$

For ease of analysis, in this section we neglect the monotonically increasing constraint on $\alpha(t)$, thus permitting an unconstrained optimization. In this case, the Euler-Lagrange equation given below must be satisfied at all extrema of $\mathcal{F}[\alpha(t)]$, i.e.

$$\frac{\partial \mathcal{F}}{\partial \alpha} - \frac{d}{dt}\frac{\partial F}{\partial \alpha'} = 0, \tag{6.18}$$

where α' denotes the derivative of $\alpha(t)$ with respect to t. Since F in (6.17) does not depend explicitly on $\alpha'(t)$, the Euler-Lagrange equation reduces to

$$\frac{\partial F}{\partial \alpha} = 0. \tag{6.19}$$

Evaluating (6.19) for the optimal warping $\alpha_*(t)$,

$$\left\{ \int_{-\infty}^{\infty} f(\alpha_*(\tau))h(t-\tau)d\tau \right\} \times \left\{ \int_{-\infty}^{\infty} f'(\alpha_*(\sigma))h(t-\sigma)d\sigma \right\} = 0 \quad \forall\, t. \tag{6.20}$$

We can interpret $f'(\alpha_*(t))$ as the result of warping $f'(t)$ with $\alpha_*(t)$, where $f'(t)$ is the derivative of $f(t)$ with respect to t. Using the chain rule for differentiation, $f'(\alpha_*(t))$ can be related to $g_*'(t)$, the derivative of $g_*(t)$, as follows:

$$g_*'(t) = \frac{d}{dt}f(\alpha_*(t)) = f'(\alpha_*(t))\alpha_*'(t),$$
$$f'(\alpha_*(t)) = \frac{g_*'(t)}{\alpha_*'(t)}. \tag{6.21}$$

A block diagram representation of (6.20) is shown in Figure 6-2. The upper and lower branches represent the highpass filtering of $f(\alpha_*(t)) = g_*(t)$ and $f'(\alpha_*(t))$ respectively. We observe that if $f(\alpha_*(t))$ is bandlimited to ω_0, the output of the top branch is zero for all t and (6.20) is satisfied, in agreement with the fact that $\varepsilon_g = 0$ necessarily corresponds to a minimum.

Note that (5.5) acts as a normalization rather than a constraint on $\alpha(t)$. Suppose that either $f(\alpha_*(t))$ or $f'(\alpha_*(t))$ is bandlimited to ω_0 for some $\alpha_*(t)$, thus satisfying (6.20). If
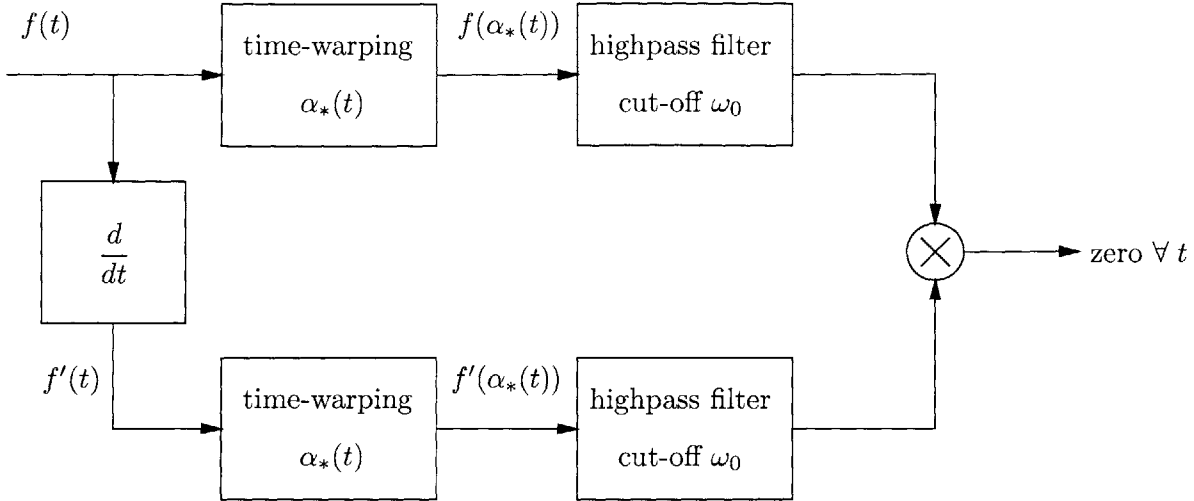
Figure 6-2: Block diagram representation of the Euler-Lagrange condition in (6.20).

(5.5) does not hold, then $\alpha_*(at)$, $|a| < 1$ is permitted and also satisfies (6.20), since it corresponds to a global dilation of a signal that is already bandlimited to ω_0. Therefore, (5.5) is required in order to normalize $\alpha_*(t)$.

In conclusion, the calculus of variations provides a necessary condition in (6.20) for a time-warping to be optimal, but does not necessarily incorporate our additional constraint that the time-warping be monotonically increasing.

6.2.2 Piecewise linear parameterization

The calculus of variations is useful for optimizing over functions of a continuous variable. As an alternative, we may consider parameterizing the warping functions $\alpha(t)$ in terms of a countable set of parameters and minimize ε_g with respect to the parameters. In this section, we only treat the case of piecewise linear warping functions. Specifically, $\alpha(t)$ is restricted to be of the form

$$\alpha(t) = \sum_{p=-\infty}^{\infty} \alpha_p \beta \left(\frac{t}{\delta} - p \right), \tag{6.22}$$

where δ is the horizontal length of every linear segment and the basis functions $\beta(t/\delta - p)$ are defined in terms of the unit triangle function $\beta(t)$:

$$\beta(t) = \begin{cases} 1 - |t|, & |t| \leq 1, \\ 0, & |t| > 1, \end{cases} \tag{6.23}$$

which is sketched in Figure 6-3. Equation (6.22) allows $\alpha(t)$ to be described in terms of the
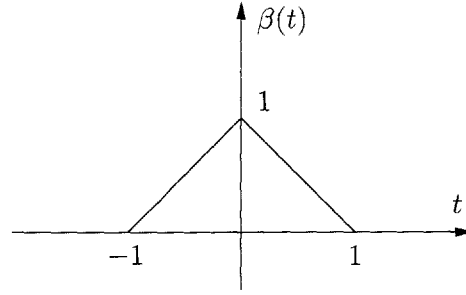

Figure 6-3: The unit triangle function $\beta(t)$.

countable set of samples $\alpha_p = \alpha(p\delta)$ taken at the boundaries between linear segments. An example of a piecewise linear $\alpha(t)$ is shown in Figure 6-4.

The derivative $\alpha'(t)$ of $\alpha(t)$ in (6.22) is piecewise constant and is given by

$$\alpha'(t) = \frac{\alpha_{p+1} - \alpha_p}{\delta} \equiv \frac{\Delta_p}{\delta}, \quad p\delta < t < (p+1)\delta, \ p \in \mathbf{Z}, \tag{6.24}$$

where $\Delta_p = \alpha_{p+1} - \alpha_p$ is the first forward difference of the parameter sequence α_p.

In principle, the segment length δ can be made arbitrarily small so that $\alpha(t)$ approximates a smooth function. It is convenient to choose $\delta = T/r$, where T is the sampling period in Figure 6-1 and r is a positive integer. Given this choice, the sampling instants t_k specified by (5.10) become

$$t_k = \alpha(kT) = \alpha(kr\delta) = \alpha_{kr}. \tag{6.25}$$

Once the sequence α_p is determined, the sequence t_k is obtained by taking every rth element of α_p.

In order for $\alpha(t)$ to be monotonically increasing, the sequence α_p must also increase monotonically, or equivalently, Δ_p must be positive for all p. As in Section 6.2.1, we again neglect the monotonically increasing constraint and perform an unconstrained minimization of ε_g. Given the parameterization of $\alpha(t)$ in (6.22), the minimization is accomplished by setting to zero the partial derivative of ε_g with respect to each parameter α_p. From (6.16) and (6.22),

$$\frac{\partial \varepsilon_g}{\partial \alpha_p} = 2 \int_{-\infty}^{\infty} \left\{ \int_{-\infty}^{\infty} f(\alpha_*(\tau))h(t-\tau)d\tau \right\} \left\{ \int_{(p-1)\delta}^{(p+1)\delta} f'(\alpha_*(\sigma))\beta\left(\frac{\sigma}{\delta} - p\right) h(t-\sigma)d\sigma \right\} dt = 0, \tag{6.26}$$
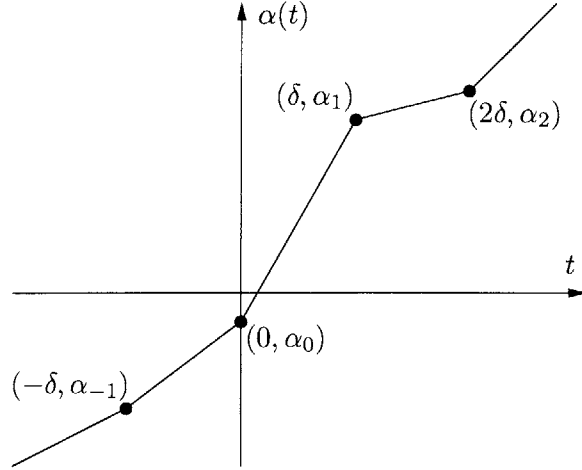
Figure 6-4: Example of a piecewise linear warping function $\alpha(t)$.

where the limits of the integral over σ are $(p-1)\delta$ and $(p+1)\delta$ because $\beta(\sigma/\delta - p) = 0$ elsewhere. As before, $\alpha_*(t)$ denotes the optimal warping function, now restricted to be piecewise linear. Substituting $g_*(\tau)$ for $f(\alpha_*(\tau))$ and (6.21) for $f'(\alpha_*(\sigma))$,

$$\int_{-\infty}^{\infty} \left\{ \int_{-\infty}^{\infty} g_*(\tau)h(t-\tau)d\tau \right\} \left\{ \int_{(p-1)\delta}^{(p+1)\delta} \frac{g_*'(\sigma)}{\alpha_*'(\sigma)} \beta\left(\frac{\sigma}{\delta} - p\right) h(t-\sigma)d\sigma \right\} dt = 0.$$

We use (6.24) to substitute for $\alpha_*'(\sigma)$ and divide the integral over σ into two halves. Rearranging, we obtain an expression for the ratio Δ_p/Δ_{p-1}:

$$\frac{\Delta_p}{\Delta_{p-1}} = -\frac{\int_{-\infty}^{\infty} \left\{ \int_{-\infty}^{\infty} g_*(\tau)h(t-\tau)d\tau \right\} \left\{ \int_{p\delta}^{(p+1)\delta} g_*'(\sigma)\beta\left(\frac{\sigma}{\delta} - p\right) h(t-\sigma)d\sigma \right\} dt}{\int_{-\infty}^{\infty} \left\{ \int_{-\infty}^{\infty} g_*(\tau)h(t-\tau)d\tau \right\} \left\{ \int_{(p-1)\delta}^{p\delta} g_*'(\sigma)\beta\left(\frac{\sigma}{\delta} - p\right) h(t-\sigma)d\sigma \right\} dt}, \quad p \in \mathbf{Z}.$$

(6.27)

The left-hand side of (6.27) may be regarded as the ratio between the slopes of $\alpha_*(t)$ on the intervals $[(p-1)\delta, p\delta]$ and $[p\delta, (p+1)\delta]$. Thus, (6.27) constrains the slopes on adjacent intervals. The constraint is implicit because $g_*(\tau)$ and $g_*'(\sigma)$ on the right-hand side of (6.27) depend on $\alpha_*(t)$, and in particular on Δ_{p-1} and Δ_p on the left-hand side.

Given the ratios in (6.27), two degrees of freedom remain in $\alpha_*(t)$: the value of a single difference Δ_p and the value of a single parameter α_p, e.g. Δ_0 and α_0 without loss of generality. Varying Δ_0 corresponds to an overall amplitude scaling on $\alpha_*(t)$. Hence, Δ_0 is fixed in principle by enforcing (5.5). The value of α_0 may be arbitrary since it corresponds

to an overall time shift of $g_*(t)$ and has no effect on its bandwidth.

Figure 6-5 shows a block diagram representation of the right-hand side of (6.27). The functions $\beta_-(t)$ and $\beta_+(t)$ are the negative-time and positive-time halves of $\beta(t)$ respectively, i.e.

$$\beta_-(t) = \begin{cases} \beta(t), & t < 0, \\ \\ 0, & t > 0, \end{cases}$$

$$\beta_+(t) = \begin{cases} 0, & t < 0, \\ \\ \beta(t), & t > 0, \end{cases}$$
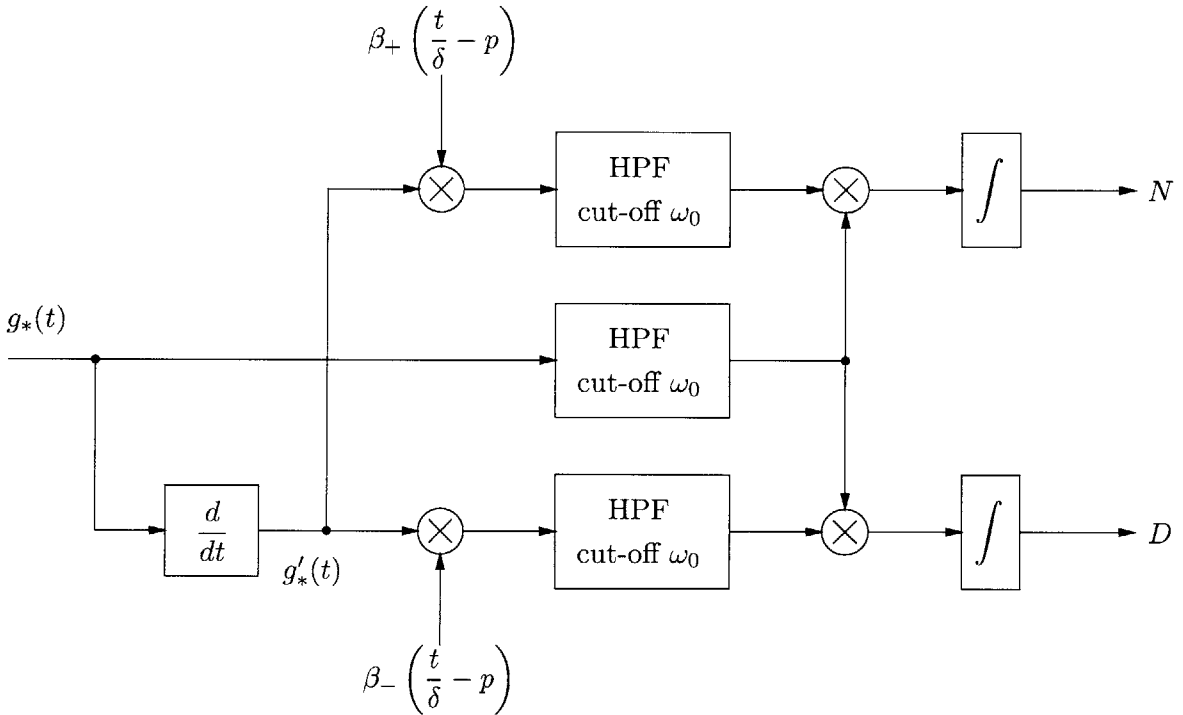
Figure 6-5: Block diagram representation of the right-hand side of (6.27), where N and D refer to the numerator and denominator and "HPF" indicates an ideal highpass filter.

We have derived the constraint in (6.27) on the optimal, piecewise linear time-warping, which is again not necessarily monotonically increasing. Equation (6.27) may not hold for the optimal, monotonically increasing $\alpha_*(t)$, since the minimum may also occur on the boundary of the region in the parameter space corresponding to monotonically increasing α_p.

6.2.3 Gradient descent

In this section, we describe a numerical gradient-descent algorithm (see e.g. [17]) for determining the warping function $\alpha_*(t)$ that minimizes ε_g. The algorithm is based on the assumption of a piecewise linear warping function as discussed in Section 6.2.2. We present the results of a MATLAB implementation of the algorithm using time-warped sinusoids as inputs.

The algorithm takes as input L samples $f[n] = f(nT)$, $n = 0, 1, 2, \ldots, L-1$, of the continuous-time signal $f(t)$, where for convenience we will set $T = 1$. In this section, the time index n takes the values $0, 1, \ldots, L-1$ unless otherwise specified. The samples $f[n]$ are taken at a sufficiently high rate for the error due to aliasing to be negligible. The values of $f(t)$ at non-integer values of t are approximated by interpolating between the samples $f[n]$.

The algorithm also requires samples $f'[n] = f'(t)|_{t=n}$ of the derivative $f'(t)$ of $f(t)$. If the samples of the derivative are not provided separately, they may be approximated by processing $f[n]$ with a discrete-time differentiator.

We wish to determine a warping function $\alpha_*(t)$ such that the sequence $g[n] = f(\alpha_*(n))$ has minimal energy ε_g above a desired maximum discrete-time frequency ω_0. Specifically, we define ε_g in terms of the K-point DFT $G[k]$ of $g[n]$ as

$$\varepsilon_g = \sum_{k=k_{min}}^{k_{max}} |G[k]|^2, \tag{6.28}$$

where k_{min} and k_{max} correspond approximately to the frequency interval $[\omega_0, 2\pi - \omega_0]$, i.e.

$$k_{min} = \left\lceil \frac{K\omega_0}{2\pi} \right\rceil,$$
$$k_{max} = \left\lfloor K \left(1 - \frac{\omega_0}{2\pi} \right) \right\rfloor. \tag{6.29}$$

If $K > L$, then $g[n]$ is zero-padded before taking the DFT. The energy ε_g is equivalently expressed in the time domain as the following circular convolution:

$$\varepsilon_g = K \sum_{m=0}^{K-1} \left[\sum_{n=0}^{L-1} g[n]h[((m-n))_K] \right]^2,$$

89

$$\varepsilon_g = K \sum_{m=0}^{K-1} \left[\sum_{n=0}^{L-1} f(\alpha(n))h[((m-n))_K] \right]^2, \qquad (6.30)$$

where $((m-n))_K$ denotes $(m-n) \bmod K$. The sequence $h[m]$, $m = 0, 1, \ldots, K-1$, is the impulse response of a highpass filter with DFT

$$H[k] = \begin{cases} 0, & 0 \leq k < k_{min}, \\ 1, & k_{min} \leq k \leq k_{max}, \\ 0, & k_{max} < k \leq K-1. \end{cases} \qquad (6.31)$$

The warping functions $\alpha(t)$ to be considered are piecewise linear functions defined on the interval $[0, L]$ by

$$\alpha(t) = \sum_{p=0}^{P} \alpha_p \beta \left(\frac{t}{\delta} - p \right), \quad 0 \leq t \leq L, \qquad (6.32)$$

where δ is chosen to be a positive integer such that $P\delta = L$. For notational convenience, we use the vector $\underline{\alpha} = [\alpha_0, \alpha_1, \ldots, \alpha_P]^T$ to represent a point in the parameter space. For $\alpha(t)$ to be monotonically increasing, we must have $\alpha_{p+1} > \alpha_p$, $p = 1, 2, \ldots, P-1$. Given the finite interval $[0, L]$, instead of requiring (5.5), we constrain the time-warping to preserve the length of the interval by fixing $\alpha_0 = 0$ and $\alpha_P = L$ so that $\alpha(L) - \alpha(0) = L$.

The algorithm requires the computation of the gradient $\underline{\nabla}\varepsilon_g$ with respect to $\underline{\alpha}$, defined as

$$\underline{\nabla}\varepsilon_g = \left[\frac{\partial \varepsilon_g}{\partial \alpha_0}, \frac{\partial \varepsilon_g}{\partial \alpha_1}, \ldots, \frac{\partial \varepsilon_g}{\partial \alpha_P} \right]^T, \qquad (6.33)$$

where we take $\partial \varepsilon_g / \partial \alpha_0 = \partial \varepsilon_g / \partial \alpha_P = 0$ since α_0 and α_P are fixed. For $p = 1, \ldots, P-1$, we differentiate (6.30) with respect to α_p, yielding

$$\frac{\partial \varepsilon_g}{\partial \alpha_p} = 2K \sum_{m=0}^{K-1} \left\{ \sum_{n=0}^{L-1} f(\alpha(n))h[((m-n))_K] \right\} \left\{ \sum_{n=0}^{L-1} f'(\alpha(n))\beta \left(\frac{n}{\delta} - p \right) h[((m-n))_K] \right\}. \qquad (6.34)$$

Define the sequences $d_p[n]$ to be

$$d_p[n] = f'(\alpha(n))\beta \left(\frac{n}{\delta} - p \right), \quad p = 1, 2, \ldots, P-1, \qquad (6.35)$$

and denote the corresponding K-point DFTs by $D_p[k]$. Using Parseval's relation, (6.34) is

90

equivalently expressed as

$$\frac{\partial \varepsilon_g}{\partial \alpha_p} = 2 \sum_{k=0}^{K-1} (G[k]H[k])(D_p[k]H[k])^*,$$

$$= 2 \sum_{k=k_{min}}^{k_{max}} G[k] D_p^*[k], \quad p = 1, 2, \ldots, P - 1. \tag{6.36}$$

Figure 6-6 shows a block diagram for a system that computes $\underline{\nabla}\varepsilon_g$ at a point $\underline{\alpha}$ in the parameter space. In a purely discrete-time implementation, the combination of time-warping and sampling is approximated by interpolating between the given samples, namely $f[n]$ and $f'[n]$. The rightmost block represents the inner product between the sequences $G[k]$ and $D_p[k]$ as given in (6.36).
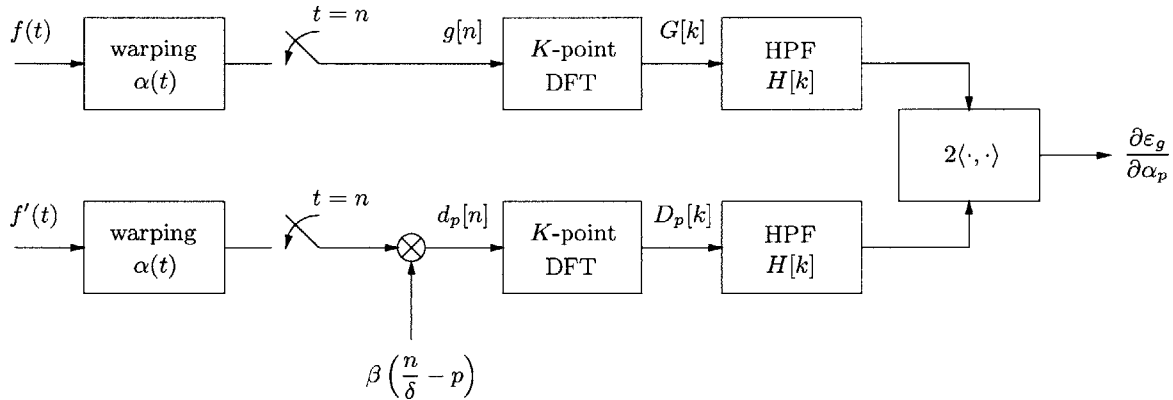

Figure 6-6: System for computing the partial derivatives $\partial \varepsilon_g / \partial \alpha_p$. The rightmost block represents the inner product given by (6.36).

We now describe the gradient-descent algorithm in terms of an iterative procedure. We use i to denote the iteration number and label quantities associated with iteration i using a superscript $^{(i)}$.

The algorithm is initialized by setting $\alpha_p^{(0)} = p\delta$ for $p = 0, 1, \ldots, P$, which yields $\alpha^{(0)}(t) = t$ and corresponds to no time-warping. Hence, $g^{(0)}[n] = f[n]$, and $\varepsilon_g^{(0)}$ is the energy of $f[n]$ above ω_0.

For each iteration i, the non-zero components of the gradient $\underline{\nabla}\varepsilon_g^{(i)}$ are computed at the point $\underline{\alpha}^{(i)}$ according to Figure 6-6. The new parameter vector $\underline{\alpha}^{(i+1)}$ is chosen in the direction of the negative gradient from $\underline{\alpha}^{(i)}$, i.e.

$$\underline{\alpha}^{(i+1)} = \underline{\alpha}^{(i)} - \Delta\alpha \cdot \underline{\nabla}\varepsilon_g^{(i)}, \tag{6.37}$$

where the step size $\Delta\alpha$ minimizes the value of $\varepsilon_g^{(i+1)}$ over the range $0 \leq \Delta\alpha < \Delta\alpha_{max}$. The maximum step size $\Delta\alpha_{max}$ is given by

$$\Delta\alpha_{max} = \min_p \left\{ \frac{\alpha_{p+1}^{(i)} - \alpha_p^{(i)}}{\left(\frac{\partial \varepsilon_g}{\partial \alpha_{p+1}}\right)^{(i)} - \left(\frac{\partial \varepsilon_g}{\partial \alpha_p}\right)^{(i)}} \right\}, \tag{6.38}$$

where the minimum is taken only over values of p, $1 \leq p \leq P-1$, for which the denominator in (6.38) is positive. The upper limit on the step size is a consequence of the monotonically increasing constraint applied to $\underline{\alpha}^{(i+1)}$.

Given (6.37), determining $\underline{\alpha}^{(i+1)}$ reduces to determining the value of $\Delta\alpha$ at which the 1-D function $\varepsilon_g^{(i+1)}(\Delta\alpha)$ has a minimum on the interval $[0, \Delta\alpha_{max})$. A variety of methods may be applied to this 1-D search. Operationally, the function $\varepsilon_g^{(i+1)}(\Delta\alpha)$ is evaluated by first determining the warping function $\alpha^{(i+1)}(t)$ corresponding to $\Delta\alpha$, and then computing the sequence $g^{(i+1)}[n] = f(\alpha^{(i+1)}(n))$, from which the energy $\varepsilon_g^{(i+1)}$ is computed.

Once the minimum of $\varepsilon_g^{(i+1)}(\Delta\alpha)$ is obtained, the corresponding parameters $\underline{\alpha}^{(i+1)}$ are used in the next iteration $i + 1$. The algorithm may be terminated upon convergence, i.e. when $\underline{\alpha}^{(i+1)} \approx \underline{\alpha}^{(i)}$ to within some tolerance, or after a desired number of iterations.

The gradient-descent algorithm was implemented using MATLAB and tested using time-warped sinusoidal signals as inputs. The input sequences $f[n]$ were obtained by time-warping a sinusoidal signal $g_0(t) = \cos(\omega_1 t)$, restricted to the interval $[0, L]$, using warping functions $\bar{\gamma}(t)$ that are piecewise linear between the points $(t, \bar{\gamma}(t)) = (\bar{\alpha}_p, p\delta)$ for $p = 0, 1, \ldots, P$. As a consequence, the inverse warping $\bar{\alpha}(t)$ has exactly the form of (6.32).

More specifically, $\bar{\alpha}_p$ was chosen as

$$\bar{\alpha}_p = \frac{aL - 1 + \sqrt{(aL - 1)^2 + 4ap\delta}}{2a}, \tag{6.39}$$

where the parameter a satisfies $|a| \leq 1/L$ to ensure monotonicity. Since $\bar{\alpha}_0 = 0$ and $\bar{\alpha}_P = L$, the length-preserving constraint is also satisfied. The corresponding $\bar{\gamma}(t)$ is a piecewise linear approximation to the quadratic function $(1 - aL)t + at^2$. Hence, the samples $f[n] = g_0(\bar{\gamma}(n))$ correspond approximately to samples of a linear FM signal.

Table 6.1 lists the parameter values used in the simulations. The frequency ω_1 was chosen so that the signals $f(t) = g_0(\bar{\gamma}(t))$ vary slowly compared to the sampling period $T = 1$, and hence the aliasing error associated with the samples $f[n]$ is small. The parameter δ controls

the fineness of the piecewise linear parameterization. It was observed that a smaller value of δ, corresponding to a greater number of degrees of freedom, yields a lower minimum value for ε_g.

parameter	symbol	value
sequence length	L	1000
frequency of $g_0(t)$	ω_1	0.01π
maximum frequency	ω_0	$1.2\omega_1$
DFT length	K	32768
length of piecewise linear segments	δ	4
number of parameters	P	250
number of iterations	I	100

Table 6.1: Parameter values used in MATLAB simulations of the gradient-descent algorithm.

Figure 6-7 indicates how $\varepsilon_g^{(i)}$ decreases with each iteration, as expected since the algorithm follows the direction of the negative gradient. The vertical axis is normalized by the total energy in $g^{(100)}[n]$, the sequence yielded by the 100th iteration. The upper and lower curves correspond to $a = -8 \times 10^{-5}$ and $a = -2 \times 10^{-5}$ respectively. We observe that $\varepsilon_g^{(i)}$ converges to a minimum value within ~ 10 iterations. The condition for convergence in the simulations is $||\underline{\alpha}^{(i+1)} - \underline{\alpha}^{(i)}|| < 0.01$, where $|| \cdot ||$ denotes the usual Euclidean distance.

Overall, the gradient-descent algorithm appears to be unsuccessful at inverting the warping functions used to generate the input sequences. Figure 6-8 plots the input sequence $f[n]$ with $a = -8 \times 10^{-5}$, the output $g^{(100)}[n]$ after 100 iterations, and the sequence $g_0[n] = g_0(n)$ from which $f[n]$ was generated. For the purposes of display, we use continuous lines to interpolate between values of discrete sequences. Figure 6-9 plots the warping function $\bar{\gamma}(t)$ corresponding to $f[n]$ in Figure 6-8, its exact inverse $\bar{\alpha}(t)$, and the inverse $\alpha^{(100)}(t)$ returned by the algorithm. As the plots illustrate, $g^{(100)}[n]$ and $\alpha^{(100)}(t)$ are very different from $g_0[n]$ and $\bar{\alpha}(t)$, the results that would have been obtained from inverting $\bar{\gamma}(t)$ exactly. We conclude therefore that $\underline{\alpha}^{(100)}$ represents a local minimum of ε_g that is close to the initial choice of $\underline{\alpha}^{(0)}$. In order to avoid converging to the nearest, not necessarily optimal local minimum, the gradient-descent algorithm may be combined with a finely-tuned initialization, or a more powerful minimization technique may be employed.
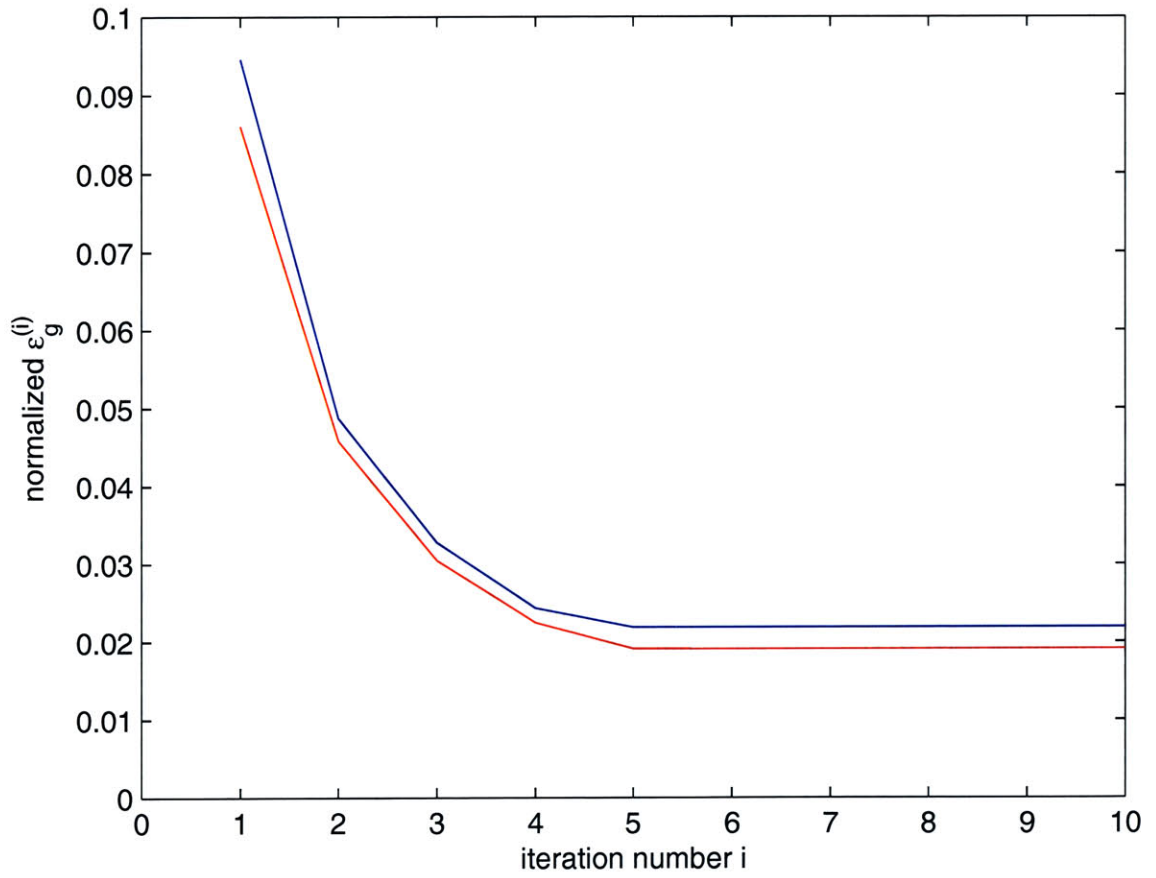
Figure 6-7: Plot of $\varepsilon_g^{(i)}$ normalized by total energy in $g^{100}[n]$ for $a = -8 \times 10^{-5}$ (upper curve) and $a = -2 \times 10^{-5}$ (lower curve).
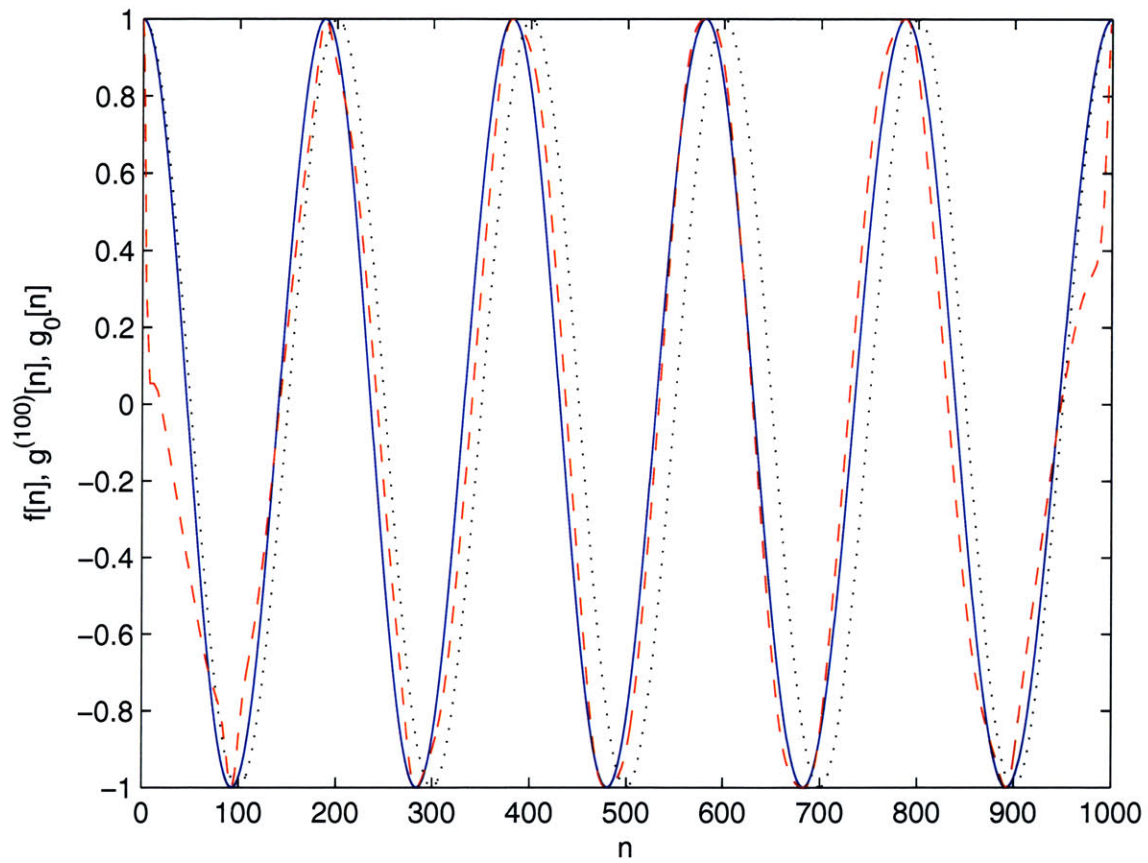
Figure 6-8: Output $g^{(100)}[n]$ (dashed line) obtained after 100 iterations of the gradient-descent algorithm with input $f[n]$ (solid line, $a = -8 \times 10^{-5}$). The desired result is $g_0[n]$ (dotted line).
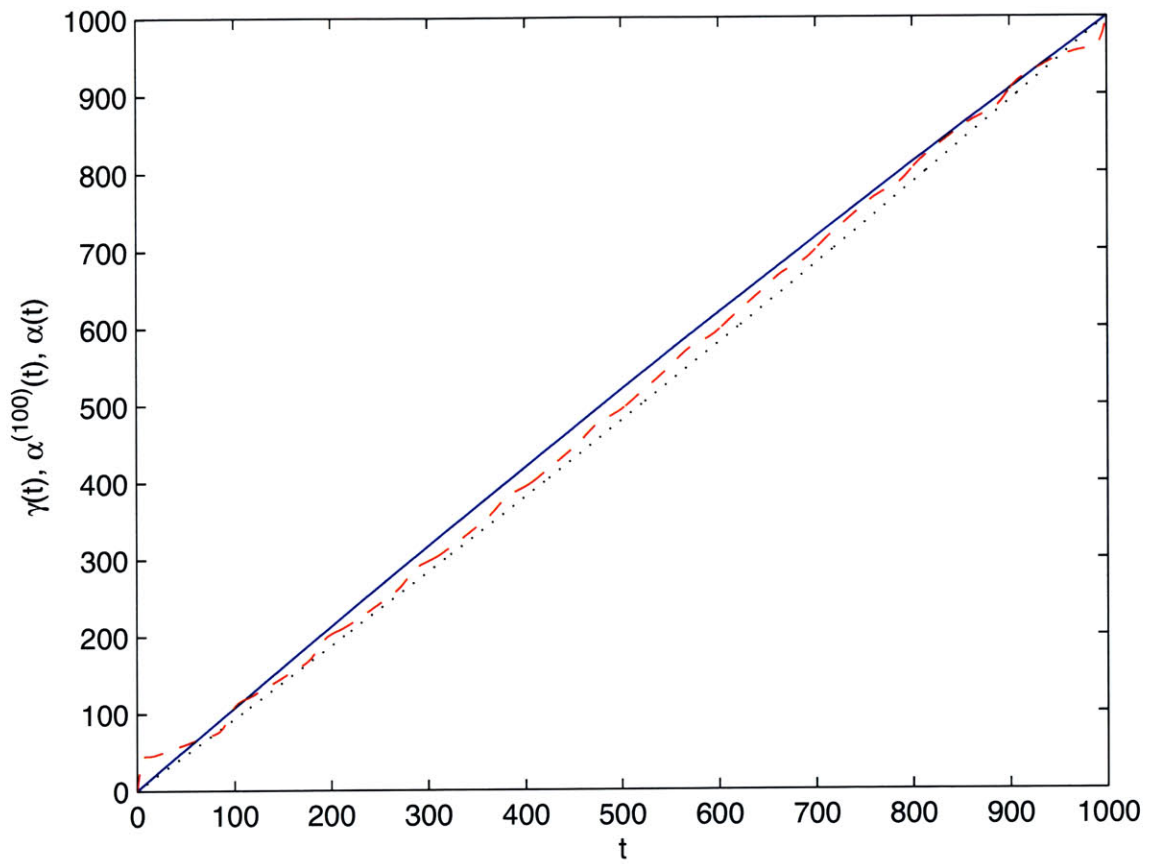
Figure 6-9: Warping function $\bar{\gamma}(t)$ (solid line) used to generate $f[n]$ in Figure 6-8, its exact inverse $\bar{\alpha}(t)$ (dotted line), and the inverse $\alpha^{(100)}(t)$ (dashed line) obtained after 100 iterations of the gradient-descent algorithm.

6.3 Determination of a time-warping based on zero-crossings

In this section, we present an alternative algorithm for determining a warping function $\alpha(t)$ that maps a signal $f(t)$ into an approximately bandlimited signal $g(t)$. However, rather than using ε_g as the metric for the quality of the solution, the algorithm of this section relies upon a more heuristic approach based on the zero-crossings of the signal. The results of a MATLAB implementation and evaluation of the algorithm are summarized.

Before discussing the algorithm, we review some relationships between a bandlimited signal and its zero-crossings. From Titchmarsh [18], if a function $q(z)$ of a complex variable $z = t + ju$ can be expressed as

$$q(z) = \frac{1}{2\pi} \int_{-\omega_0}^{\omega_0} Q(\omega) e^{j\omega z} d\omega, \qquad (6.40)$$

then $q(z)$ is real-valued, entire, and completely specified up to a scaling by an infinite product involving its zeroes:

$$q(z) = q(0) \prod_{m=-\infty}^{\infty} \left(1 - \frac{z}{z_m}\right), \qquad (6.41)$$

where $q(0)$ is assumed to be non-zero for simplicity, and the zeroes z_m are ordered such that $|z_m| \leq |z_{m+1}|$. Furthermore, the moduli of the zeroes are spaced on average according to the Nyquist rate associated with ω_0, i.e.

$$\lim_{m \to \infty} \frac{|z_m|}{m} = \frac{\pi}{\omega_0}. \qquad (6.42)$$

By restricting z to be real, we obtain a function $q(t)$ of a real variable that is bandlimited to ω_0 and has as its zero-crossings the subset of $\{z_m, m \in \mathbf{Z}\}$ for which z_m is real.

Based on [18], Bond and Cahn [19] developed a construction for a bandlimited signal having a specified set of N zero-crossings within the interval $t \in \left[-\frac{T}{2}, \frac{T}{2}\right]$. The maximum frequency ω_0 of the constructed signal has a lower bound of $\pi N/T$. Outside of $\left[-\frac{T}{2}, \frac{T}{2}\right]$, the zeroes are assumed to be real and to occur uniformly at the Nyquist spacing π/ω_0. It was observed in [19] that the amplitude of the constructed signal depends approximately on the spacings between nearby zero-crossings: the amplitude tends to be higher if the zero-crossings are farther apart, and lower if the zero-crossings are closer together.

We contrast the result of [19] with Logan's theorem [20], which states that a signal is uniquely specified by its zero-crossings provided that the bandwidth of the signal is less than one octave, i.e. an interval $[B, 2B]$ for some frequency B, and that there are no common zeroes between the signal and its Hilbert transform, except for simple real zeroes. Logan's theorem does not hold in general for baseband-limited signals, which are not uniquely specified by their zero-crossings. In particular, the baseband-limited construction of [19] is one of many signals having the same bandwidth and zero-crossings. It may be modified by the addition of a finite number of complex zeroes without altering the bandwidth.

Using the results of [18] and [19], we develop an iterative algorithm based on the following heuristic approach. The signal $f(t)$ is given on a finite interval $[0, L]$, from which its zeroes z_m, $m = 1, 2, \ldots, M$, can be determined. The zeroes z_m are all assumed to be of first order, a condition that can be achieved by the addition of an appropriate constant. We wish to map $f(t)$ into an approximately bandlimited signal $g(t)$ by means of a time-warping. Toward this end, we construct a bandlimited signal $q(t)$ that has the same zero-crossings z_m (and only those zero-crossings) on $[0, L]$ and zero-crossings outside of $[0, L]$ with average spacing equal to that in $[0, L]$. The signal $q(t)$ is then normalized to $f(t)$, e.g. by scaling $q(t)$ so that the energies of $q(t)$ and $f(t)$ are equal.

We consider the ratio

$$r(t) = \begin{cases} \left| \dfrac{q(t)}{f(t)} \right|, & 0 \le t \le L, \quad f(t) \ne 0, \\ \left| \dfrac{q'(t)}{f'(t)} \right|, & 0 \le t \le L, \quad f(t) = 0, \end{cases} \tag{6.43}$$

where the right-hand side for $f(t) = 0$ is obtained using l'Hôpital's rule. As Figure 6-10 suggests, in a region where $r(t) < 1$, $f(t)$ has a larger amplitude than the bandlimited signal $q(t)$ with the same local set of zero-crossings. Following the observation of [19], in order for a bandlimited signal to have the same amplitude as $f(t)$, its zero-crossings should be more widely spaced. Accordingly, $f(t)$ should be locally dilated where $r(t) < 1$ to yield the appropriate zero spacing. Similarly, if $r(t) > 1$, $f(t)$ has an amplitude smaller than $q(t)$ and should therefore be locally compressed.

Thus, we choose the derivative $\alpha'(t)$ of the warping function to be of the form

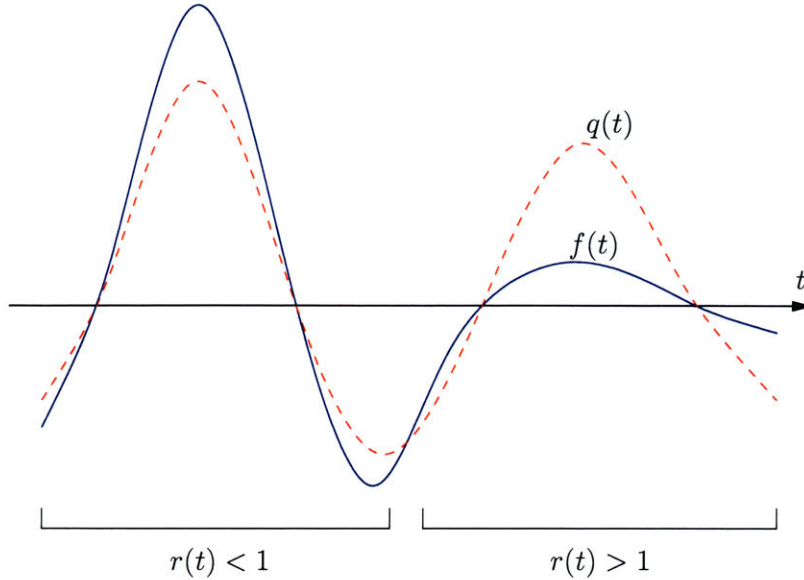$$\alpha'(t) = a \left(r(t) \right)^p, \quad 0 \le t \le L, \tag{6.44}$$

Figure 6-10: Sketch of $f(t)$ (solid line) and a bandlimited signal $q(t)$ (dashed line) sharing the same zeroes.

where a and p are positive constants, and a is chosen to satisfy the length-preserving constraint, i.e. with

$$\alpha(t) = \int_0^t \alpha'(\tau)d\tau, \tag{6.45}$$

we have $\alpha(0) = 0$ and $\alpha(L) = L$. Note that $\alpha(t)$ is monotonically increasing since $\alpha'(t) > 0$. We obtain a new signal $g(t) = f(\alpha(t))$ by time-warping $f(t)$ with $\alpha(t)$. The procedure may then be iterated with $g(t)$ taking the place of $f(t)$.

A discrete-time adaptation of the foregoing algorithm was implemented in MATLAB. As in Section 6.2.3, the input to the algorithm is a sequence $f[n] = f(t)|_{t=n}$ of samples of $f(t)$, where the time index n takes the values $0, 1, 2, \ldots, L$. We again assume that $f(t)$ varies slowly enough for the aliasing error to be negligble, and that $f(t)$ at non-integer values of t may be approximated by interpolating between the samples $f[n]$.

The iteration number is denoted by i and quantities associated with iteration i are denoted by a superscript $^{(i)}$. The algorithm is initialized by setting $g^{(0)}[n] = f[n]$. For each iteration i, $i = 0, 1, \ldots$, the following steps are performed:

1. The zero-crossings $z_m^{(i)}$, $m = 1, 2, \ldots, M$, of $g^{(i)}(t)$ are determined, either by identifying zeroes in the sequence $g^{(i)}[n]$, or by interpolating between samples whenever a sign change occurs.

2. The bandlimited signal $q^{(i)}(t)$ is constructed from the zero-crossings $z_m^{(i)}$ by assuming

that the pattern of zero-crossings repeats periodically with period L, i.e. $q^{(i)}(t)$ has zero-crossings at $z_m^{(i)} + rL$ for all m and $r \in \mathbf{Z}$. $q^{(i)}(t)$ is then sampled at $t = n$, resulting in the sequence

$$q^{(i)}[n] = Q^{(i)} \prod_{m=1}^{M} \sin\left(\frac{\pi}{L}\left(n - z_m^{(i)}\right)\right), \tag{6.46}$$

with normalizing constant $Q^{(i)}$ chosen so that $q^{(i)}[n]$ and $g^{(i)}[n]$ have the same energy.

3. Samples of $\alpha'^{(i)}(t)$ are computed as

$$\alpha'^{(i)}(n) = \begin{cases} \left|\dfrac{q^{(i)}[n]}{g^{(i)}[n]}\right|^p, & g^{(i)}[n] \neq 0, \\[4mm] \left|\dfrac{q^{(i)}[n+1] - q^{(i)}[n-1]}{g^{(i)}[n+1] - g^{(i)}[n-1]}\right|^p, & g^{(i)}[n] = 0, \end{cases} \tag{6.47}$$

where $p \approx 0.25$ as determined empirically. The right-hand side of (6.47) for $g^{(i)}[n] = 0$ represents an approximation to the ratio of derivatives in (6.43). In addition, $\alpha'^{(i)}(n)$ may be further regularized by imposing a maximum local dilation or compression factor α'_{max}, e.g. through hard-limiting if $\alpha'^{(i)}(n)$ exceeds the range $[1/\alpha'_{max}, \alpha'_{max}]$.

4. Samples $\alpha^{(i)}(n)$ of the warping function are computed by numerically integrating $\alpha'^{(i)}(n)$. The sequence $\alpha^{(i)}(n)$ is then normalized so that $\alpha^{(i)}(0) = 0$ and $\alpha^{(i)}(L) = L$.

5. The new sequence $g^{(i+1)}[n]$ is obtained by time-warping $f(t)$, i.e.

$$g^{(i+1)}[n] = f(\alpha^{(i)}(n)),$$

where samples of $f(t)$ at non-integer times are approximated by interpolation.

The algorithm may be repeated for a desired number of iterations, or until it converges to a final sequence $g[n]$.

The algorithm was evaluated using time-warped sinusoidal signals as inputs. Specifically, the sinusoidal signal $g_0(t) = \cos(\omega_1 t)$ with $\omega_1 = 0.01\pi$ was time-warped using functions of the form

$$\bar{\gamma}(t) = (1 - aL)t + at^2, \quad 0 \leq t \leq L, \tag{6.48}$$

where $|a| \leq 1/L$ and $L = 1000$. As noted in Section 6.2.3, $\bar{\gamma}(t)$ is length-preserving

and monotonically increasing. The input sequence $f[n]$ is given by $f[n] = g_0(\bar{\gamma}(n))$, $n = 0, 1, \ldots, L$.

In Figure 6-11, we plot the input $f[n]$ with $a = 1/L = 10^{-3}$, the resulting sequence $g^{(50)}[n]$ after 50 iterations of the algorithm, and the sequence $g_0[n] = g_0(n)$ of samples of the original sinusoid. The sequences $g^{(50)}[n]$ and $g_0[n]$ differ only by a small shift over most of the displayed region. We conclude in this case that the algorithm is successful in inverting the time-warping $\bar{\gamma}(t)$, yielding an approximately bandlimited sequence. Furthermore, the agreement between $g^{(50)}[n]$ and $g_0[n]$ improves as $|a|$ decreases, as expected since a smaller value for $|a|$ corresponds to a more modest time-warping.
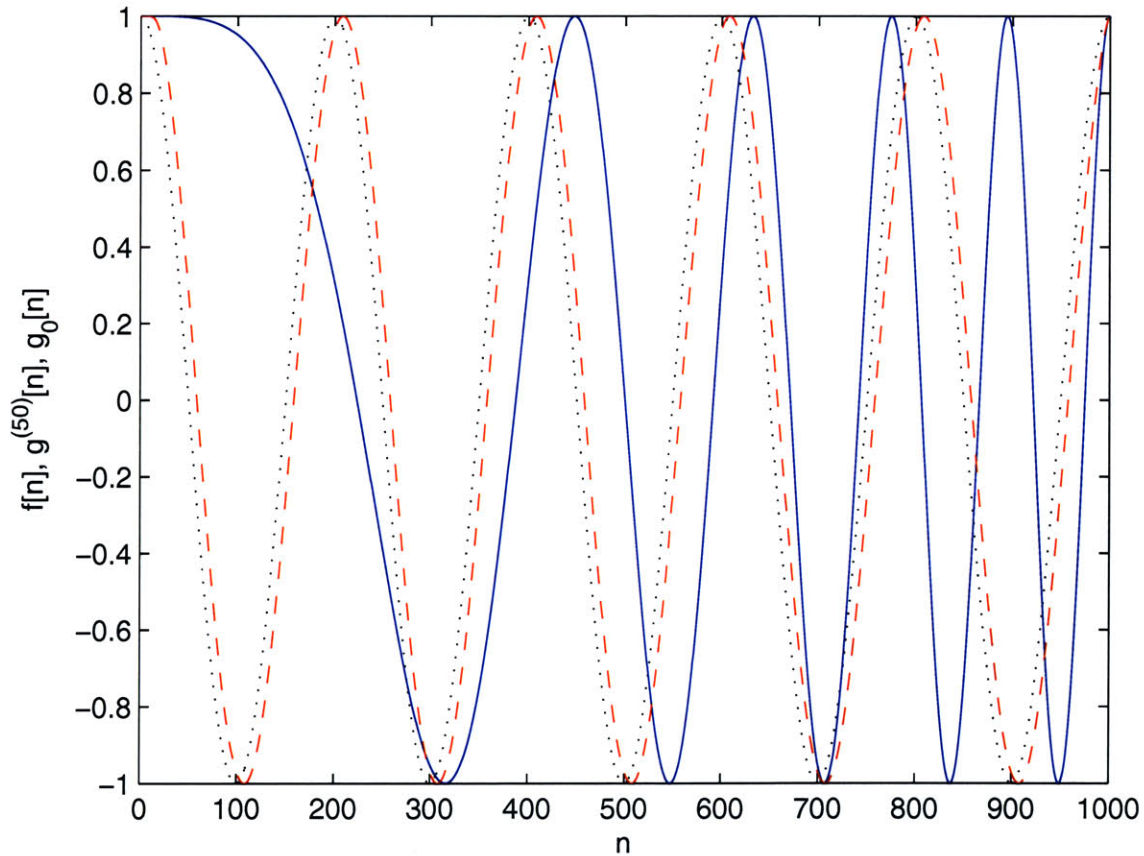

Figure 6-11: Input sequence $f[n]$ (solid line), sequence $g^{(50)}[n]$ (dashed line) obtained after 50 iterations of the zero-crossings algorithm, and sinusoidal sequence $g_0[n]$ (dotted line) used to generate $f[n]$ with $a = 10^{-3}$.

The algorithm was also applied to time-warped, bandlimited white noise. White noise sequences consisting of samples uniformly distributed on $[-1, 1]$ were filtered using a length $L + 1$ Parks-McClellan lowpass filter with cut-off frequency ω_1, resulting in approximately

bandlimited sequences $g_0[n]$. We assume that each sequence $g_0[n]$ corresponds to an underlying continuous-time signal $g_0(t)$ that can be evaluated by interpolating $g_0[n]$. The input sequences are given by $f[n] = g_0(\bar{\gamma}(n))$ with $\bar{\gamma}(t)$ specified in (6.48) and $a = 7 \times 10^{-4}$.

Figures 6-12 and 6-13 show plots of the input sequences $f[n]$ corresponding to two different white noise realizations, the output sequences $g^{(20)}[n]$ after 20 iterations, and the sequences $g_0[n]$ from which the inputs were generated. In Figure 6-12, there is approximate agreement between $g^{(20)}[n]$ and $g_0[n]$, a result that represents only about 20% of the trials. The remainder of the trials are represented by Figure 6-13, where $g^{(20)}[n]$ is very different from $g_0[n]$ and also exhibits undesirable artifacts near $n = 0$ and between $n = 700$ and $n = 800$ caused by excessive local time-warping.
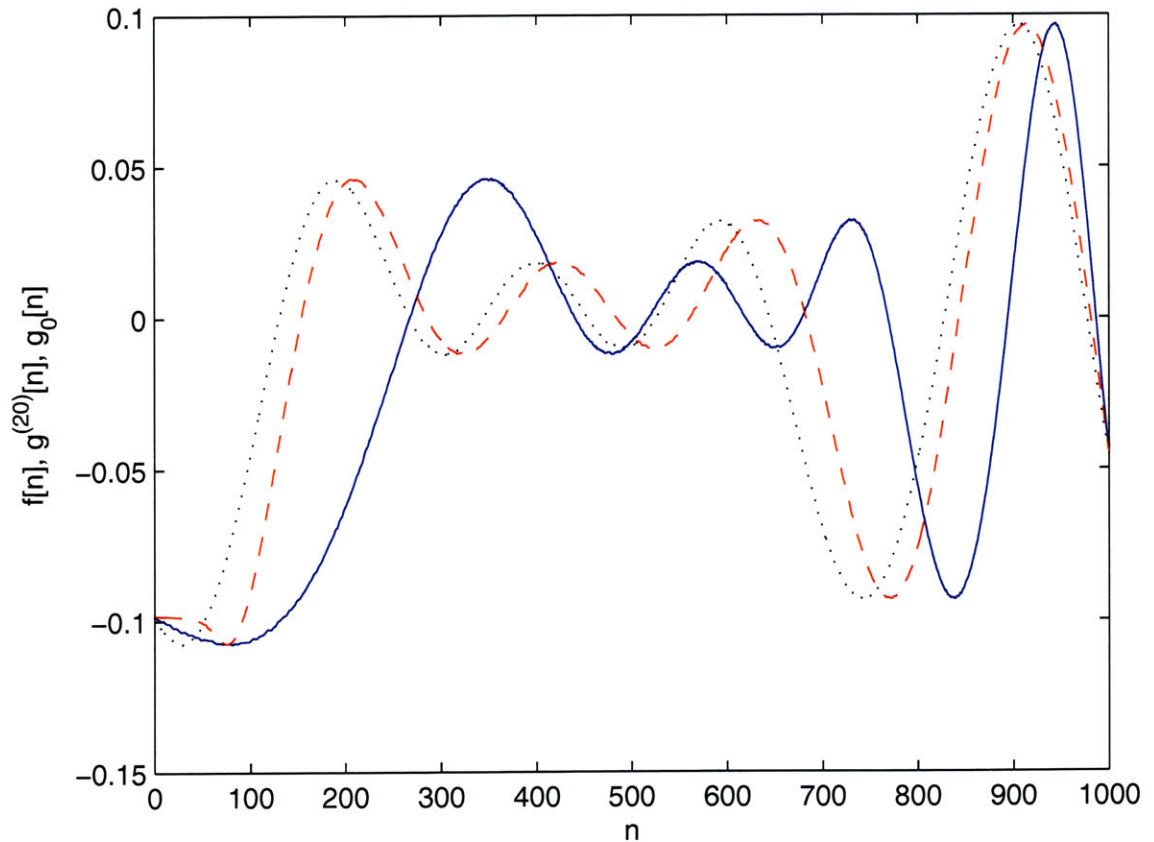

Figure 6-12: Input sequence $f[n]$ (solid line), sequence $g^{(20)}[n]$ (dashed line) obtained after 20 iterations of the zero-crossings algorithm, and bandlimited white noise $g_0[n]$ (dotted line) used to generate $f[n]$ with $a = 7 \times 10^{-4}$.

The poor performance of the algorithm as demonstrated in Figure 6-13 can be related to the regularity of the occurrence of zero-crossings in the input signal. The inputs in Figures
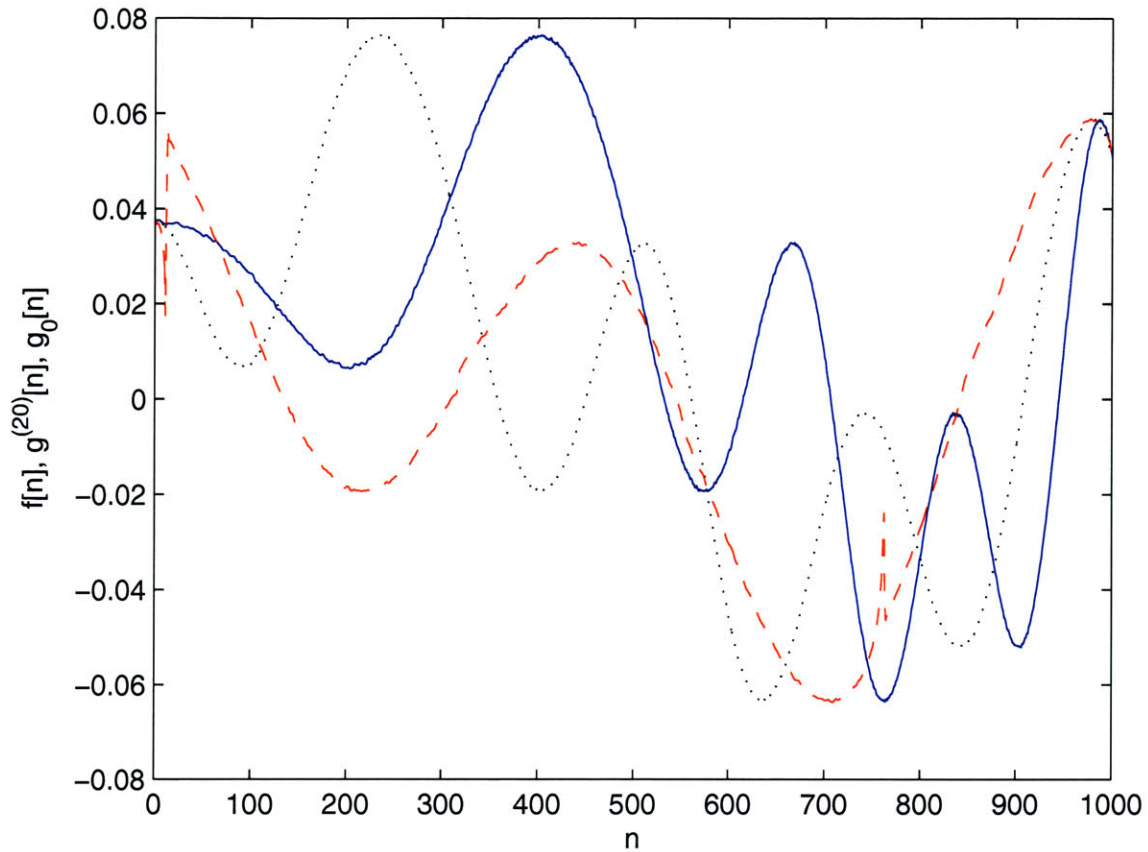
Figure 6-13: Input $f[n]$ (solid line), output $g^{(20)}[n]$ (dashed line) after 20 iterations, and bandlimited white noise $g_0[n]$ (dotted line) corresponding to a noise realization different from the one in Figure 6-12.

6-12 and 6-11 have the property that zero-crossings occur between nearly every pair of adjacent local extrema. We expect the algorithm to perform well in these cases as they correspond to the intuition in Figure 6-10 on which the algorithm is based. In contrast, $f[n]$ in Figure 6-13 has fewer zero-crossings on $[0, L]$, separated in some cases by several local extrema. The lack of regular zero-crossings results in a poorly-controlled time-warping.

Bibliography

[1] A. J. Jerri, "The Shannon sampling theorem – its various extensions and applications – a tutorial review," *Proceedings of the IEEE*, vol. 65, no. 11, pp. 1565–1596, November 1977.

[2] A. W. Rihaczek, *Principles of High-Resolution Radar*, ser. Applied Mathematical Sciences. Norwood, Massachusetts: Artech House, 1996, vol. 42.

[3] J. S. Lim, *Two-Dimensional Signal and Image Processing*. Upper Saddle River, NJ: Prentice-Hall, Inc., 1990.

[4] K. Horiuchi, "Sampling principle for continuous signals with time-varying bands," *Information and Control*, vol. 13, no. 1, pp. 53–61, 1968.

[5] J. J. Clark, M. R. Palmer, and P. D. Lawrence, "A transformation method for the reconstruction of functions from nonuniformly spaced samples," *IEEE Transactions on Acoustics, Speech, and Signal Processing*, vol. 33, no. 4, pp. 1151–1165, October 1985.

[6] Y. Y. Zeevi and E. Shlomot, "Nonuniform sampling and antialiasing in image representation," *IEEE Transactions on Signal Processing*, vol. 41, no. 3, pp. 1223–1236, March 1993.

[7] L. Cohen, *Time-Frequency Analysis*. Upper Saddle River, NJ: Prentice-Hall, Inc., 1995.

[8] N. N. Bruller, N. Peterfreund, and M. Porat, "Optimal sampling and instantaneous bandwidth estimation," in *Proceedings of the IEEE International Symposium on Time-Frequency and Time-Scale Analysis*, vol. 1, Pittsburgh, USA, October 1998, pp. 113–115.

[9] T. A. C. M. Claasen and W. F. G. Mecklenbrauker, "On stationary linear time-varying systems," *IEEE Transactions on Circuits and Systems*, vol. 29, no. 3, pp. 169–184, March 1982.

[10] L. A. Zadeh, "Time-varying networks, I," *Proceedings of the IRE*, vol. 49, pp. 1488–1503, October 1961.

[11] G. W. Wornell, *Signal Processing with Fractals: A Wavelet-Based Approach.* Upper Saddle River, NJ: Prentice-Hall, Inc., 1996.

[12] J. L. Yen, "On nonuniform sampling of bandwidth-limited signals," *IEEE Transactions on Circuit Theory*, vol. 3, no. 4, pp. 251–257, December 1956.

[13] K. Yao and J. B. Thomas, "On some stability and interpolatory properties of nonuniform sampling expansions," *IEEE Transactions on Circuits and Systems*, vol. 14, no. 4, pp. 404–408, December 1967.

[14] J. R. Higgins, "A sampling theorem for irregularly spaced sample points," *IEEE Transactions on Information Theory*, vol. 22, no. 5, pp. 621–622, September 1976.

[15] P. Weiss, "An estimate of the error arising from misapplication of the sampling theorem," *Notices of the American Mathematical Society*, no. 10.351, pp. Abstract 601–51, 1963.

[16] I. M. Gelfand, S. V. Fomin, and R. A. Silverman, *Calculus of Variations.* Mineola, NY: Courier Dover Publications, 2000.

[17] D. G. Luenberger, *Introduction to Linear and Nonlinear Programming.* Reading, MA: Addison-Wesley Publishing Company, 1973.

[18] E. C. Titchmarsh, "The zeros of certain integral functions," *Proceedings of the London Mathematical Society*, vol. 25, pp. 283–302, May 1926.

[19] F. E. Bond and C. R. Cahn, "On sampling the zeros of bandwidth limited signals," *IRE Transactions on Information Theory*, vol. IT-4, pp. 110–113, September 1958.

[20] B. F. Logan, Jr., "Information in the zero-crossings of bandpass signals," *Bell System Technical Journal*, vol. 56, pp. 487–510, April 1977.